UNIFIED FORMULATION FOR EVALUATION AND VISUALIZATION OF ELECTRIC AND MAGNETIC FIELDS INSIDE WAVEGUIDES AND CAVITY RESONATORS

by

Zahid Hasan

A thesis submitted to the Faculty and the Board of Trustees of the Colorado School of Mines in partial fulfillment of the requirements for the degree of Master of Science (Electrical Engineering).

Golden, Colorado

Date _____

Signed: _____
Zahid Hasan

Signed: _____
Dr. Atef Z. Elsherbeni
Thesis Advisor

Signed: _____
Dr. Peter Aaen
Committee Member

Signed: _____
Dr. Mona ElHelbawy
Committee Member

Golden, Colorado

Date: _____

Signed: _____
Dr. Peter Aaen
Professor and Department Head
Department of Electrical Engineering

ABSTRACT

Waveguides and cavity resonators play an important role in microwave applications and optical systems. Applications include filters, antennas, and electromagnetic sources, such as magnetrons and lasers. They can also be used to enhance the sensitivity of sensors. Electromagnetic (EM) simulation helps optimize device configuration for better performance in the desired frequency band. With the aid of simulation software expensive reworks can be avoided. The computation and visualization of EM fields inside waveguides and cavity resonators is challenging even in simple rectangular cross sections. This problem becomes more complex when dealing with circular, sectoral, and coaxial geometries. The research presented in this thesis provides an efficient and cost-effective solution to these challenges; An interactive software (WGC version 3) that has been developed to enhance and expedite the design and testing process through the computation and visualization of the electric and magnetic field distribution inside waveguides and cavity resonators.

The software features a user-friendly interface through which users can select one of seven different configurations and specify parameters of their design, such as structure dimensions, Transverse Electric (TE) mode or Transverse Magnetic (TM) mode, mode number, operating frequency, number of points of any of the field components along the x, y, and z axis for rectangular structures, and any 2D plane angles between 0° to 360° for cylindrical structures. Both transverse and longitudinal field components can be visualized in vector, color contour or both. The software makes it easy for users to see how the changes of physical dimensions and operating frequency affect the field distribution. Moreover, the user interface allows users to select how visualizations of the field distribution are generated and displayed. Five selection

options are made available: electric and magnetic field with vector; electric field vector; magnetic field vector; electric field strength; and magnetic field strength. Field distributions can be displayed as static images or video animations using appropriate sequencing of computed field values. The software provides all necessary warning messages to users for invalid input parameters.

The software has been designed in MATLAB App Designer platform. The executable code has been tested and verified on a personal computer (PC) platform running Windows 10 operating system. Mathematical expressions of the field components used in this software were derived from the classical solution of the wave equations using the separation of variables technique in cartesian coordinates for rectangular configurations and cylindrical coordinates for all other configurations. Results obtained using this software were validated against values found in the literature for similar types of problems, and results show perfect agreement.

The work developed in this thesis makes it possible for microwave engineers to quickly model and obtain information about the performance of their designs. It has great potential in enhancing the teaching and learning of microwave engineering. Visualizations produced by the software can greatly improve learners' ability to understand how electromagnetic waves propagate through guided structures. Furthermore, it provides a cost-effective alternative to commercial software packages, such as Ansys High Frequency Structure Simulator (HFSS), and Computer Simulation Technology (CST) Studio Suite for such applications.

TABLE OF CONTENTS

ABSTRACT…….……. iii

LIST OF FIGURES…….…….viii

ACKNOWLEDGEMENTS…….……..xii

CHAPTER 1 INTRODUCTION…….…….1

1.1 Motivation and Background …….1

1.2 The Need for Software …….…....2

1.3 Thesis Organization and Overview.…….…….4

CHAPTER 2 MATHEMATICAL DERIVATION OF FIELD EQUATIONS…….……5

2.1 Waveguide and Cavity…….…….5

2.2 General Equation Derivation…….5

2.2.1 Rectangular Cross-Section…….……6

2.2.2 Circular and Coaxial Cross-Section...…….……...10

2.2.3 Sectoral and Sectoral-Coaxial Cross-Section...……..13

2.2.4 Baffle and Baffle-Coaxial Cross-Section...……15

CHAPTER 3 SOFTWARE DESIGN…...…….……...16

3.1 MATLAB App Designer Platform.…….16

3.2 Graphical User Interface Development …….....17

3.2.1 WGC flowchart of the Software……...……..17

3.3 Layout and Operation of the Software…….…….19

3.3.1 Main Window…….19

3.3.2 Geometry Selection……20

3.3.3 Parameters Screen…….……20

3.3.4 Figures of EM Fields…...…….……..22

3.3.5 Video Animations of EM Fields….……....22

3.3.6 Programming and Special Functions ..…...……....23

CHAPTER 4 ILLUSTRATED EXAMPLES.……..…….…….....24

4.1 Waveguide ……...……..24

4.1.1 Rectangular Waveguide…….25

4.1.2 Circular Waveguide.……..37

4.1.3 Coaxial Waveguide……42

4.1.4 Sectoral Waveguide……...46

4.1.5 Baffle Waveguide……..49

4.1.6 Sectoral-Coaxial Waveguide…….52

4.1.7 Baffle-Coaxial Waveguide……55

4.2 Cavity…….....58

4.2.1 Rectangular Cavity ……..……58

4.2.2 Circular Cavity …….....62

4.2.3 Coaxial Cavity……..……...65

4.2.4 Sectoral Cavity……..……...67

4.2.5 Baffle Cavity……..……..69

4.2.6 Sectoral-Coaxial Cavity……..…….71

4.2.7 Baffle-Coaxial Cavity……..……72

CHAPTER 5 CONCLUSIONS.……..…75

5.1 Summary of Results……...75

5.2 Implications……...75

5.3 Future Work……...76

REFERENCES……..77

APPENDIX A ZEROS FOR BESSEL FUNCTION……..80

A.1 Matlab Programming...…...……..82

LIST OF FIGURES

Figure 2.1 Different cross-sections of waveguides and cavity resonators…….6

Figure 2.2 Rectangular cross-section of waveguide or cavity……..7

Figure 2.3 Cross-section of waveguide and cavity, circular (a) and coaxial (b) ……..…10

Figure 2.4 Sectoral and sectoral-coaxial cross-section of waveguide and cavity……...13

Figure 2.5 Circular baffle and baffle-coaxial waveguide and cavity resonator……..15

Figure 3.1 WGC (version 3) flow chart…….....…….18

Figure 3.2 Main window of the software……..……..19

Figure 3.3 Geometry selection (option menu) window of the software..……..20

Figure 3.4 Parameters Screen window for rectangular waveguide and cavity….……..22

Figure 4.1 Light color change with switch position.……...24

Figure 4.2 Illustrated example of how to start with the software….……25

Figure 4.3 "Rectangular" push button selection in the option menu.……...26

Figure 4.4 Initial parameters screen window for rectangular cross-section…….……..26

Figure 4.5 All valid inputs for rectangular waveguide.……..27

Figure 4.6 Drop-down menu for plotting different figures……...……..27

Figure 4.7 Checking the error message for wrong mode number….……..28

Figure 4.8 Other error messages for rectangular waveguide….……..29

Figure 4.9 Vector plot of rectangular waveguide at x-y plane for TE_{01} mode…….30

Figure 4.10 E-field and H-field of rectangular waveguide at x-y plane for TE_{01} mode……31

Figure 4.11 Vector plot of rectangular waveguide at x-z plane for TE_{01} mode…….31

Figure 4.12 E-field and H-field of rectangular waveguide at x-z plane for TE_{01} mode……...33

Figure 4.13 Vector plot of rectangular waveguide at y-z plane for TE_{01} mode……33

Figure 4.14 H-field of rectangular waveguide at y-z plane for TE_{01} mode……..….....33

Figure 4.15 Vector plot of rectangular waveguide at x-y plane for TM_{11} mode……...…...34

Figure 4.16 E-field and H-field of rectangular waveguide at x-y plane for TM_{11} mode……35

Figure 4.17 Vector plot of rectangular waveguide at x-z plane for TM_{11} mode.…….35

Figure 4.18 E-field and H-field of rectangular waveguide at x-z plane for TM_{11} mode……..36

Figure 4.19 Vector plot of rectangular waveguide at y-z plane for TM_{11} mode…..……..….36

Figure 4.20 E-field and H-field of rectangular waveguide at y-z plane for TM_{11} mode…...…36

Figure 4.21 Initial parameter screen window for circular waveguide……37

Figure 4.22 Parameters screen showing input and disable options for circular waveguide…….38

Figure 4.23 Error message for invalid mode number in circular waveguide…..…….39

Figure 4.24 For all valid input "Run" button is activated. …….39

Figure 4.25 Vector plot of circular waveguide at x-y axis for TM_{11} mode…..……...…..40

Figure 4.26 E-field and H-field of circular waveguide for TM_{11} mode……..…….41

Figure 4.27 Vector plot of circular waveguide for TM_{11} mode at 60° plane……...41

Figure 4.28 E-field and H-field of circular waveguide for TM_{11} mode at 60° plane…..….…...42

Figure 4.29 Parameters screen of coaxial waveguide…….……43

Figure 4.30 Vector plot of coaxial waveguide for TM_{12}…..…….....43

Figure 4.31 E-Field and H-Field of coaxial waveguide for TM_{12}…….……44

Figure 4.32 Vectors and field strength of coaxial waveguide at 60° plane angle for TM_{12} mode…….……45

Figure 4.33 Vector plots of coaxial waveguide for (a) TM_{11} (b) TE_{11} (c) TM_{21} (d) TE_{21}…….….46

Figure 4.34 Parameters screen for sectoral waveguide……...……47

Figure 4.35 Vector plot of (a) 90° and (b) 270° sectoral waveguide for TE_{21} mode……...……...48

Figure:4.36 E-Field and H-Field for 90° and 270° sectoral waveguide for TE_{21} mode……..……..49

Figure 4.37 Parameters screen of Baffle waveguide……...……..…..50

Figure 4.38 Vector plot of Baffle waveguide for TE_{11} mode……...……..….51

Figure 4.39 E-field and H-field of baffle waveguide for TM_{11}……52

Figure 4.40 Field vectors for (a) TE_{21} (b) TE_{31} (c) TE_{41} mode in baffle waveguide……..52

Figure 4.41 Parameters screen for sectoral-coaxial waveguide……...……53

Figure 4.42 Field vectors of 90° and 180° sectoral coaxial waveguide for TM_{11} mode……..……..54

Figure 4.43 E-Field and H-Field of 90° and 180° sectoral-coaxial waveguide……...55

Figure 4.44 Parameters screen of baffle-coaxial waveguide……...56

Figure 4.45 Field vectors of baffle-coaxial waveguide for TE_{21} mode……56

Figure 4.46 E-Field and H-Field of baffle-coaxial waveguide for TE_{21} mode……57

Figure 4.47 Parameters screen for rectangular cavity……..58

Figure 4.48 Vector plot of rectangular cavity at x-y plane for TE_{112}……59

Figure 4.49 E-field and H-field of rectangular cavity at x-y plane for TE_{112}……...60

Figure 4.50 Vector plot of rectangular cavity at x-z plane for TE_{112}……60

Figure 4.51 E-field and H-field of rectangular cavity at x-z plane for TE_{112}……..61

Figure 4.52 Vector plot of rectangular cavity at y-z plane for TE_{112}……..61

Figure 4.53 E-field and H-field with vector plot of rectangular cavity at y-z plane for TE_{112}…61

Figure 4.54 Parameters screen for circular cavity……..……..62

Figure 4.55 Vector plot of circular cavity at x-y plane for TE_{221}……63

Figure 4.56 E-field and H-field of circular cavity at x-y plane for TE_{221}……64

Figure 4.57 Vector plot of circular cavity at 120° plane cut for TE_{111}…….……..64

Figure 4.58 E-field and H-field of circular cavity at 120° plane cut for TE_{111}…….……..65

Figure 4.59 Field vectors of coaxial cavity for TM_{211} mode……66

Figure 4.60 E-field and H-field of coaxial cavity for TM_{211} mode……..67

Figure 4.61 Field vectors of 180° sectoral cavity for TM_{212} mode……..……..……67

Figure 4.62 E-Field and H-Field of 180° sectoral cavity for TM_{212} mode……...……68

Figure 4.63 Field vectors of 120° sectoral cavity for TM_{121} mode……..……68

Figure 4.64 E-Field and H-Field of 120° sectoral cavity for TM_{121} mode……..……....69

Figure 4.65 Field vectors of baffle cavity for TM_{122} mode……..70

Figure 4.66 E-Field and H-Field of baffle-coaxial cavity for TM_{122} mode……..71

Figure 4.67 Field vectors of 45° sectoral-coaxial cavity for TM_{211} mode……..….71

Figure 4.68 E-Field and H-Field of sectoral-coaxial cavity for TM_{211} mode……..72

Figure 4.69 Field vectors of baffle-coaxial cavity for TE_{212} mode……73

Figure 4.70 E-Field and H-Field of baffle-coaxial cavity for TE_{212} mode……..74

ACKNOWLEDGEMENTS

As a novice in the programming, this thesis has been the hardest and most fruitful project I have ever done. Now, I found myself much more confident to work in software designing and enjoying working on this platform. I would like to thank a large number of people and dedicate this work to them. Without them, this project would have been much more complicated and perhaps not even possible.

First of all, I would like to thank my advisor Dr. Atef Elsherbeni, for the countless hours that he spent with me verifying my work, providing meaningful suggestions based on his extensive experience, and also for teaching me everything I know about EM field theory, simulation and coding for MATLAB. He is truly a caring advisor and mentor and I have been lucky to work with him these past few months.

I want to also thank Dr. Peter Aaen, Martha Sanchez-Hayre, Yiming Chen, Robert Jones, and but most importantly Andres Velasco, the previous graduate student of ARC research group who helped me to use MATLAB App Designer platform and Dr. Mona ElHelbawy who helped me in carefully reviewing and editing the thesis with me. Andres Velasco provided me with all necessary study materials and online resources to make me feel confident to work in App Designer. Dr. Peter Aaen and Martha made all arrangement to support me financially throughout this thesis. Yiming and Robert helped me to find coding issues. You all have had an impact in how I have performed in this project, and I want to thank you all.

To my parents, Matin and Rabeya, my love and my friend, Shanta, and my sister Jenny

CHAPTER 1

INTRODUCTION

In many microwave applications, electromagnetic waves need to be guided from one location to another using waveguides and cavity resonators. A waveguide is a hollow conductive metal pipe used to carry high-frequency radio waves, particularly microwaves. Rectangular cross-sections are the simplest and most commonly used waveguides. Circular metallic tubes are appropriate for applications such as radars. Coaxial waveguides are well suited for long-distance transmission because the central conductor is shielded from external electrical noise by the outer conducting material. On the other hand, cavity resonators consist of a closed metal structure that confines electromagnetic waves in the microwave region. These electromagnetic waves bounce back and forth between the walls of the cavity. Understanding the electromagnetic wave distribution inside waveguide and cavity resonators helps microwave engineers in the design manufacturing, testing and installation of electronic components in systems used to transmit and receive microwave signals.

1.1 Motivation and Background

The history of the development of waveguides is more than 100 years old. It was first discovered by George C. Southworth who played an important role in radar system design [1]. An electromagnetic field cannot be seen directly [17], only its effects can be observed. Nowadays, technology is growing faster, and millimeter and sub-millimeter waves applications require a combination of active and passive devices. Usually, waveguide-based transmission lines are preferred in the design of low-loss filters, hybrid couplers, power dividers, antennas,

etc. [2]. These applications require microwave devices to operate at higher frequencies (above 100 GHz). For operating at this frequency bands, waveguide feature size needs to be smaller and tolerance requirements need to be tightened. In medical applications, there is a growing need for wireless sensing systems [16]. Passive wireless sensors such as those used in harsh environmental conditions are generally composed of resonant circuits [3]. Cavity resonators are the most commonly used component in passive wireless sensors. For cavity resonators, EM waves bounce back and forth between the cavity walls which produce field oscillations. Evanescent-mode cavity resonators inherently fulfill the need for high frequency passive wireless sensor applications because the size can be greatly reduced. But, with the growing demand for high speed, smaller size devices that consume less power, conventional manufacturing is becoming more and more challenging every day [4]. To the demands for small size and low-power consumption, microwave engineers must fully understand electromagnetic wave propagation inside waveguides and cavity resonators.

1.2 The Need for Software

WGC (version 2.1) was developed by Dr. Atef Elsherbeni and Dr. Clayborne Taylor, Jr. in 1994 to compute and visualize EM field distribution inside waveguides and cavity resonators using an interactive BASIC language for a personal computer running DOS operating system [5]. The executable code of the software was available for the IBM-PC computer family, but it is no longer useable due to recent changes and advancements in computing technology and operating systems. Several software packages for designing and simulating microwave devices and transmission lines, such as Ansys HFSS, CST, and ADS are being used nowadays. For example, the design and simulation of a coplanar and air-gap waveguide transmission line using ADS has been introduced in [6, 7]. CST Studio Suite has been used for similar design problem [8, 9, 10]

and similarly HFSS as in [11, 12, 13]. These software packages are not only expensive, but they also require substantial memory and computational resources to compute and visualize field components inside such configurations of waveguides and cavities. Other software packages like COCAFIL [14] and XFdtd [15] are available, but they require substantial memory and computational resources. A web application to visualize the field pattern inside waveguide has been recently introduced in [26], but it is limited to waveguides with rectangular and circular cross-sections. The software package introduced in this thesis aims to overcome those challenges. WGC (version 3) allows users to visualize the electric and magnetic field distribution inside several types of waveguides and cavity resonators (rectangular, circular, coaxial, baffle, sectoral, sectoral-coaxial, and baffle-coaxial) almost instantaneously on current PC platform. Advantages of using this software include the ability to model a wide variety of waveguide and cavity resonators, less memory requirements and computation time. WGC (version 3) features a user-friendly interface that makes easy for users to quickly model, compute and generate figures and video animations of the EM field distribution within their design structure to assess the performance of their design.

WGC (version 3) allows user to observe the change of electric and magnetic fields distribution for different dimensions of the physical or electrical parameters of the cross-sections at different plane cuts. Also, users do not need to limit their interest in any specific mode of operation or order. They have a lot of flexibility in choosing among shapes, dimensions, mode numbers, plane views (x-y, x-z and y-z). Moreover, this software is capable of generating video animations of field distribution as the view angle and position changes. The code is executable on all modern computer families with installed MATLAB version 2021a and later versions. No internet connectivity is needed to run this software.

1.3 Thesis Organization and Overview

This Thesis work is divided into five chapters.

- Chapter 1 provides the motivation and background information and highlights the significance of this work.
- Chapter 2 presents the theoretical foundation and mathematical formulations used to compute and visualize EM fields inside various waveguides and cavity resonator types.
- Chapter 3 provides software design details and describes the graphical user interface.
- Chapter 4 presents examples of different waveguide and cavity resonator models and simulations results.
- Chapter 5 summarizes the research and development of WGC and introduces future directions for research.

CHAPTER 2

MATHEMATICAL DERIVATION OF FIELD EQUATIONS

The objective of this chapter is to introduce the field equations for different configurations of waveguide and cavity resonators used in WGC (version 3). The mathematical expressions of the field components are derived from the classical solution of the wave equation using the separation of variables technique.

2.1 Waveguide and Cavity

Waveguides and cavity resonators play an important role in microwave applications [18]. Waveguides have definite boundaries which direct the propagation of electromagnetic waves and prevent them from scattering outside the guide. On the other hand, cavity resonators can be considered short-circuited transmission lines and are constructed by short-circuiting the waveguides. The boundary walls of waveguides and cavity resonators are highly conductive materials and, thus, the electromagnetic energy is confined [19]. The modes of wave propagation in the waveguides and cavity resonators can be classified into two types: transverse electric (TE) mode and transverse magnetic (TM) mode.

2.2 General Equations Derivation

General equations of the propagating field components inside waveguides and cavity resonators are presented in this section. Seven different cross-sections are considered. These are rectangular, circular, sectoral, baffle, coaxial, sectoral coaxial, and baffle coaxial (see Figure 2.1). The electromagnetic wave is propagating along the z-axis and the boundary walls are

assumed to be perfectly conductive. The medium inside the waveguides and the cavity resonators are filled with homogeneous, isotropic, and lossless material with permeability denoted by μ and permittivity denoted by ϵ. The field equations for TE and TM modes are obtained after solving the Helmholtz wave equation inside the guide using the separation of variables technique. For rectangular geometry, the Cartesian coordinates system is considered and for the circular, sectoral, baffle, coax, sectoral coax, and baffle coax, the cylindrical coordinates system is used [20].

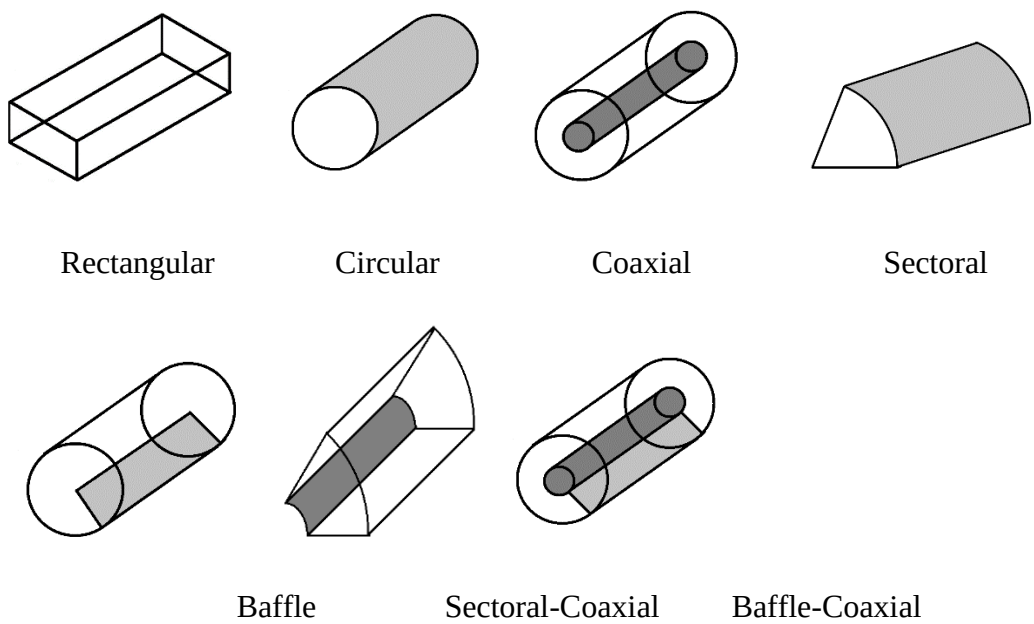

Figure 2.1: Different cross-sections of waveguides and cavity resonators.

2.2.1 Rectangular Cross-Section

Rectangular waveguides are one of the earliest types of transmission lines which are commonly used for the transport of radio frequency signals at frequencies in the SHF band (3–30 GHz) and higher [21]. On the other hand, rectangular cavity has been commonly used in

Electron Paramagnetic Resonance (EPR), Nuclear Magnetic Resonance (NMR), and Magnetic Resonance Imaging (MRI) experiments, [22]. The fields in a rectangular waveguide and cavity resonator consist of several propagating modes which depend on the electrical dimensions, the type, and the position of excitation. Assuming the inner dimensions of the rectangular waveguide are a and b and d along the x, y, and -z axes as shown in Figure 2.2. A rectangular waveguide supports TM or TE mode but not TEM mode because a hollow rectangular waveguide does not have any inner conductor. TEM mode is characterized by electric fields and magnetic fields perpendicular to each other and perpendicular to the direction of propagation. If a TEM mode exists inside a waveguide, it must have at least two conductors so that the electric fields can have a start and an end. For a hollow waveguide, there is no inner conductor, hence electric fields create loops and that is why TEM mode is not an option in this configuration.

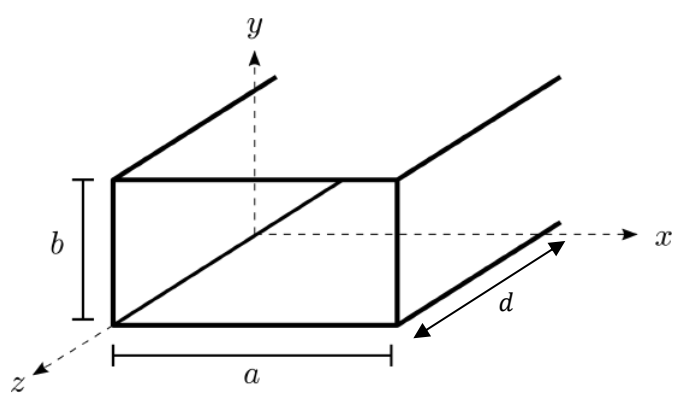

Figure 2.2: Rectangular cross-section of a waveguide or cavity.

For TE_z modes in rectangular cross-section of a waveguide or a cavity, the field equations are given by:

$$E_x(x,y,z,t) = \frac{\beta_y}{\epsilon} cos(\beta_x x)\, sin(\beta_y y) \begin{cases} A_{mn}\cos(\omega t - \beta_z z) \\ A_{mnl} cos(\omega t)\, sin(\beta_z z) \end{cases} \tag{2.1}$$

$$E_y(x,y,z,t) = \frac{\beta_x}{\epsilon} sin(\beta_x x)\, cos(\beta_y y) \begin{cases} A_{mn}\cos(\omega t - \beta_z z) \\ A_{mnl} cos(\omega t)\, sin(\beta_z z) \end{cases} \tag{2.2}$$

$$E_z(x,y,z,t) = 0 \tag{2.3}$$

$$H_x(x,y,z,t) = \frac{\beta_x \beta_z}{\omega\mu\epsilon} sin(\beta_x x)\, cos(\beta_y y) \begin{cases} A_{mn}\cos(\omega t - \beta_z z) \\ A_{mnl} sin(\omega t) cos(\beta_z z) \end{cases} \tag{2.4}$$

$$H_y(x,y,z,t) = \frac{\beta_y \beta_z}{\omega\mu\epsilon} cos(\beta_x x)\, sin(\beta_y y) \begin{cases} A_{mn}\cos(\omega t - \beta_z z) \\ A_{mnl} sin(\omega t) cos(\beta_z z) \end{cases} \tag{2.5}$$

$$H_z(x,y,z,t) = \frac{{\beta_c}^2}{\omega\mu\epsilon} cos(\beta_x x)\, cos(\beta_y y) \begin{cases} A_{mn}\sin(\omega t - \beta_z z) \\ A_{mnl} sin(\omega t) sin(\beta_z z) \end{cases} \tag{2.6}$$

For TM_z modes the corresponding field equations can be written as

$$E_x(x,y,z,t) = -\frac{\beta_x \beta_z}{\omega\mu\epsilon} cos(\beta_x x)\, sin(\beta_y y) \begin{cases} B_{mn}\cos(\omega t - \beta_z z) \\ B_{mnl} sin(\omega t) cos(\beta_z z) \end{cases} \tag{2.7}$$

$$E_y(x,y,z,t) = -\frac{\beta_y \beta_z}{\omega\mu\epsilon} sin(\beta_x x)\, cos(\beta_y y) \begin{cases} B_{mn}\cos(\omega t - \beta_z z) \\ B_{mnl} sin(\omega t) sin(\beta_z z) \end{cases} \tag{2.8}$$

$$E_z(x,y,z,t) = \frac{{\beta_c}^2}{\omega\mu\epsilon} sin(\beta_x x)\, sin(\beta_y y) \begin{cases} B_{mn}\sin(\omega t - \beta_z z) \\ B_{mnl} sin(\omega t) cos(\beta_z z) \end{cases} \tag{2.9}$$

$$H_x(x,y,z,t) = \frac{\beta_y}{\mu} sin(\beta_x x)\, cos(\beta_y y) \begin{cases} B_{mn}\cos(\omega t - \beta_z z) \\ B_{mnl} cos(\omega t) cos(\beta_z z) \end{cases} \tag{2.10}$$

$$H_y(x,y,z,t) = -\frac{\beta_x}{\mu} cos(\beta_x x)\, sin(\beta_y y) \begin{cases} B_{mn}\cos(\omega t - \beta_z z) \\ B_{mnl} cos(\omega t) cos(\beta_z z) \end{cases} \tag{2.11}$$

$$H_z(x,y,z,t) = 0 \tag{2.12}$$

Here,

$$\beta_z = \begin{cases} \sqrt{\beta^2 - {\beta_c}^2}; & \text{for waveguides} \\ \dfrac{\pi l}{d}; & \text{for cavity resonators} \end{cases} \tag{2.13}$$

$$\beta = \omega\sqrt{\mu\epsilon}; \quad \beta_c = \sqrt{{\beta_x}^2 + {\beta_y}^2} \tag{2.14}$$

where μ and ϵ are the permeability and the permittivity of vacuum, respectively.

$$\mu = 4\pi \times 10^{-7} \text{ H/m}; \epsilon = 8.854 \times 10^{-12}\text{F/m}$$

$$\beta_x = \frac{m\pi}{a}; \quad \beta_y = \frac{n\pi}{b} \tag{2.15}$$

In most of the equations there are two entries. The top part is for waveguides and the bottom one is for cavity resonators. The variables a, b, d in these equations are the dimensions along x, y and $-z$ axes, respectively. The values of m and n starts from 0 but cannot be equal to 0 at the same time for TE modes. For TM modes the values of m and $n = 1, 2, 3, \ldots$ The constants A_{mn} and B_{mn} are the amplitudes of the mode designated by the integers m and n. And for the cavity resonator subscript $l = 0, 1, 2, 3, \ldots$ for TM modes and $l = 1, 2, 3, 4, \ldots$ for TE modes. Like waveguides the constants A_{mnl} and B_{mnl} are the amplitude of the mode designated by integers m, n and l. The value of m, n and l is the half-period variation of the field components along x, y and z axis, respectively. The cut-off frequency, f_c of a rectangular waveguide is calculated as $f_c = \frac{\beta_c}{2\pi\sqrt{\mu\epsilon}}$ and for the rectangular cavity, the resonant frequency is given by $f_r = \frac{\beta_r}{2\pi\sqrt{\mu\epsilon}}$; where

$$\beta_r = \sqrt{{\beta_x}^2 + {\beta_y}^2 + {\beta_z}^2} \tag{2.16}$$

2.2.2 Circular and Coaxial Cross-Section

For the cross-section of circular waveguide and cavity, the radius is denoted by a and for the coaxial cross-section, a is the inner radius and b is the outer radius. The parameter d is the dimension along the propagation of waves as shown in Figure 2.3.

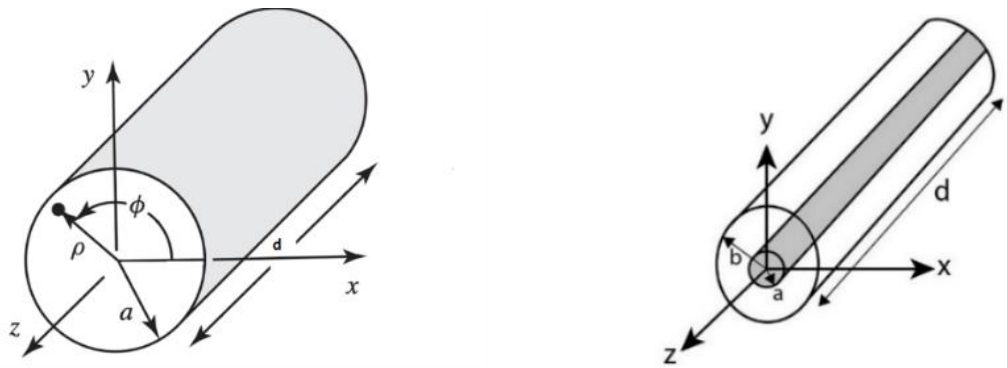

(a) (b)

Figure 2.3: Cross-section of a waveguide and cavity, circular (a) and coaxial (b).

The field components for TE_z modes can be written as

$$E_\rho(\rho,\phi,z,t) = \frac{m}{\varepsilon\rho} g_m(\beta_\rho\rho)\sin(m\phi)\begin{cases} A_{mn}\cos(\omega t - \beta_z z) \\ A_{mnl}\cos(\omega t)\, sin(\beta_z z) \end{cases} \tag{2.17}$$

$$E_\phi(\rho,\phi,z,t) = \frac{\beta_\rho}{\varepsilon} g'_m(\beta_\rho\rho)\cos(m\phi)\begin{cases} A_{mn}\cos(\omega t - \beta_z z) \\ A_{mnl}\cos(\omega t)\, sin(\beta_z z) \end{cases} \tag{2.18}$$

$$E_z(\rho,\phi,z,t) = 0 \tag{2.19}$$

$$H_\rho(\rho,\phi,z,t) = -\frac{\beta_\rho\beta_z}{\varepsilon} g'_m(\beta_\rho\rho)\cos(m\phi)\begin{cases} A_{mn}\cos(\omega t - \beta_z z) \\ A_{mnl} sin(\omega t)\, cos(\beta_z z) \end{cases} \tag{2.20}$$

$$H_\phi(\rho,\phi,z,t) = \frac{m\beta_z}{\omega\mu\varepsilon\rho} g_m(\beta_\rho\rho)\sin(m\phi)\begin{cases} A_{mn}\cos(\omega t - \beta_z z) \\ A_{mnl} sin(\omega t)\, cos(\beta_z z) \end{cases} \tag{2.21}$$

$$H_z(\rho,\phi,z,t) = \frac{1}{\omega\mu\varepsilon} g_m(\beta_\rho \rho)\cos(m\phi)\begin{cases} A_{mn}(\beta_\rho)^2 \sin(\omega t - \beta_z z) \\ A_{mnl}(\beta^2 - {\beta_z}^2) sin(\omega t)\ sin(\beta_z z) \end{cases} \tag{2.22}$$

And for the TM_z modes, the corresponding field components are

$$E_\rho(\rho,\phi,z,t) = -\frac{\beta_\rho \beta_z}{\varepsilon\omega\mu} g'_m(\beta_\rho \rho)\cos(m\phi)\begin{cases} B_{mn}\cos(\omega t - \beta_z z) \\ B_{mnl} sin(\omega t)\ sin(\beta_z z) \end{cases} \tag{2.23}$$

$$E_\phi(\rho,\phi,z,t) = \frac{m\beta_z}{\omega\mu\varepsilon\rho} g_m(\beta_\rho \rho)\sin(m\phi)\begin{cases} B_{mn}\cos(\omega t - \beta_z z) \\ B_{mnl} sin(\omega t)\ sin(\beta_z z) \end{cases} \tag{2.24}$$

$$E_z(\rho,\phi,z,t) = \frac{(\beta_\rho)^2}{\omega\mu\varepsilon} g_m(\beta_\rho \rho)\cos(m\phi)\begin{cases} B_{mn}\sin(\omega t - \beta_z z) \\ B_{mnl} sin(\omega t)\ cos(\beta_z z) \end{cases} \tag{2.25}$$

$$H_\rho(\rho,\phi,z,t) = -\frac{m}{\mu\rho} g_m(\beta_\rho \rho)\sin(m\phi)\begin{cases} B_{mn}\cos(\omega t - \beta_z z) \\ B_{mnl} cos(\omega t)\ cos(\beta_z z) \end{cases} \tag{2.26}$$

$$H_\phi(\rho,\phi,z,t) = -\frac{\beta_\rho}{\mu} g'_m(\beta_\rho \rho)\cos(m\phi)\begin{cases} B_{mn}\cos(\omega t - \beta_z z) \\ B_{mnl} cos(\omega t)\ cos(\beta_z z) \end{cases} \tag{2.27}$$

$$H_z(\rho,\phi,z,t) = 0 \tag{2.28}$$

where

$$\beta_\rho = \begin{cases} \frac{X'_{mn}}{a}; & \text{for TE modes} \\ \frac{X_{mn}}{a}; & \text{for TM modes} \end{cases} \tag{2.29}$$

$$\beta_z = \begin{cases} \sqrt{\beta^2 - {\beta_\rho}^2}; & \text{for waveguides} \\ \frac{\pi l}{d}; & \text{for cavity resonators} \end{cases} \tag{2.30}$$

In the above equations the prime indicates the derivative of the function with respect to its full argument. Here the function

$$g_m(\beta_\rho \rho) = \begin{cases} J_m(\beta_\rho \rho); & \text{for TE and TM circular cross} - \text{sections} \\ Y_m(\beta_\rho \rho) - J_m(\beta_\rho \rho)\dfrac{Y_m(\beta_\rho b)}{J_m(\beta_\rho b)}; & \text{for TM coaxial cross} - \text{sections} \\ Y_m(\beta_\rho \rho) - J_m(\beta_\rho \rho)\dfrac{Y'_m(\beta_\rho b)}{J'_m(\beta_\rho b)}; & \text{for TE coaxial cross} - \text{sections} \end{cases} \tag{2.31}$$

In equation (2.31) J_m indicates the Bessel function of first kind and Y_m indicates the Bessel function of second kind. X_{mn} and X'_{mn} in equation (2.29) are the zeros of $g_m(\beta_\rho \rho)$ and $g'_m(\beta_\rho \rho)$, respectively. The $\frac{Y_m(\beta_\rho b)}{J_m(\beta_\rho b)}$ and $\frac{Y'_m(\beta_\rho b)}{J'_m(\beta_\rho b)}$ are the constant for TM and TE coaxial cross-sections, respectively. The derivative of equation (2.31) can be written as

$$g'_m(\beta_\rho \rho) = \begin{cases} J'_m(\beta_\rho \rho); & \text{for TE and TM circular cross} - \text{sections} \\ Y'_m(\beta_\rho \rho) - J'_m(\beta_\rho \rho)\dfrac{Y_m(\beta_\rho b)}{J_m(\beta_\rho b)}; & \text{for TM coaxial cross} - \text{sections} \\ Y'_m(\beta_\rho \rho) - J'_m(\beta_\rho \rho)\dfrac{Y'_m(\beta_\rho b)}{J'_m(\beta_\rho b)}; & \text{for TE coaxial cross} - \text{sections} \end{cases} \tag{2.32}$$

where from [28],

$$J'_m(\beta_\rho \rho) = -J_{m+1}(\beta_\rho \rho) + \frac{m}{\beta_\rho \rho} J_m(\beta_\rho \rho) \tag{2.33}$$

and $Y'_m(\beta_\rho \rho)$ can be obtained in the same way as $J'_m(\beta_\rho \rho)$ shown in equation (2.33).

To find the zeros of equations (2.31) and (2.32), one needs to find the zeroes of the Bessel function. The approximation of the first three roots of any order Bessel function were generated using a least-squares fit of the roots. The approximation is used to start the iteration of Halley's method. Details about finding zeros of Bessel function is documented in Appendix A1.

For both TE and TM mode in circular and coaxial cross-section of waveguide subscript $m = 0, 1, 2, 3, \ldots$ and subscript $n = 1, 2, 3, 4, \ldots$ For cavity, l is defined by $l = 1, 2, 3, \ldots$ for TE modes

and $l = 0, 1, 2, 3, ...$ for TM modes. The cut-off frequency of a waveguide is denoted by f_c and the resonant frequency of a cavity is denoted by f_r. f_c is calculated as

$$(f_c)_{mn} = \frac{\beta_\rho}{2\pi\sqrt{\mu\epsilon}} \tag{2.34}$$

and the resonant frequency, f_r is given by

$$(f_r)_{mn} = \frac{\sqrt{{\beta_\rho}^2 + {\beta_z}^2}}{2\pi\sqrt{\mu\epsilon}} \tag{2.35}$$

2.2.3 Sectoral and Sectoral-Coaxial Cross-Section

The field expressions for sectoral and sectoral-coaxial cross-section are similar to the field equations presented in section 2.2.2. The geometry of sectoral and sectoral-coaxial cross-section are shown in Figure 2.4. The only difference is the value of m. For sectoral and sectoral-coaxial cross-section subscript m is a rational number and it is written by

$$m = \frac{p\pi}{\phi_0} \tag{2.36}$$

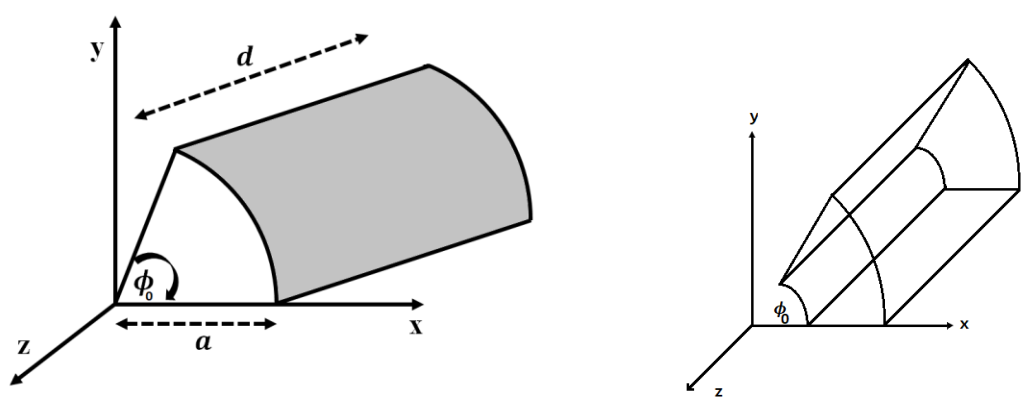

Figure 2.4: Sectoral and sectoral-coaxial cross-section of a waveguide and cavity.

Here, p is an integer whose value is defined as $p = 0, 1, 2, 3, \ldots$ for TE modes and $p = 1, 2, 3, \ldots$ for TM modes and ϕ_0 is the sectoral angle. The interpretation of p is similar to the integer m for circular and coaxial cross-section. Besides, to satisfy the boundary conditions at $\phi_0 = 0$ degree only in the TM_z mode field expressions, $\cos(m\phi)$ should be replaced by $\sin(m\phi)$ and the term $\sin(m\phi)$should be replaced by the $-\cos(m\phi)$. The TM_z mode field equations are given here for better understanding.

$$E_\rho(\rho, \phi, z, t) = -\frac{\beta_\rho \beta_z}{\varepsilon\omega\mu} g'_m(\beta_\rho \rho) \sin(m\phi) \begin{cases} B_{mn}\cos(\omega t - \beta_z z) \\ B_{mnl} sin(\omega t)\ sin(\beta_z z) \end{cases} \tag{2.37}$$

$$E_\phi(\rho, \phi, z, t) = -\frac{m\beta_z}{\omega\mu\varepsilon\rho} g_m(\beta_\rho \rho) \cos(m\phi) \begin{cases} B_{mn}\cos(\omega t - \beta_z z) \\ B_{mnl} sin(\omega t)\ sin(\beta_z z) \end{cases} \tag{2.38}$$

$$E_z(\rho, \phi, z, t) = \frac{(\beta_\rho)^2}{\omega\mu\varepsilon} g_m(\beta_\rho \rho) \sin(m\phi) \begin{cases} B_{mn}\sin(\omega t - \beta_z z) \\ B_{mnl} sin(\omega t)\ cos(\beta_z z) \end{cases} \tag{2.39}$$

$$H_\rho(\rho, \phi, z, t) = \frac{m}{\mu\rho} g_m(\beta_\rho \rho) \cos(m\phi) \begin{cases} B_{mn}\cos(\omega t - \beta_z z) \\ B_{mnl} cos(\omega t)\ cos(\beta_z z) \end{cases} \tag{2.40}$$

$$H_\phi(\rho, \phi, z, t) = -\frac{\beta_\rho}{\mu} g'_m(\beta_\rho \rho) \sin(m\phi) \begin{cases} B_{mn}\cos(\omega t - \beta_z z) \\ B_{mnl} cos(\omega t)\ cos(\beta_z z) \end{cases} \tag{2.41}$$

$$H_z(\rho, \phi, z, t) = 0 \tag{2.42}$$

The field components for TE_z modes can be written as

$$E_\rho(\rho, \phi, z, t) = \frac{m}{\varepsilon\rho} g_m(\beta_\rho \rho) \sin(m\phi) \begin{cases} A_{mn}\cos(\omega t - \beta_z z) \\ A_{mnl}\cos(\omega t)\ sin(\beta_z z) \end{cases} \tag{2.43}$$

$$E_\phi(\rho, \phi, z, t) = \frac{\beta_\rho}{\varepsilon} g'_m(\beta_\rho \rho) \cos(m\phi) \begin{cases} A_{mn}\cos(\omega t - \beta_z z) \\ A_{mnl}\cos(\omega t)\ sin(\beta_z z) \end{cases} \tag{2.44}$$

$$E_z(\rho, \phi, z, t) = 0 \tag{2.45}$$

$$H_\rho(\rho,\phi,z,t) = -\frac{\beta_\rho\beta_z}{\varepsilon} g'_m(\beta_\rho\rho)\cos(m\phi)\begin{cases} A_{mn}\cos(\omega t-\beta_z z) \\ A_{mnl} sin(\omega t)\ cos(\beta_z z)\end{cases} \tag{2.46}$$

$$H_\phi(\rho,\phi,z,t) = \frac{m\beta_z}{\omega\mu\varepsilon\rho} g_m(\beta_\rho\rho)\sin(m\phi)\begin{cases} A_{mn}\cos(\omega t-\beta_z z) \\ A_{mnl} sin(\omega t)\ cos(\beta_z z)\end{cases} \tag{2.47}$$

$$H_z(\rho,\phi,z,t) = \frac{1}{\omega\mu\varepsilon} g_m(\beta_\rho\rho)\cos(m\phi)\begin{cases} A_{mn}(\beta_\rho)^2\sin(\omega t-\beta_z z) \\ A_{mnl}(\beta^2-{\beta_z}^2) sin(\omega t)\ sin(\beta_z z)\end{cases} \tag{2.48}$$

2.2.4 Baffle and Baffle-Coaxial Cross-Section

To enhance the directivity of EM fields a conducting plate is places inside the hollow waveguides and cavity resonators (see Figure 2.5) and these configurations field equations are similar to the section 2.2.3 except for the value of ϕ_0. For baffle and baffle-coaxial waveguides and cavity resonators $\phi_0 = 2\pi$.

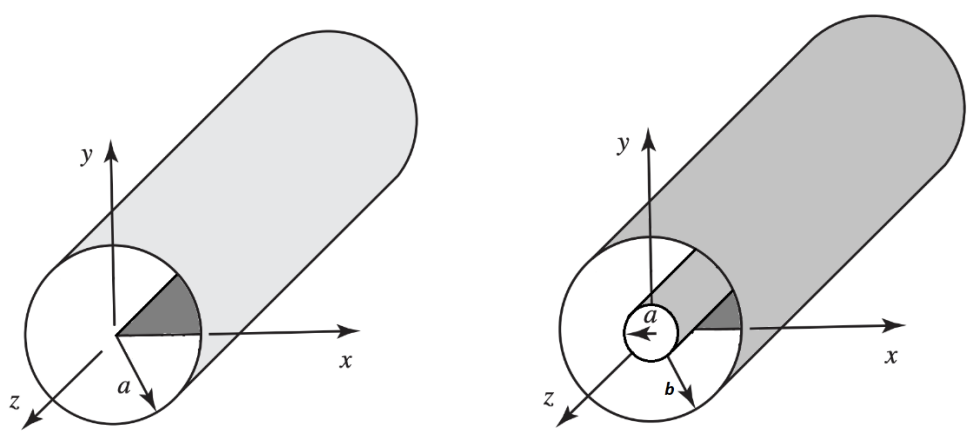

Figure 2.5: Circular baffle and baffle-coaxial waveguide and cavity resonator.

CHAPTER 3

SOFTWARE DESIGN

This chapter provides the design configuration of the software which will visually represent the electric and magnetic field distribution inside waveguides and cavity resonators for different modes of operation. The full software package is designed in the MATLAB App designer platform. First, field equations in this document have been verified with existing figures documented in [24, 25]. Then in MATLAB App designer, two windows are created to access the cross-sections of different waveguides and cavity resonators and later seven different windows are designed for seven different configurations of waveguides and cavity resonators.

3.1 MATLAB App Designer Platform

App designer helps to design professional apps. Simple drag and drop visual components in the app designer window help to layout the design of the graphical user interface (GUI) and use the integrated editor to quickly program its behavior. App designer has two view options, one is design view and another one is code view. In the design view window, one can easily layout the visual components from the component library. Each component has callback options that allow commanding individual components separately. Callback functions allow working in the code view window. Also, the code view window has property, functions, and app input arguments options which give the freedom to work in multiple app window settings. App Designer can automatically check for coding problems using the Code Analyzer. Standalone applications can be created by using MATLAB Compiler and Simulink Compiler to share them royalty-free with other users [23].

3.2 Graphical User Interface Development

Our software has nine different windows. The front window is called the main menu which will guide users to the next option menu. There a user can select which cross-section of waveguide and cavity they want to select. After that, the user will be able to draw figures or create a movie for a different mode of operations in waveguide and cavity.

3.2.1 WGC flowchart of the Software

This software works in a sequential way. When a user puts all the information correctly, then this software will create a figure or video of the electromagnetic field inside the waveguide or cavity for different modes of operation. If the user fails to put the right information, then the software will give warnings and tell the user what needs to be done. The flowchart of this software is given below.

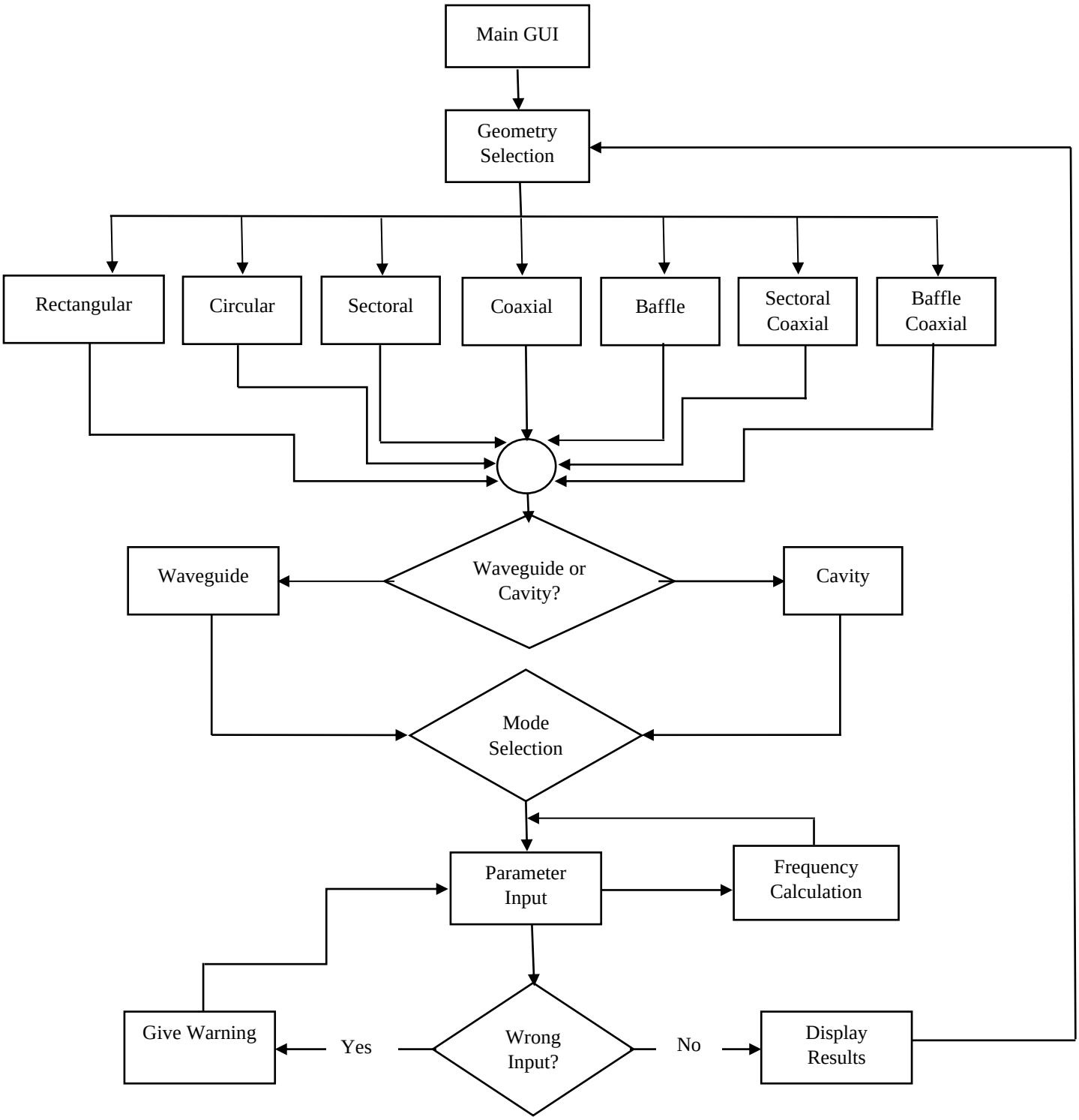

Figure 3.1: WGC (version 3) flow chart.

3.3 Layout and Operation of the Software

The layout of the software is mainly categorized into four main windows. Those are Main Window, Geometry Selection, and Parameters Screen and Output Screen (Figure Creation and Video Creation). Each of them is described below.

3.3.1 Main Window

The window that will appear when a user runs the software is called the main window. In this window at the top of the left corner, there is a button called help. If the user selects this button, he/she will find two options there. One is about the app and the other will help the user find the contact details of the authors. In the main window, there is a big button called "Get Started". When the user presses that button it will lead him/her to the next window. The figures that are shown in Figure 3.2 are originally in Gif format and those are generated by using this software. The main window is shown here as a figure (see Figure 3.2).

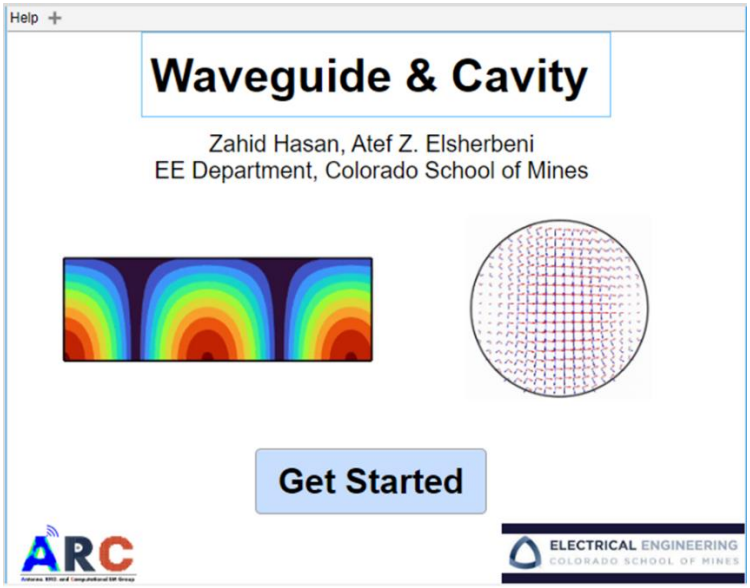

Figure 3.2: Main window of the software.

3.3.2 Geometry Selection

In the geometry selection (Options Menu) window, there are seven different cross-sections are included. Those are rectangular, circular, sectoral, baffle, coaxial, sectoral-coaxial, baffle-coaxial cross-sections. For better understanding, each of the cross-sections has been shown in the figure format. When the user clicks the button beside those pictures, the next window will open, and this geometry selection window will close automatically. The geometry selection window is shown in Figure 3.3.

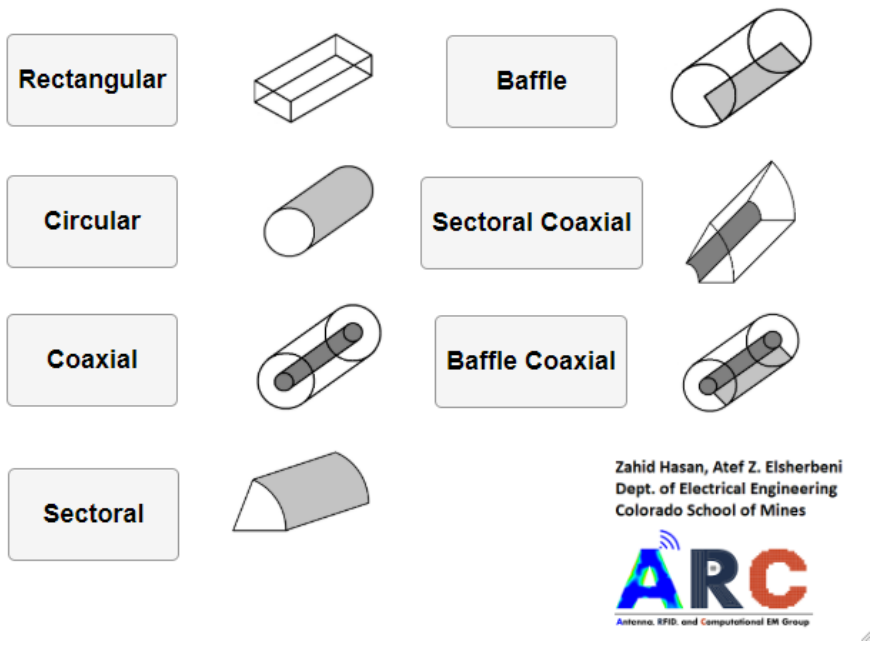

Figure 3.3: Geometry selection (Option Menu) window of the software.

3.3.3 Parameters Screen

The parameters screen window is different for different geometry selections. Each of them has a common waveguide or cavity selection button, mode choice option, input for waveguide and cavity dimensions, operation frequency, and plane cut option. Also, there are cut-off,

resonant frequency calculator option which depends on the dimensions of the cross-sections of waveguides and cavity resonators. The waveguide and cavity selection button will enable or disable some options (which are not needed) in the parameter screens. In the waveguide and cavity dimension box, three different units (cm, mm, and inch) are added in the drop-down menu. There is also an input for the number of points along the x, y, and z-axis. It will give the users the flexibility to see the propagation of electromagnetic waves as to how they want to see them. In the bottom of the left corner, there are two options for figure creation and video creation. Users can save their works as a picture as well as a video. In the figure creation and video creation buttons, there are 5 different options in the drop-down menu. These are vector plot, E-field strength, H-field strength, E-field strength with vector, and H-field strength with vector. At the end of the right corner of the window there are three buttons called “Check”, “Run”, and “Return” buttons. The “Check” button checks all the input parameters. If there is an error in the input parameters, this “Check” button will show users warning messages. Also, if the user puts some wrong inputs while trying to find the cut-off and resonance frequency for waveguides and cavity resonators, this “calculate” button will also show some warning messages. Initially, the “Run” button is kept deactivated so that users can easily understand the mistakes if they do any by pressing the “Check” button. If there is no error, the “Run” button will be activated and the user will be able to see the picture or the video according to his/her options selection. Right below the Create figure and Video box, there is a text area where the user can see the message about the current figure or video creation. The “Return” button will get the user back to the geometry selection window to work further with the app. The parameters screen for rectangular cross-section is shown in Figure 3.4.

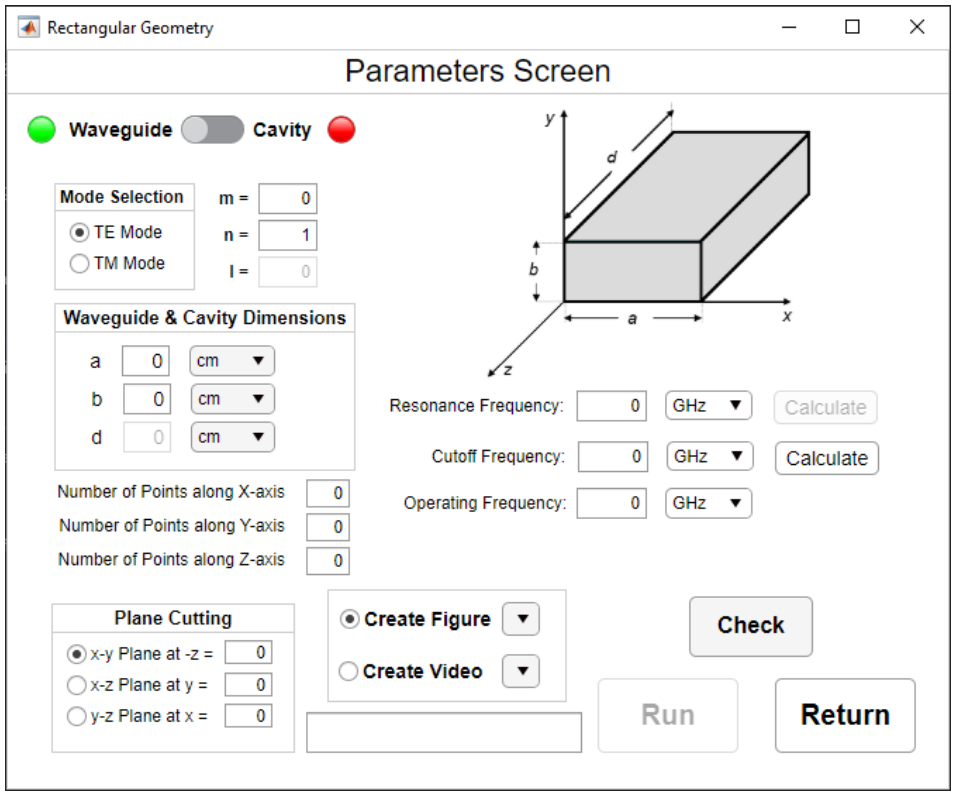

Figure 3.4: Parameters screen window for rectangular waveguide and cavity.

3.3.4 Figures of EM Fields

When the user selects the “Create Figure” button, initially, it is selected for the vector plot. But the user can change the view option by pressing the drop-down menu just beside the button. After creating one figure the user does not need to exit the figure window to see another configuration of input parameters. This will help the user to compare figures by placing them side by side. And after that, the user can save those images in whichever directory they want to select.

3.3.5 Video Animations of EM Fields

The video creation option is pretty much similar to the figure creation option. For creating a video, more time is needed than figure creation. So, at that time a progress bar and successful bar

are included so that the user can understand that the video is being created, and it will take some time. When the video creation is completed, a success message will appear and telling the user that the movie creation is successful. In the next chapter, all of these processes and how the software is working will be described.

3.3.6 Programming and Special Functions

Before implementing the code in the App Designer platform, code for all cross-sections has been written as MATLAB script. Figures are validated against values found in the literature for similar types of problems, and results show perfect agreement with each other. Field equations in previous chapters have been used to create figures and video animations of all configurations. Code for the rectangular geometry is straight forward and no special functions are needed. But for the circular and all other cross-sections, a special function is used to generate the zeros of the Bessel function. The function is called “besselzeros.m” for circular, sectoral and baffle cross-sections and “gmzeros.m” for coaxial, sectoral-coaxial, and baffle-coaxial cross-sections. The procedure for computing the Bessel function is described in Appendix A.

CHAPTER 4

ILLUSTRATED EXAMPLES

This chapter provides illustrated examples of software functionality. For both waveguide and cavity resonators, the cross-sections can be grouped into two categories: rectangular, and circular. Sectoral cross-sections of 90°, 180°, and 270° are part of full circular cross-sections, coaxial cross-sections have a conducting core inside the circular cross-sections. For the baffle configuration, a conducting plate is placed inside the circular cross-section.

4.1 Waveguide

Each of the parameters screens has the option to switch between waveguide and cavity. The default position of the switch is for waveguide. When a user slides the switch to cavity, the red light next to it turns green and the green light next to the waveguide turns red. When the user changes the switch position back to waveguide, the light color will change again. This way, a user receives feedback from the software confirming which of the two configurations is active. Figure 4.1 shows light color is changes as the switch moves from waveguide to cavity.

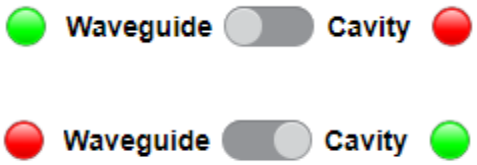

Figure 4.1: Light color change with switch position.

4.1.1 Rectangular Waveguide

Step by step operation of the software for the rectangular waveguide is shown below.

Step 1: Click “Get Started” button in the main window.

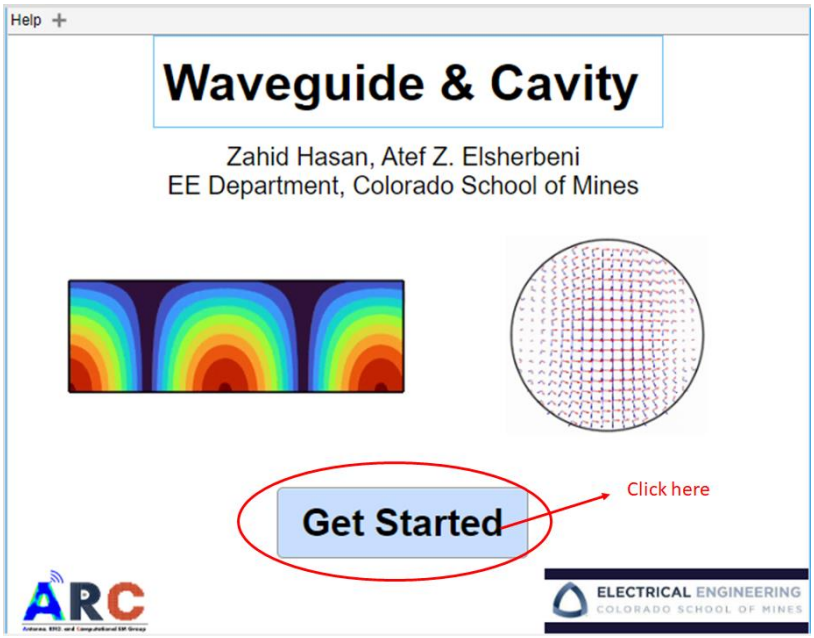

Figure 4.2: Illustrated example of how to start with the software.

Step 2: Choose “Rectangular” push button for working with rectangular cross-section.

Step 3: Enter valid inputs and check all of them by clicking “Check” button.

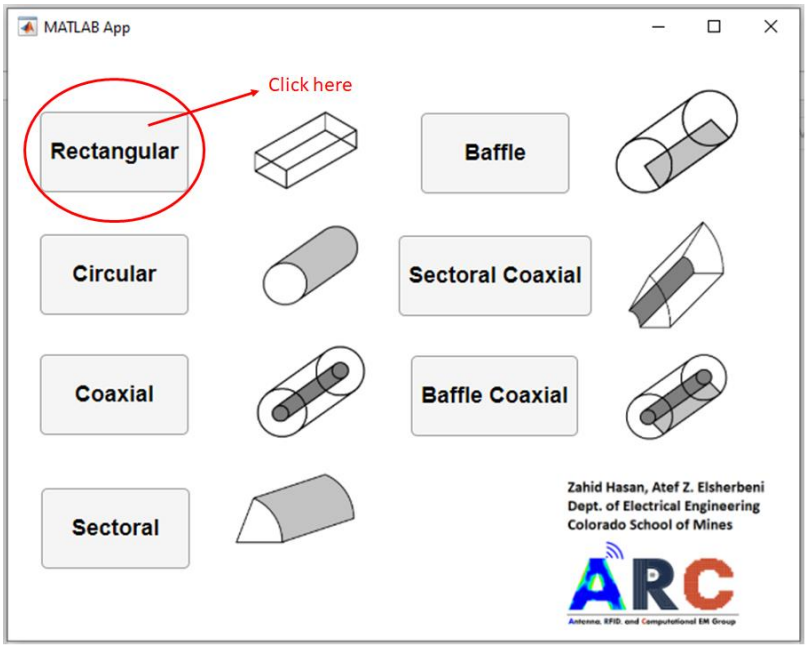

Figure 4.3: “Rectangular” push button selection in the option menu.

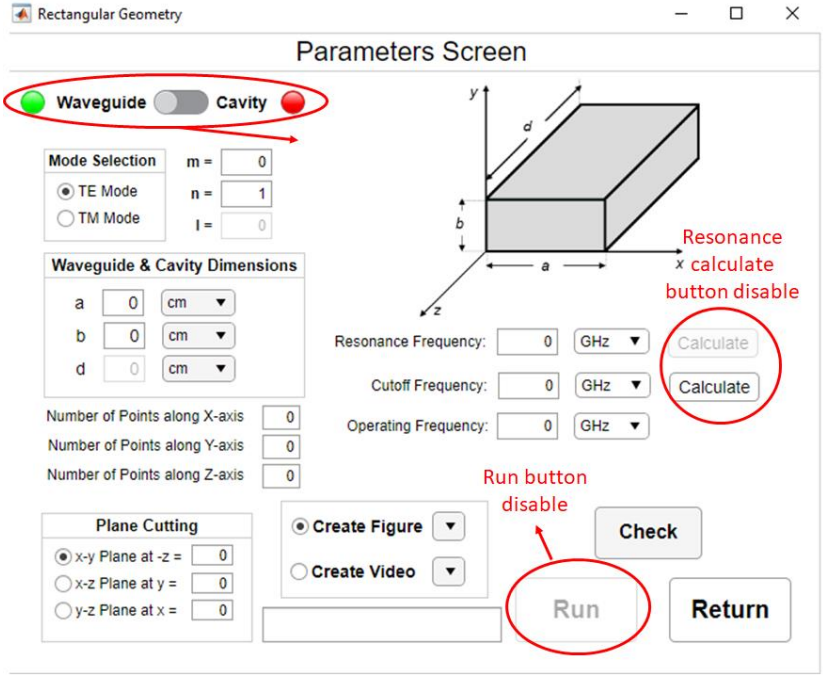

Figure 4.4: Initial parameters screen window for rectangular cross-section.

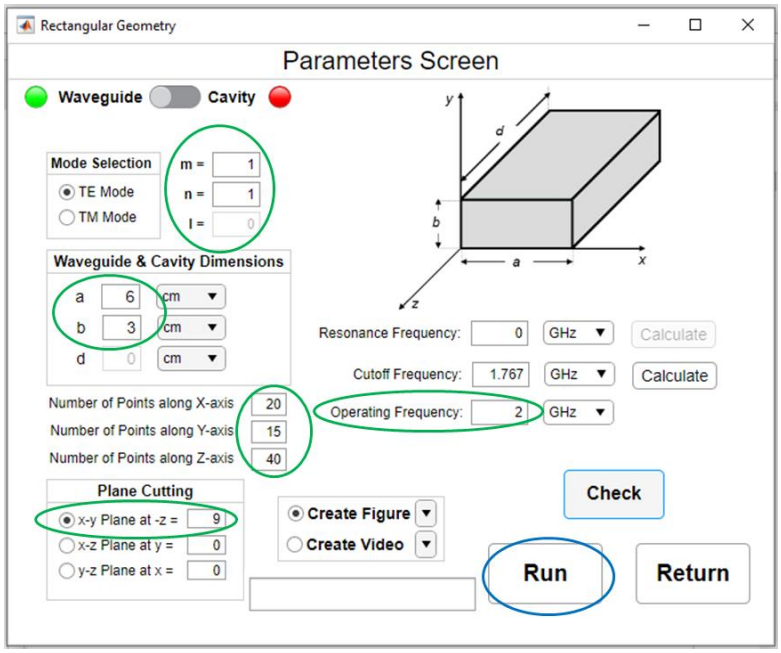

Figure 4.5: All valid inputs for rectangular waveguide.

In Figure 4.5 all inputs are valid and those are marked with green circle. After clicking the "Check" button no error is shown and that enables the "Run" button.

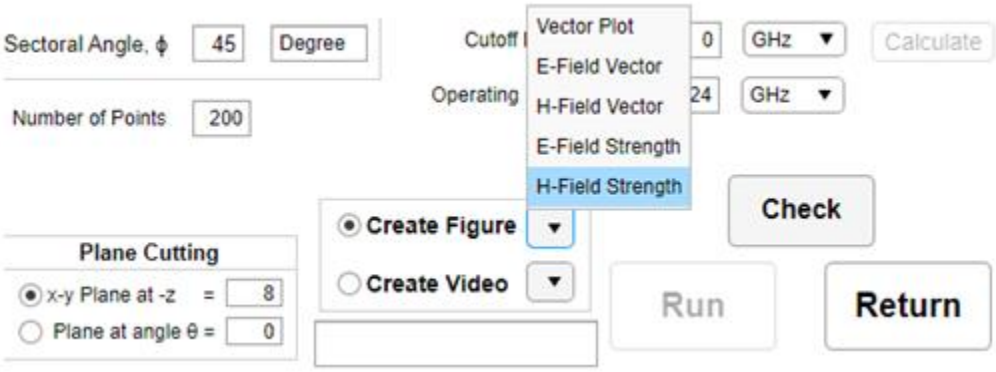

Figure 4.6: Drop-down menu for plotting different figures.

Figure 4.6 shows the drop-down menu for different figure creation options. As mentioned in previous chapter, user can create video or figure in five different ways: electric and magnetic field with vector; electric field vector; magnetic field vector; electric field strength; and magnetic field strength. Now, we enter invalid inputs to check warning messages in the parameters screen of the rectangular waveguide.

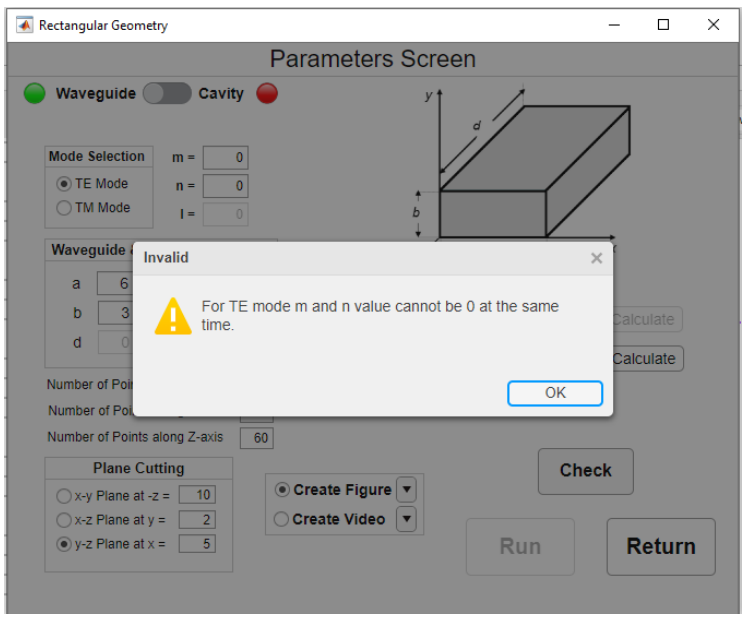

Figure 4.7: Checking the error message for invalid mode number.

For TE mode, m and n values can be 0 but not at the same time. This error message clearly tells the user what the correction should be. While checking the error, the software automatically disables the “Run” button and this makes the user understand some corrections need to be done. Similarly, some other error messages are checked in the below.

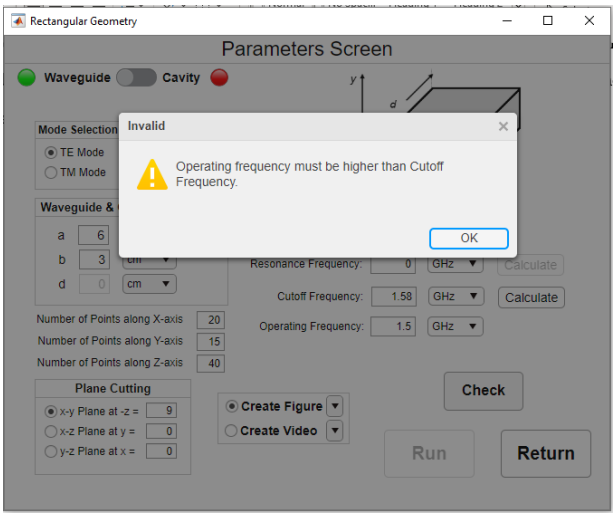

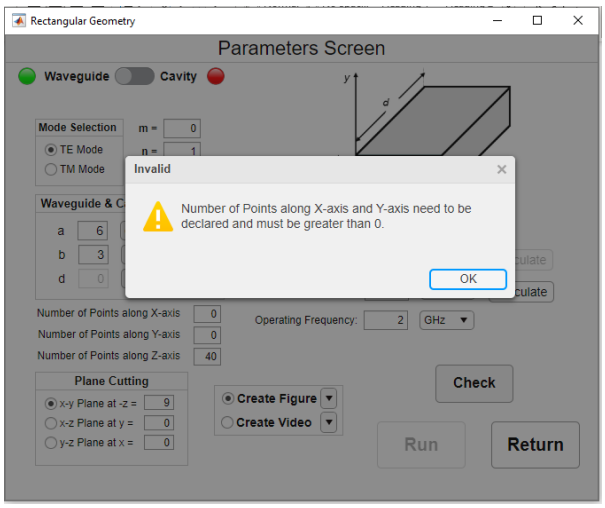

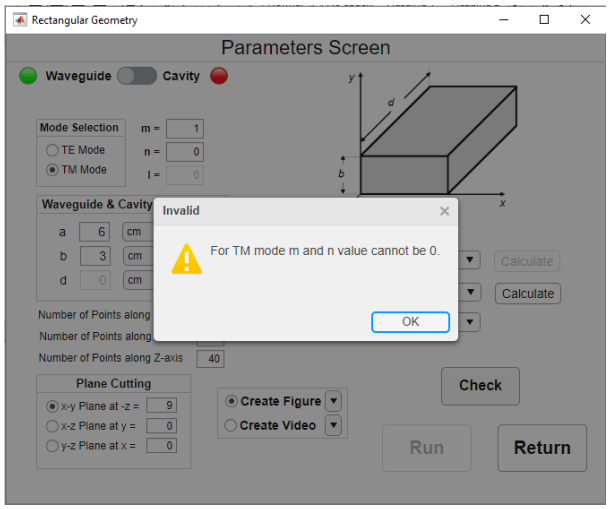

Figure 4.8: Other error messages for rectangular waveguide.

For valid inputs, some figures of the rectangular waveguide for different views are shown here. Figures 4.9 shows the vector plot, Figure 4.10 shows field strength of the rectangular waveguide at x-y plane for TE_{01} mode.

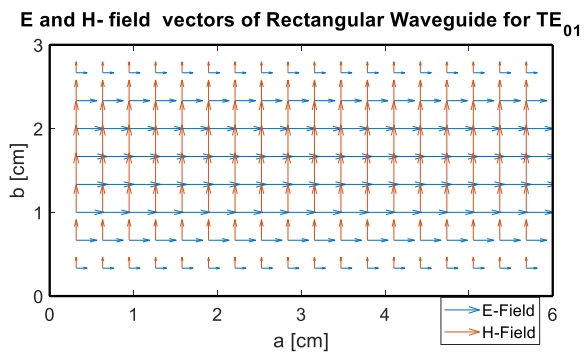

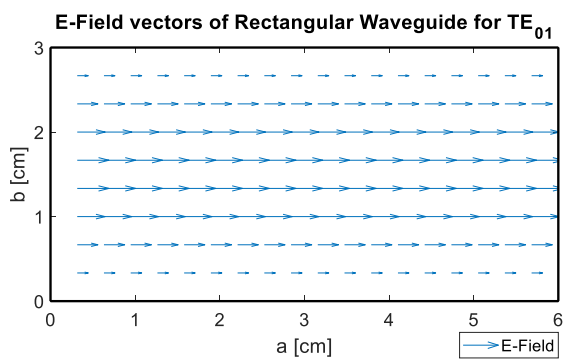

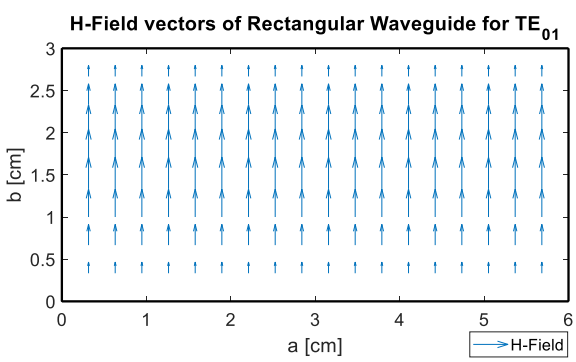

TE_{01} *Mode*

a = 6 cm

b = 3 cm

x-y plane cut in –z = 8 cm

Cutoff frequency, fc = 1.58 GHz

Operating frequency, f =2.0 GHz

Figure 4.9: Vector plot of rectangular waveguide at x-y plane for TE_{01} mode.

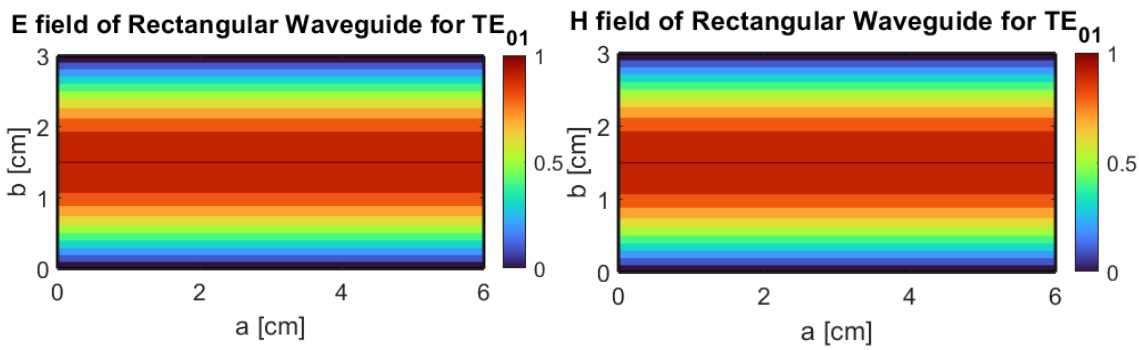

Figure 4.10: E-field and H-field of rectangular waveguide at x-y plane for TE_{01} mode.

Vector plot of rectangular waveguide at x-z plane is shown in Figure 4.11 and in Figure 4.12, field strength is presented for TE_{01} mode.

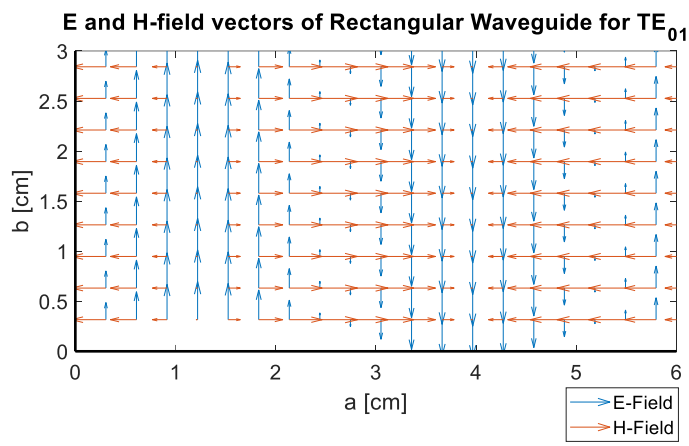

Figure 4.11: Vector plot of rectangular waveguide at x-z plane for TE_{01} mode.

Figure 4.11 continued.

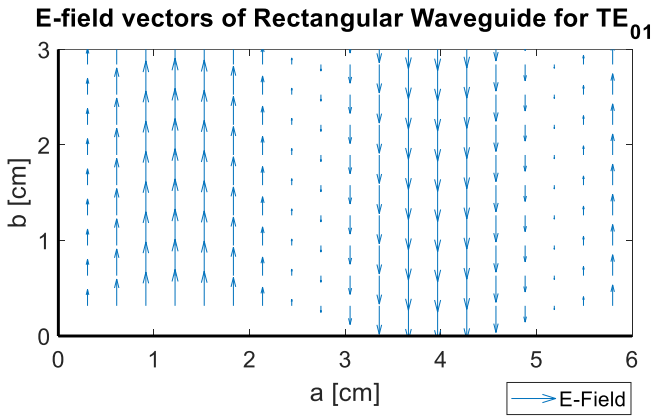

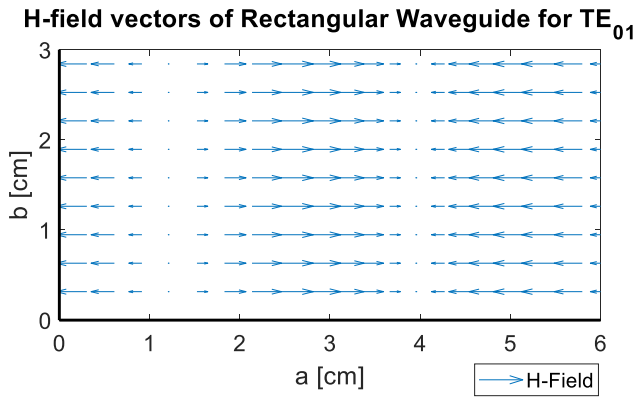

And Figures 4.13 and 4.14 show the vector plot and E and H-field strength inside the rectangular waveguide, respectively. At the y-z plane, the electric field is zero and that is clearly noticeable in these figures where the magnetic field is circulating around the boundary walls.

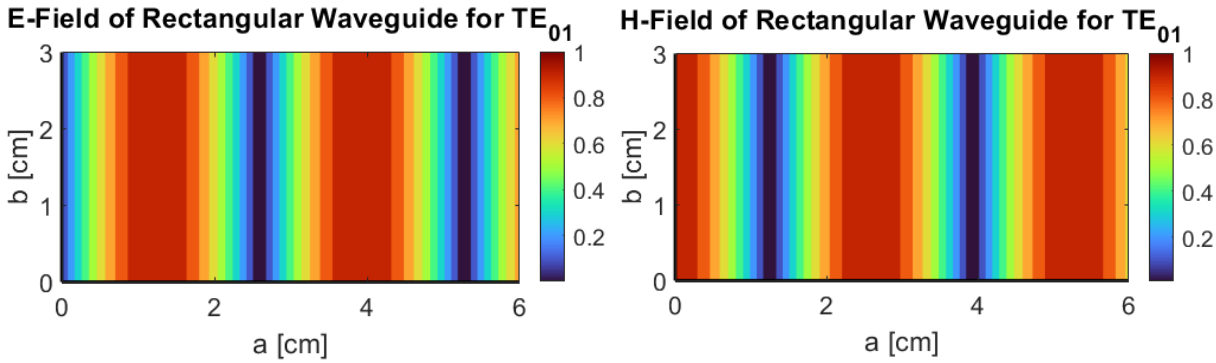

Figure 4.12: E-field and H-field of rectangular waveguide at x-z plane for TE_{01} mode.

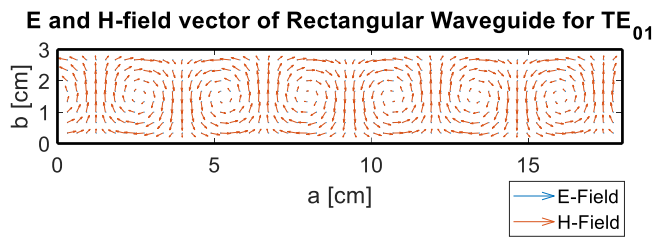

Figure 4.13: Vector plot of rectangular waveguide at y-z plane for TE_{01} mode.

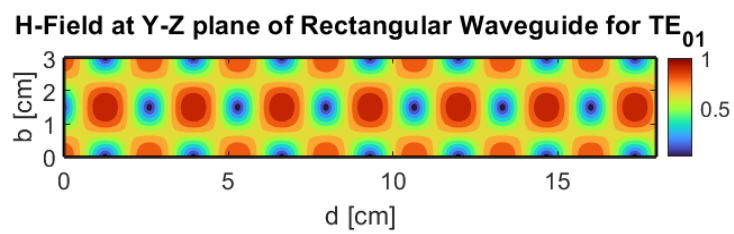

Figure 4.14: H-field of rectangular waveguide at y-z plane for TE_{01} mode.

Now, the TM button is selected in the mode selection box. For that, again cut-off frequency has been calculated and the operating frequency is kept higher than that of the cut-off frequency. Figures 4.15 shows the vector plot of the electric and magnetic field inside the rectangular waveguide, Figures 4.16 shows field strength at x-y plane for TM_{11} mode. Figure 4.17 and

Figure 4.19 show the vector plot at x-z and y-z plane for the same mode number, respectively, and Figure 4.18 and Figure 4.20 show field strength of those.

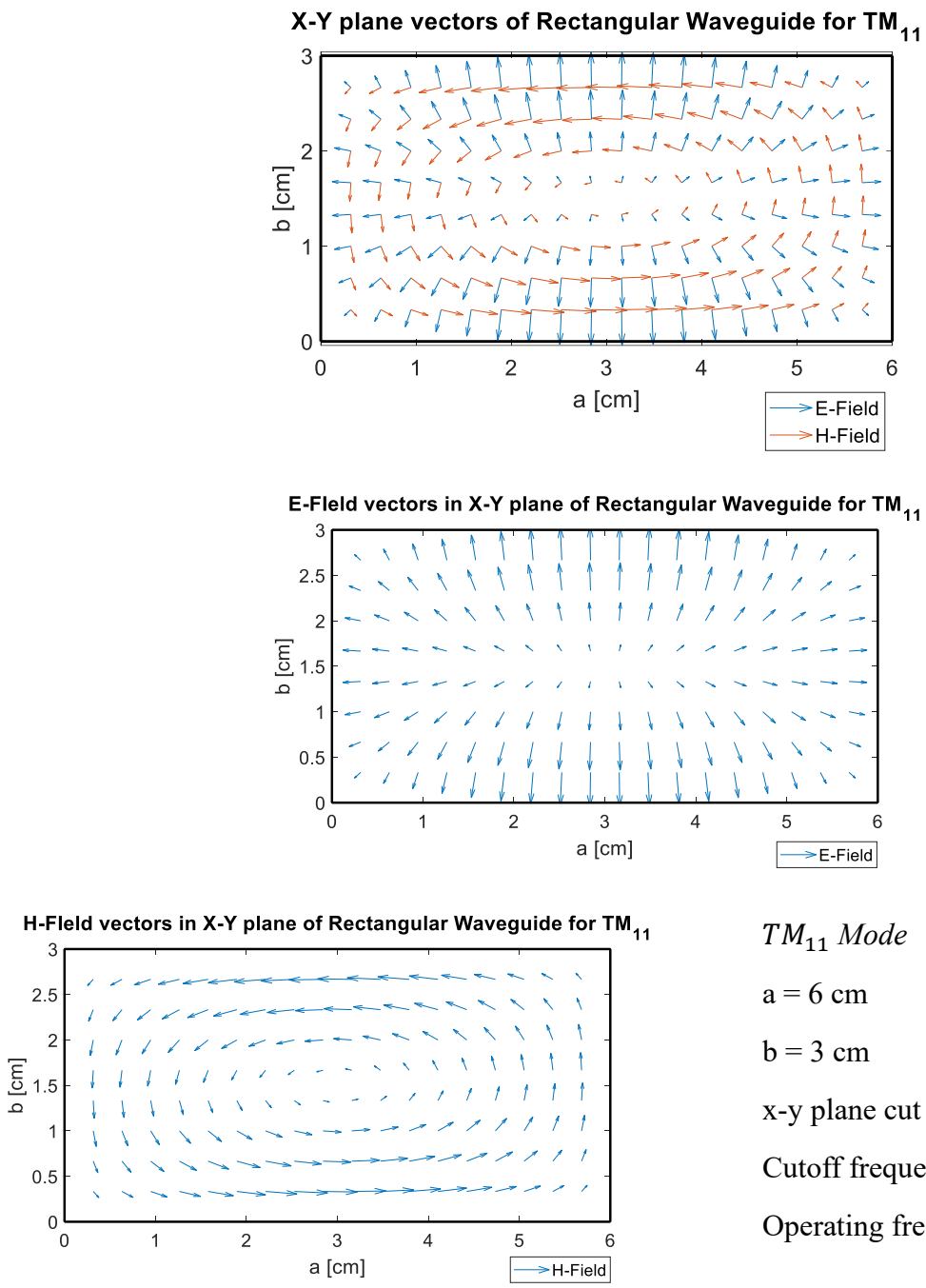

TM_{11} *Mode*

a = 6 cm

b = 3 cm

x-y plane cut in –z = 8 cm

Cutoff frequency, fc = 1.76 GHz

Operating frequency, f =2.0 GHz

Figure 4.15: Vector plot of rectangular waveguide at x-y plane for TM_{11} mode.

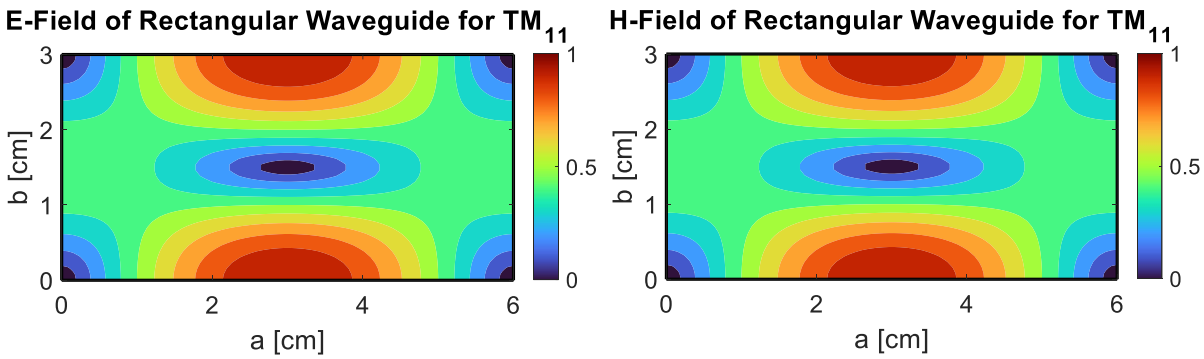

Figure 4.16: E-field and H-field of rectangular waveguide at x-y plane for TM_{11} mode.

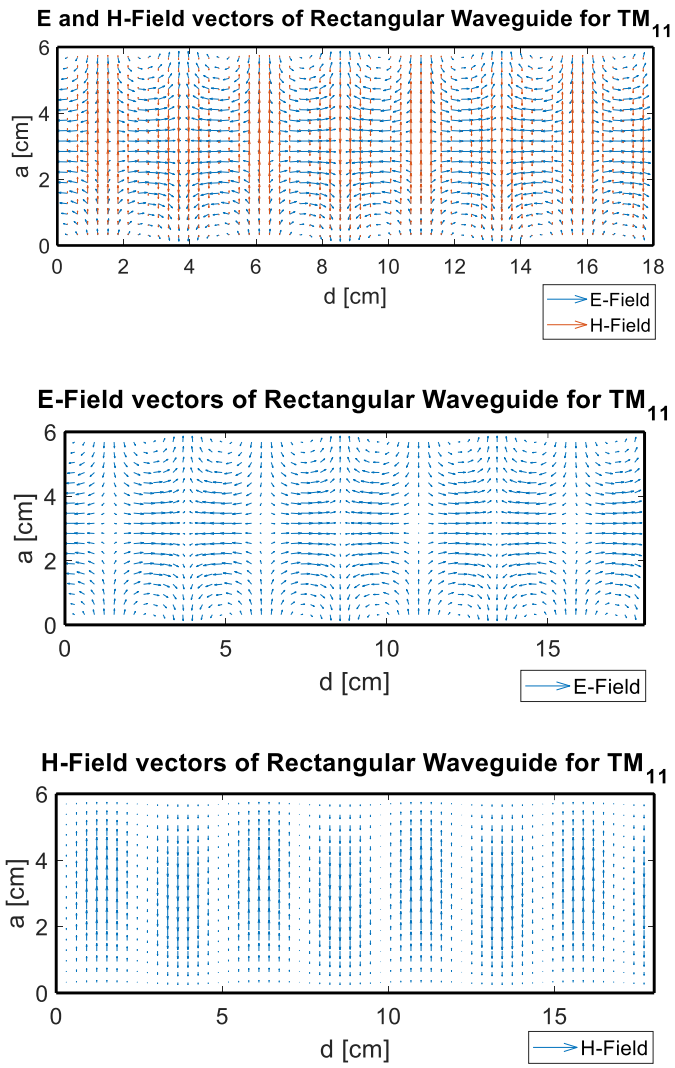

Figure 4.17: Vector plot of rectangular waveguide at x-z plane for TM_{11} mode.

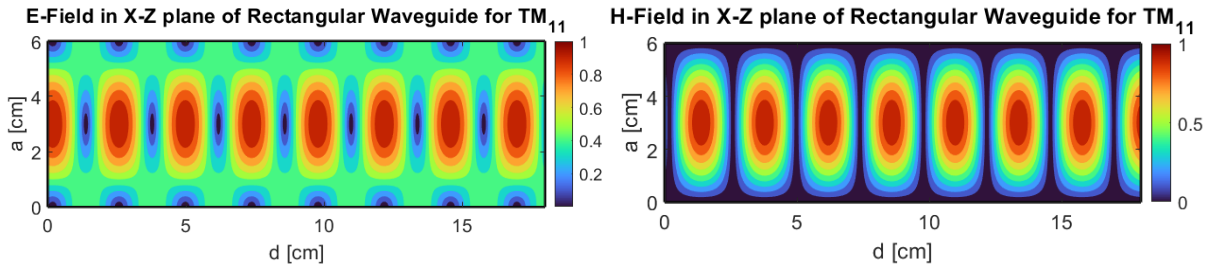

Figure 4.18: E-field and H-field of rectangular waveguide at x-z plane for TM_{11} mode.

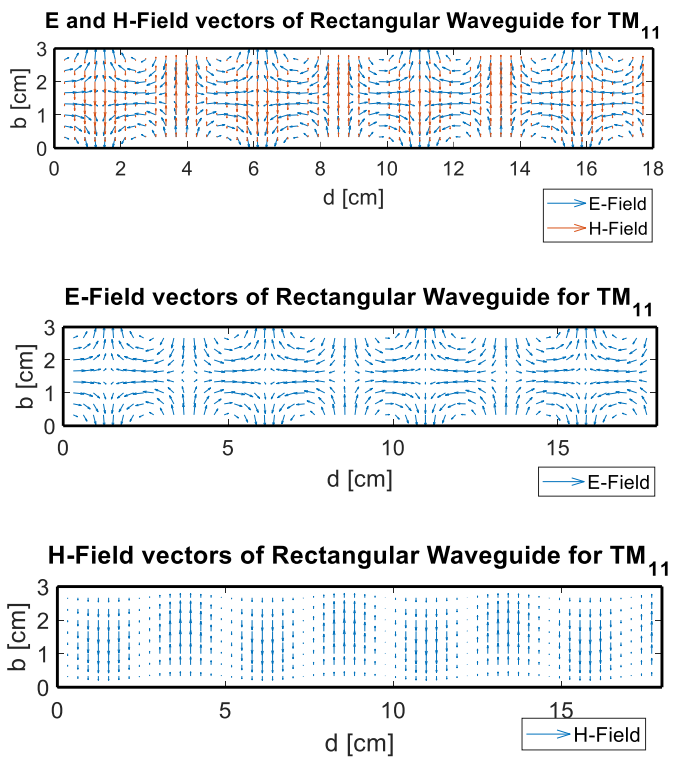

Figure 4.19: Vector plot of rectangular waveguide at y-z plane for TM_{11} mode.

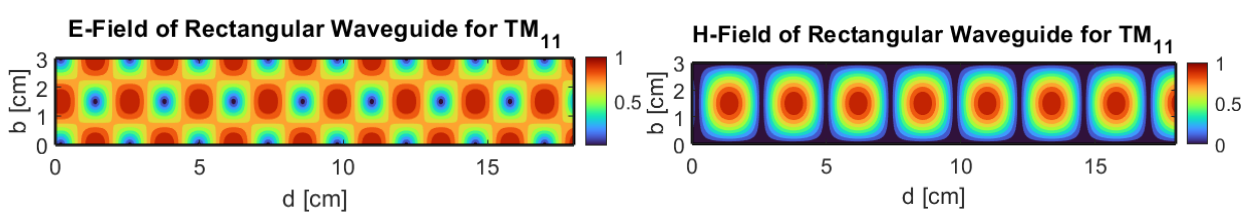

Figure 4.20: E-field and H-field of rectangular waveguide at y-z plane for TM_{11} mode.

4.1.2 Circular Waveguide

Like rectangular waveguides, steps are similar to the circular waveguide till the parameters screen. In the parameters screen, some inputs are different. For circular waveguides, users need to only input the radius of the waveguide in the waveguide dimensions box. Switching over TE and TM mode will give the different values of cut-off frequency for the same mode number. Just like rectangular waveguide, the “Check” button will verify whether the inputs are valid or not. For any invalid input, the “Run” button will remain disabled. If there are no errors, pressing the “Check” button will enable the “Run” button for execution.

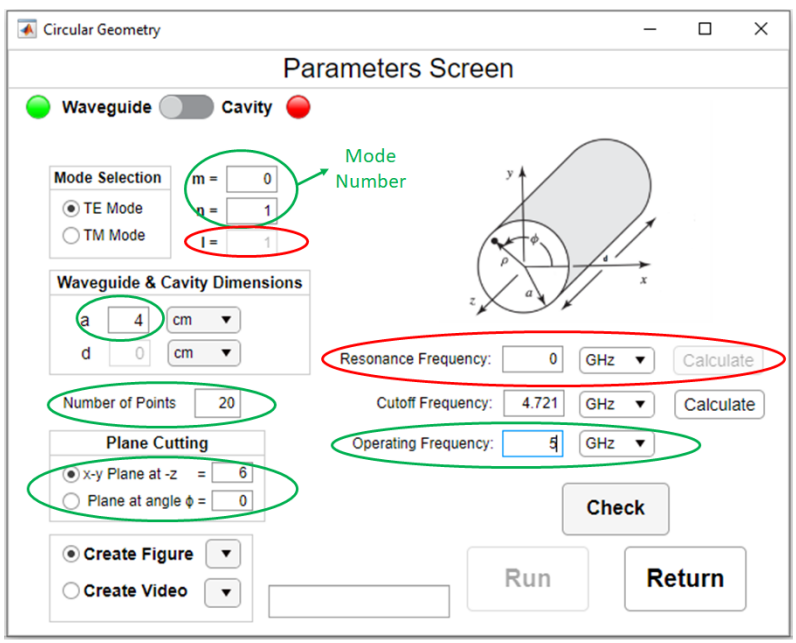

Figure 4.21: Initial parameter screen window for circular waveguide.

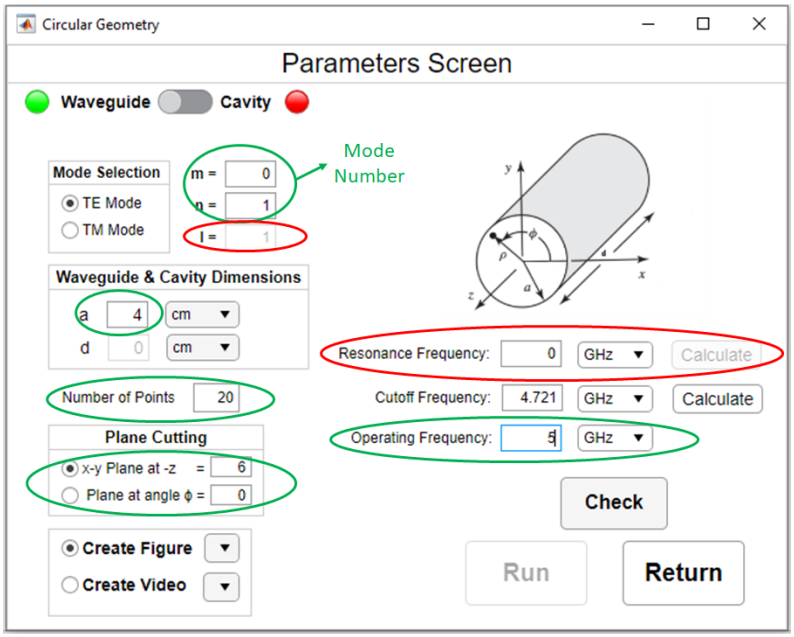

Figure 4.22: Parameters screen showing input and disable options for circular waveguide.

Figures 4.21 and 4.22 show the parameter input options and disable field for waveguide selection mode. All green circles indicate input fields and red circles indicate disable fields. For wrong mode number, both the check button and cut-off frequency calculate button show error messages. Mode number n cannot be zero in both TE and TM mode of operation for circular waveguide. Putting the value of $n = 0$ in the parameters screen, the error message is shown in Figure 4.23.

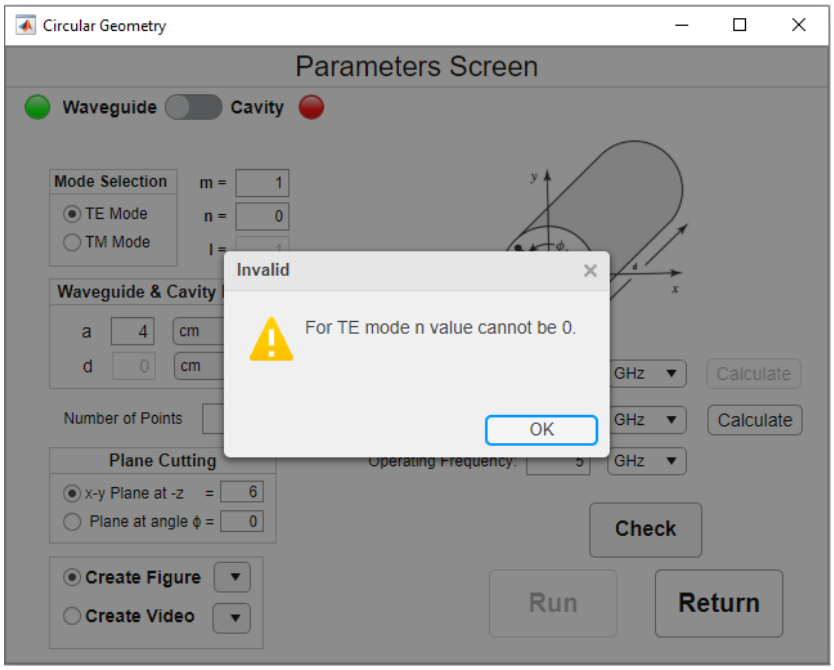

Figure 4.23: Error message for invalid mode number in circular waveguide.

If every input is valid, then the “Check” button enables the “Run” button (see Figure 4.24).

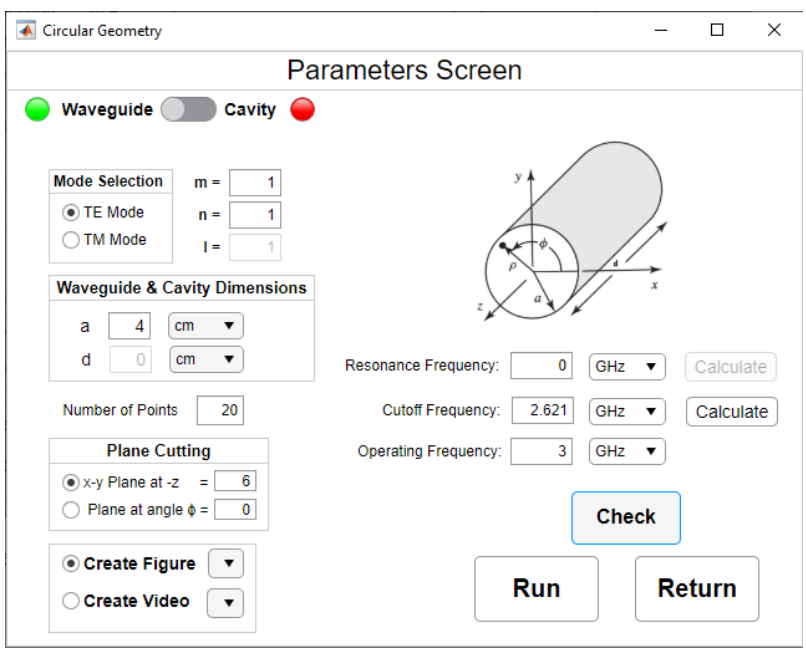

Figure 4.24: For all valid input “Run” button is activated.

Some examples of electric and magnetic fields distribution inside circular waveguide at different plane cut are shown in Figures 4.25, 4.26, 4.27, and 4.28.

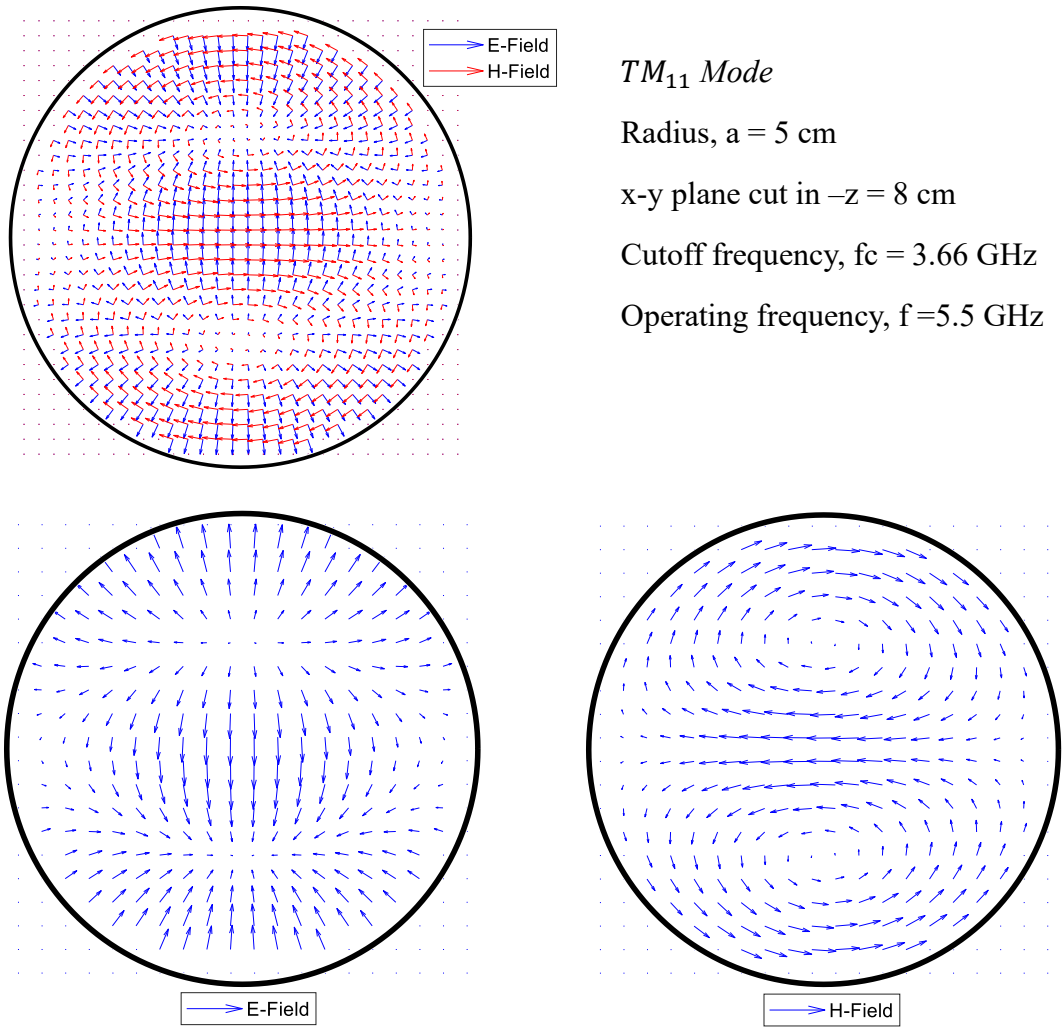

Figure 4.25: Vector plot of circular waveguide at x-y axis for TM_{11} mode.

Figure 4.25 shows the vector of electric and magnetic fields inside the circular waveguide. Field maps are also shown in Figure 4.26. This figure shows where the E-Field and H-Field are strong. The field distribution in Figure 4.26 is identical because the field strength of both electric

and magnetic fields is denser in the same location. The differences can be observed using the vector plots as the arrow directions are different.

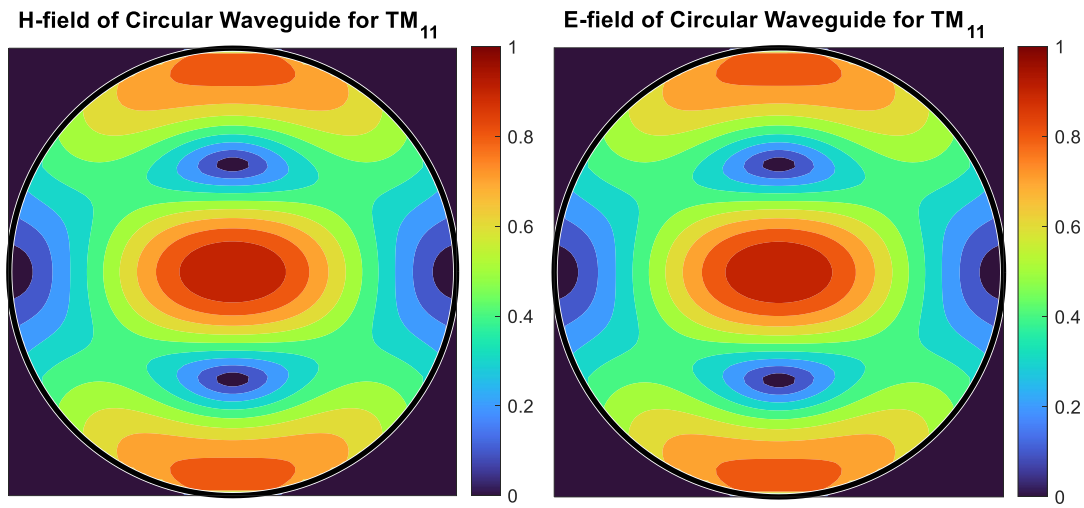

Figure 4.26: E-field and H-field of circular waveguide for TM_{11} mode.

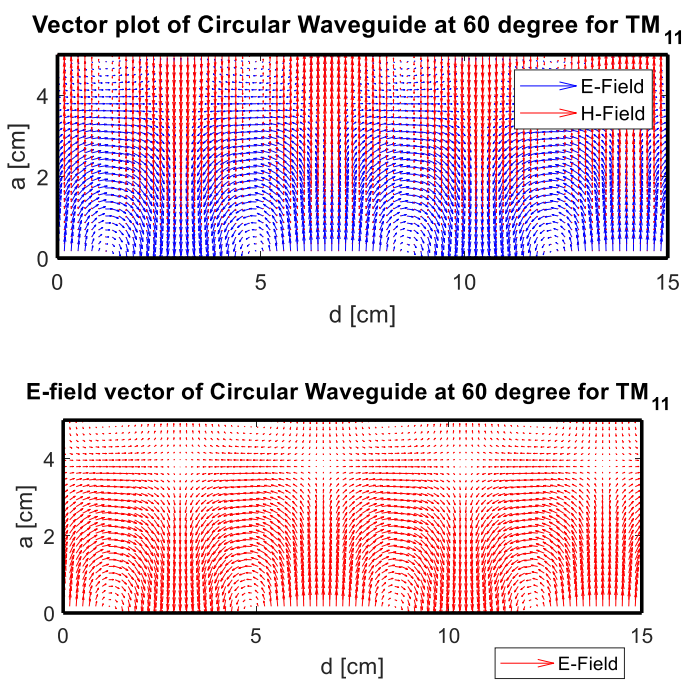

Figure 4.27: Vector plot of circular waveguide for TM_{11} mode at 60° plane.

Figure 4.27 continued.

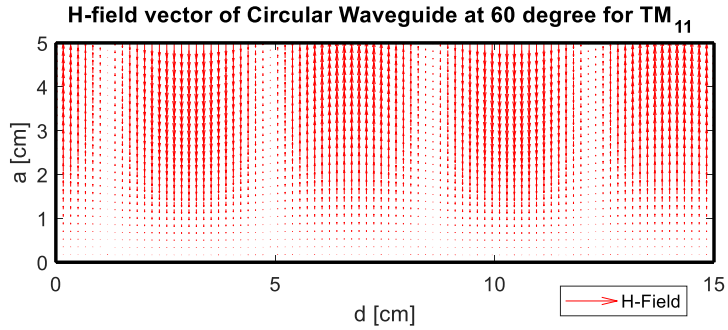

Field vectors at 60° plane angle are presented in Figure 4.27 for TM_{11} mode. Contour plot helps user understand the field strength inside the hollow waveguide and that is shown in Figure 4.28.

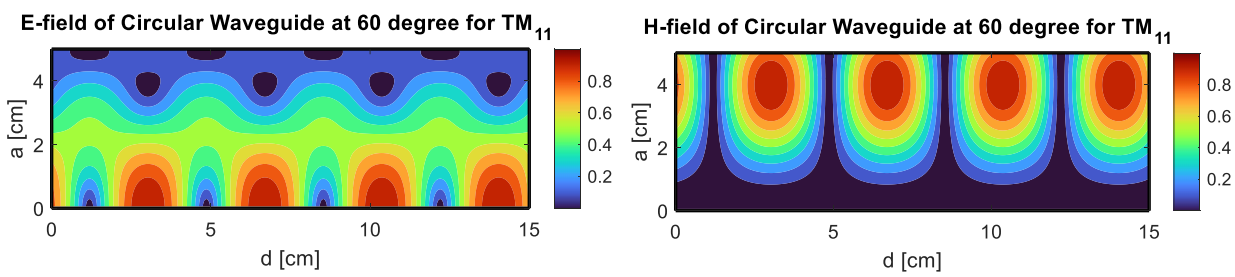

Figure 4.28: E-field and H-field of circular waveguide for TM_{11} mode at 60° plane.

4.1.3 Coaxial Waveguide

In the coaxial waveguide a conducting core is placed inside the hollow cylindrical waveguide. This conducting core helps to active the TEM mode in this transmission line. The parameters screen is shown in Figure 4.29. For the coaxial cross-section, an extra dimension is included in the waveguide and cavity dimension box. The dimension of the inner radius a is the radius of the conducting core and the outer radius is b.

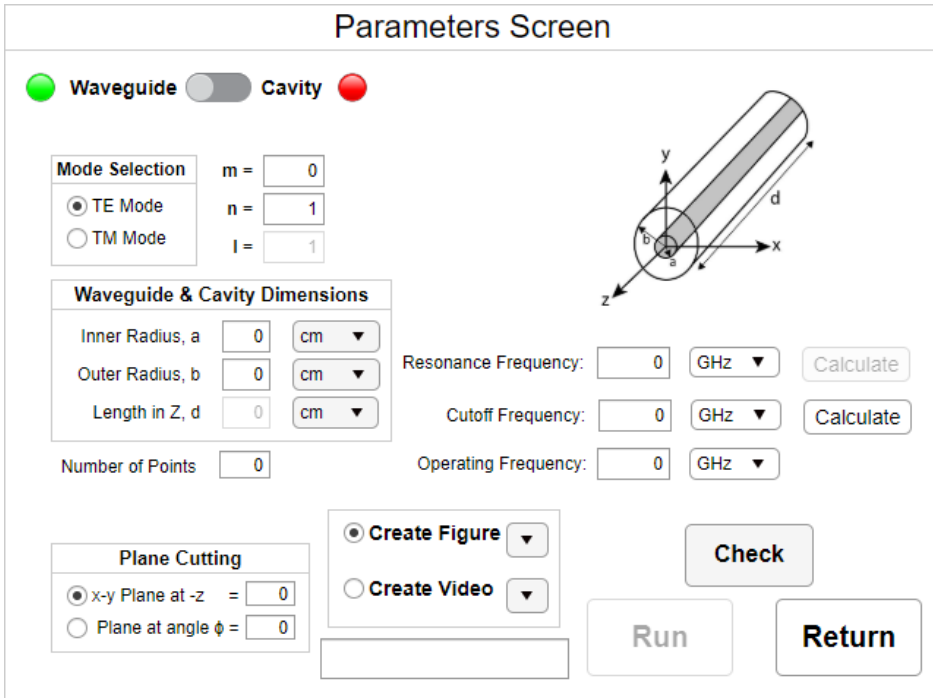

Figure 4.29: Parameters screen of coaxial waveguide.

Like circular waveguide, the software will generate some warning messages for invalid inputs. The cavity switch enables the mode number l, length in -z axis d and the resonance calculate button. The vector plots and field strength for TM_{12} mode is shown in Figures 4.30 and 4.31.

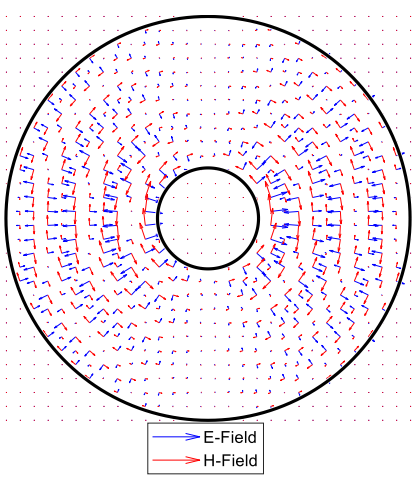

TM_{12} Mode

Inner radius, a = 1 cm

Outer radius, b = 4 cm

x-y plane cut in –z = 8 cm

m = 1

n = 2

Cutoff frequency, fc = 25.43 GHz

Operating frequency, f = 26 GHz

Figure 4.30: Vector plot of coaxial waveguide for TM_{12}.

Figure 4.30 continued.

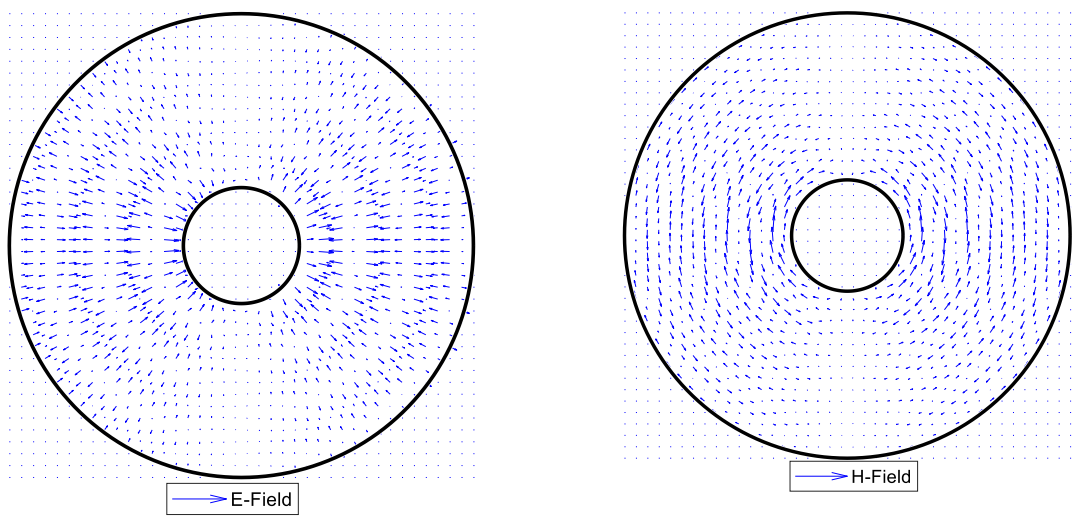

Also here, the field maps are identical but the arrow direction is different. Figure 4.32 shows the vectors and field strength of coaxial waveguide at 60° plane angle for TM_{12} mode.

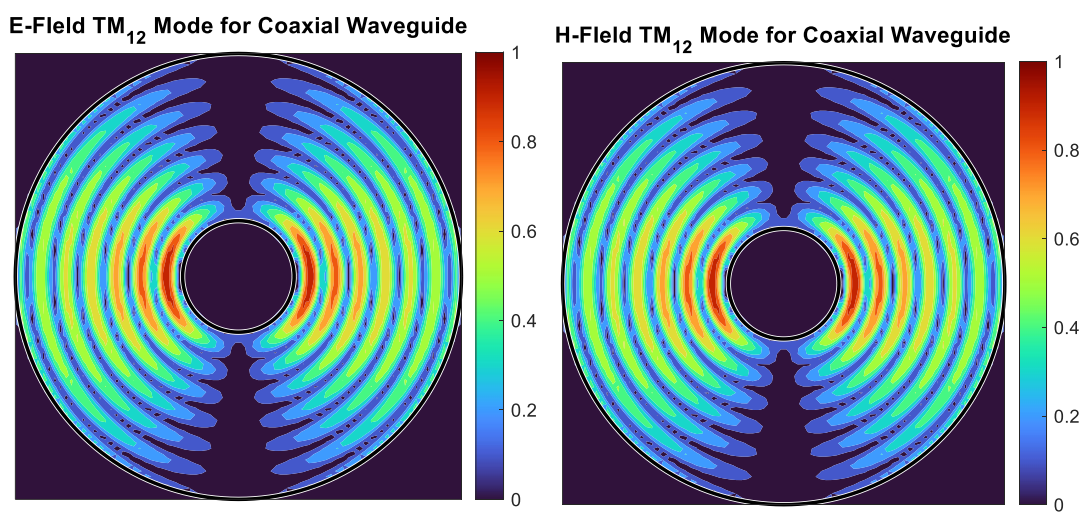

Figure 4.31: E-Field and H-Field of coaxial waveguide for TM_{12}.

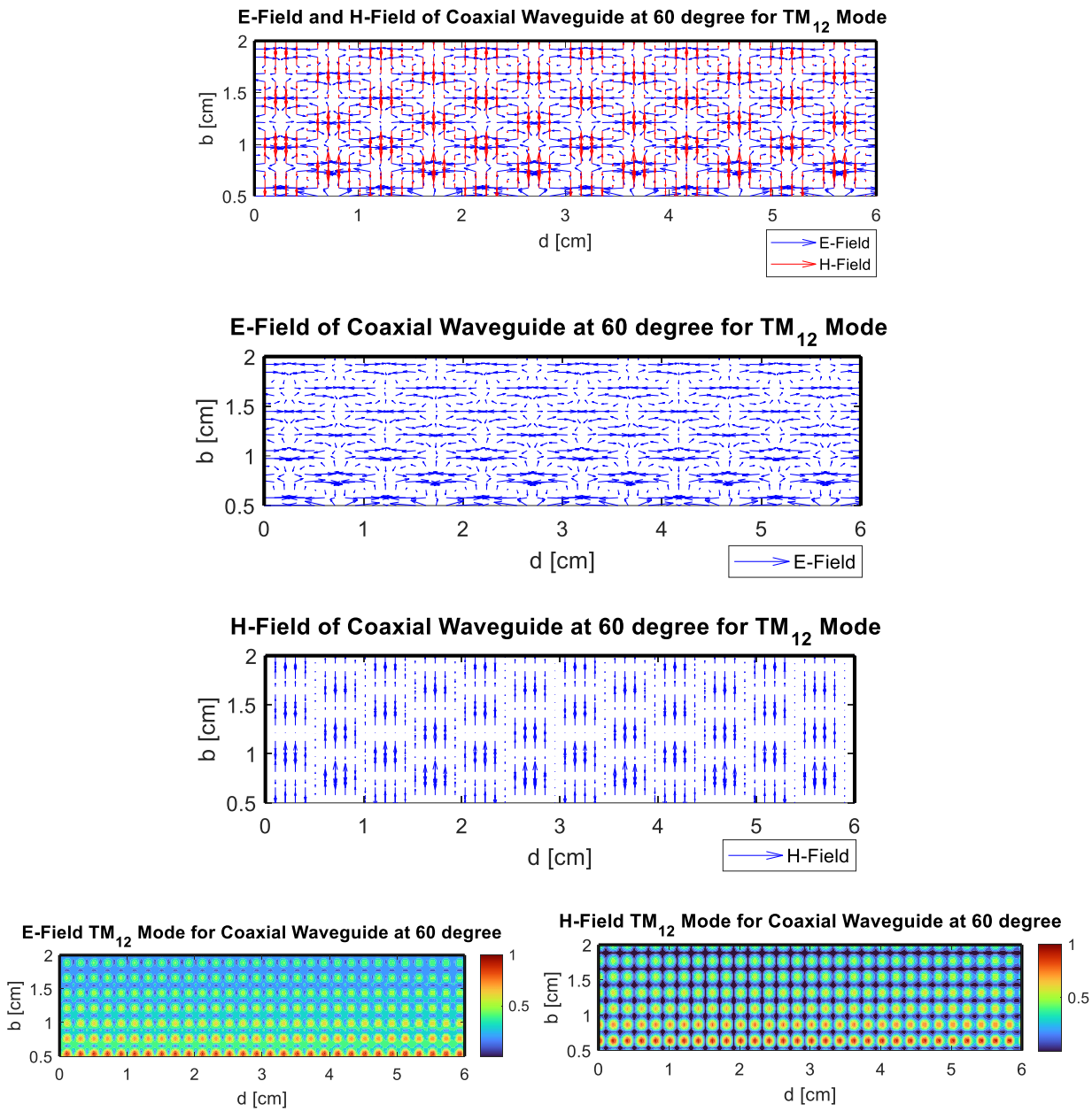

Figure 4.32: Vectors and field of coaxial waveguide at 60° plane angle for TM_{12} mode.

Some other vector plots for different modes in coaxial waveguide are shown below.

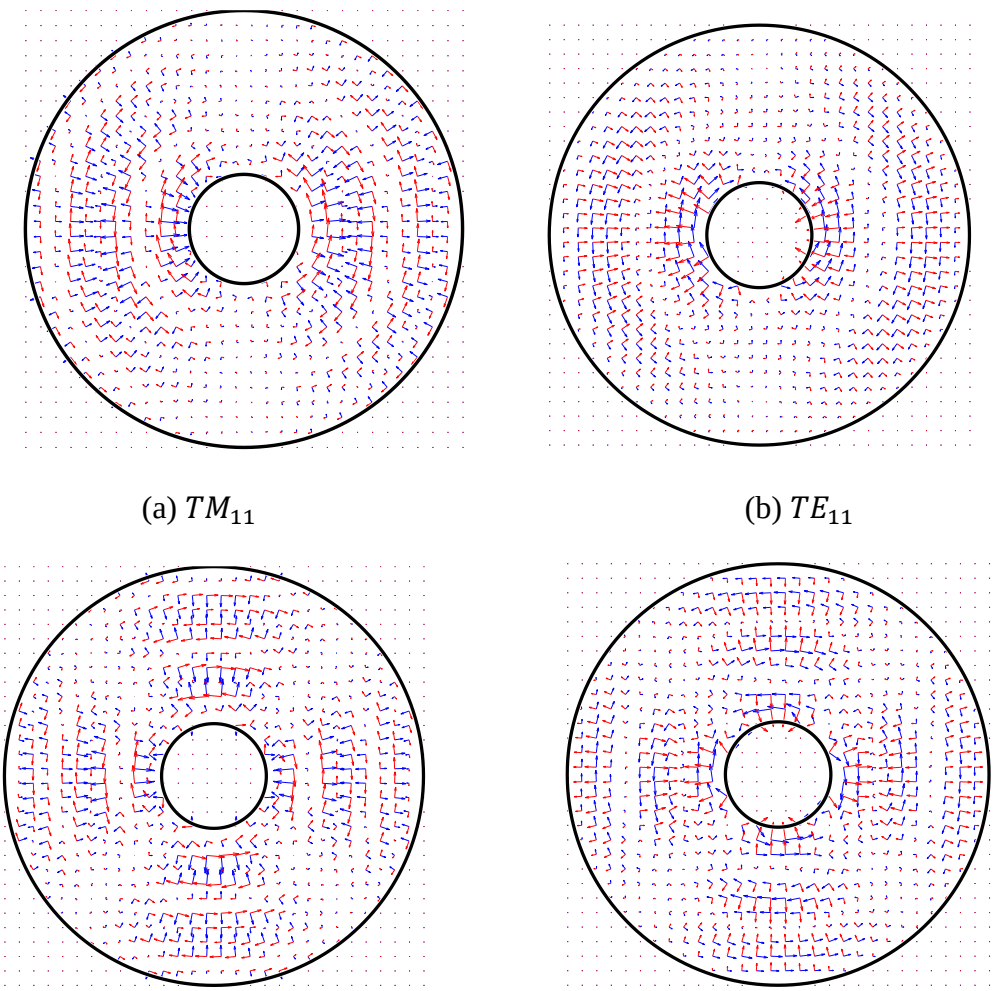

(a) TM_{11} (b) TE_{11}

(c) TM_{21} (d) TE_{21}

Figure 4.33: Vector plots of coaxial waveguide for (a) TM_{11} (b) TE_{11} (c) TM_{21} (d) TE_{21}.

4.1.4 Sectoral Waveguide

When the cylindrical waveguide is cut with different angles then it is called the sectoral waveguide. Sectoral waveguide can be any arbitrary angle from 1 to 360°. The parameter screen of the sectoral waveguide is shown in Figure 4.34. Here, ϕ_0 is the sectoral angle and p is the

integer for mode number. For TE mode $p = 0, 1, 2, 3, \ldots$ and for TM mode $p = 1, 2, 3, \ldots$ Some figures for 90° and 270°sectoral waveguide are documented here and compared with the previous work presented in [25].

Parameters screen of the sectoral waveguide is shown in Figure 4.34. The angle$\phi_0$for the sectoral cross-section is arbitrary and that gives users flexibility to select any angle from 0 to 360°.

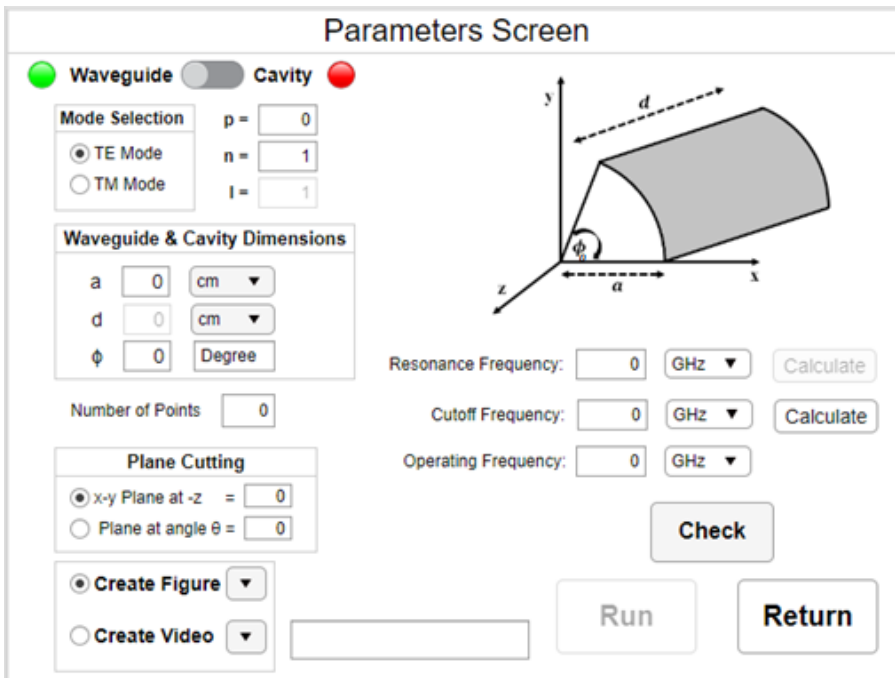

Figure 4.34: Parameters screen for sectoral waveguide.

Some field vectors of sectoral waveguide at different ϕ_0 angle are shown in Figure 4.35. Here $90^{\circ}$and 270°sectoral angle is selected. Figure 4.36 shows the field strength inside these sectoral waveguides. TE_{21} mode is selected for both structures. Cutoff frequency is calculated for 90° sectoral waveguide and 270°sectoral waveguide is 5.07 GHz and 2.15 GHz, respectively. Operating frequency is selected 6 GHz 90° sectoral and 3 GHz for 270°sectoral.

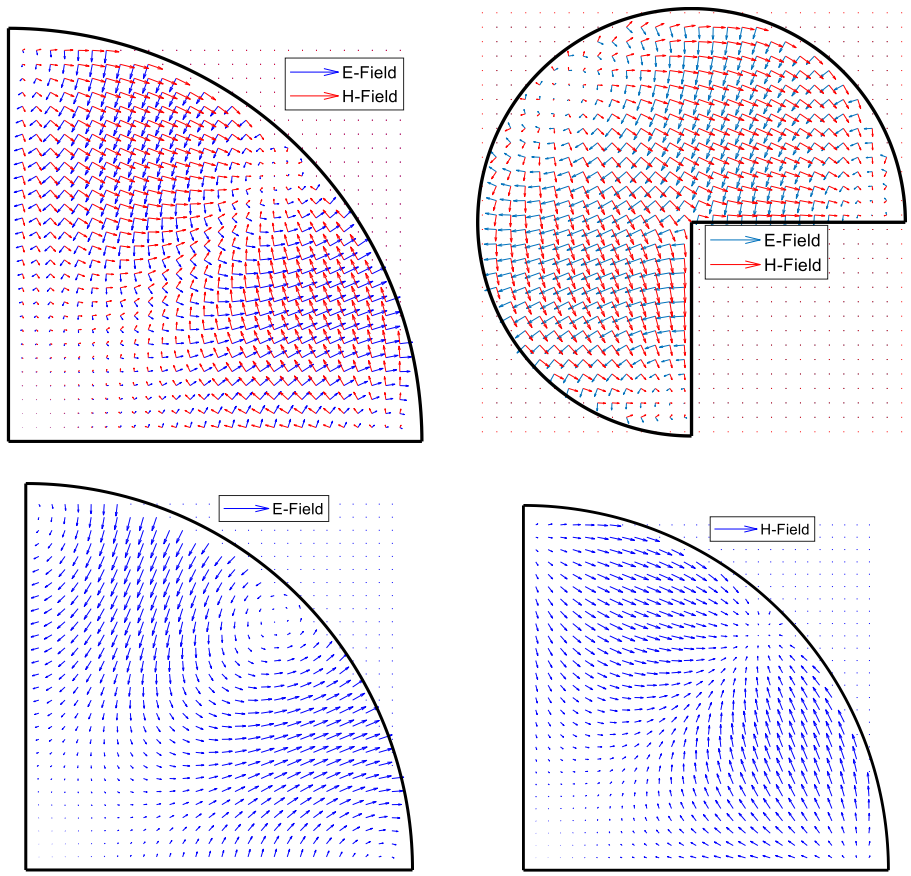

(a) 90° sectoral

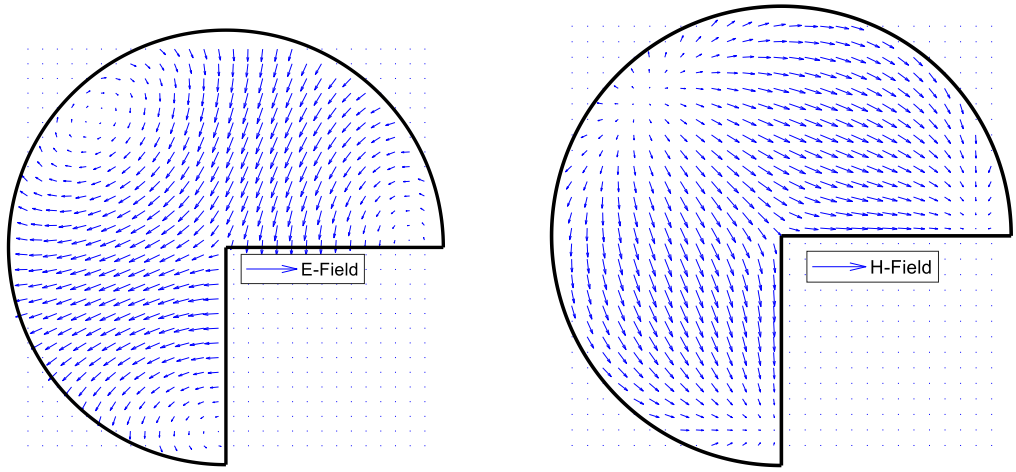

(b) 270° sectoral

Figure 4.35: Vector plot of (a) 90°and (b) 270°sectoral waveguide for TE_{21} mode.

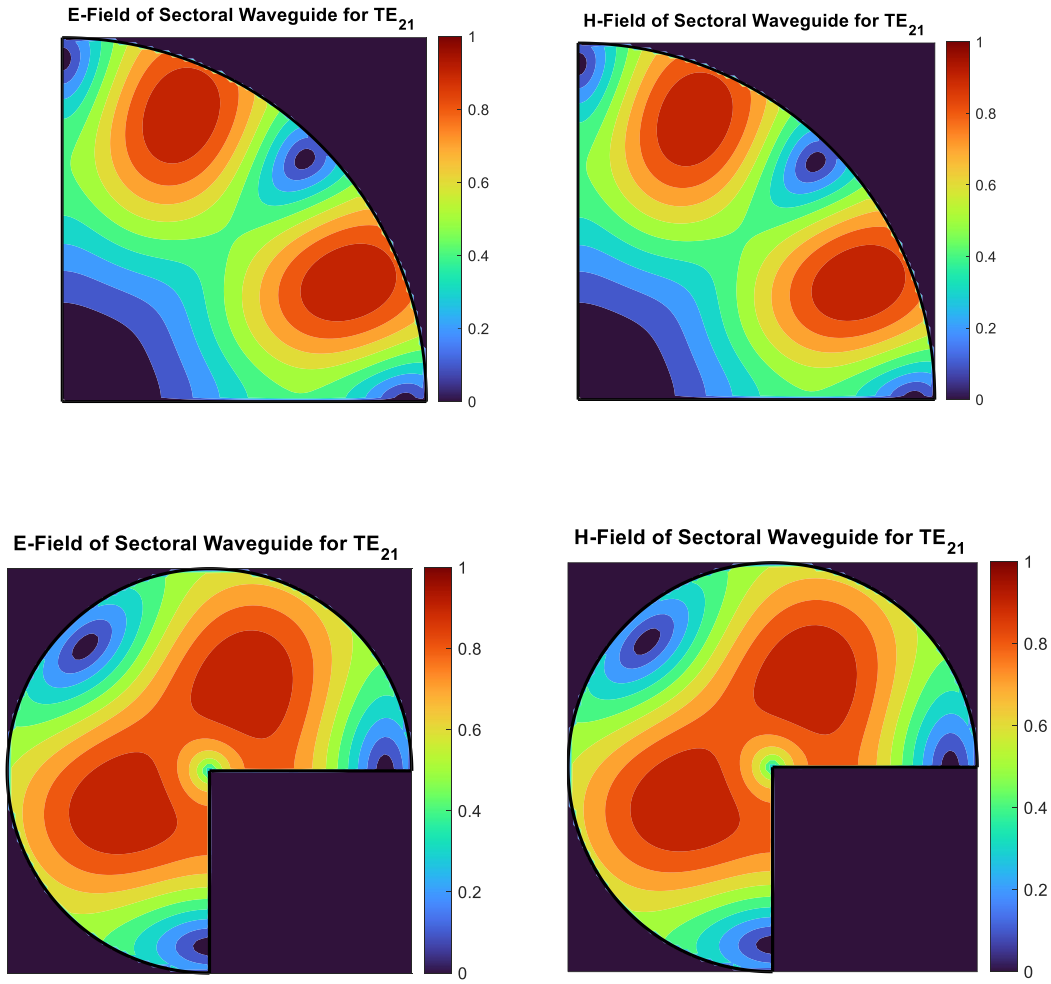

Figure:4.36: E-Field and H-Field for 90° and 270°sectoral waveguide for TE_{21} mode.

4.1.5 Baffle Waveguide

As previously mentioned in chapter 2, that a baffle waveguide is created by the insertion by a metal plate into the hollow circular waveguide. The parameters screen of the baffle waveguide is shown in Figure 4.37. All the parameters here are as same as circular waveguide only difference is the parameter p. Mode number m is replaced here by p because the value of m is non integer for the baffle waveguide.

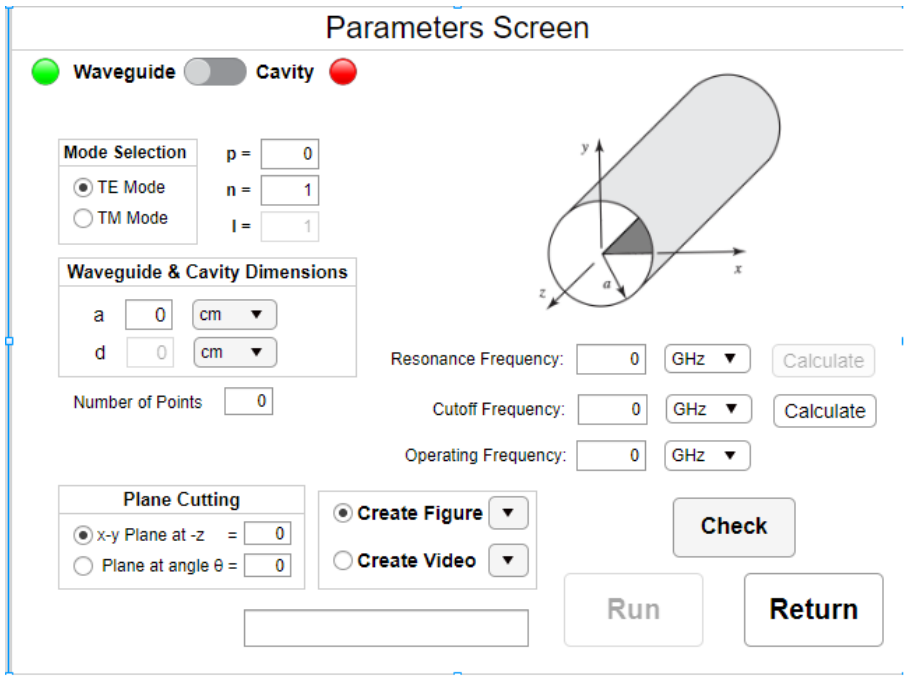

Figure 4.37: Parameters screen of Baffle waveguide.

Field pattern has been verified for the TE_{11} mode. Vector plots and field strength for both E-Field and H-Field are shown in Figure 38 and 39, respectively.

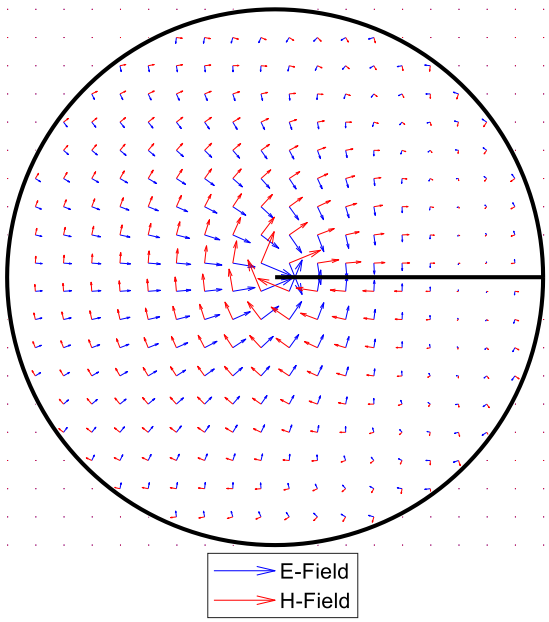

TE_{11} *mode*

Radius, a = 5 cm

Cutoff frequency, fc = 1.11 GHz

Operating frequency, f = 2 GHz

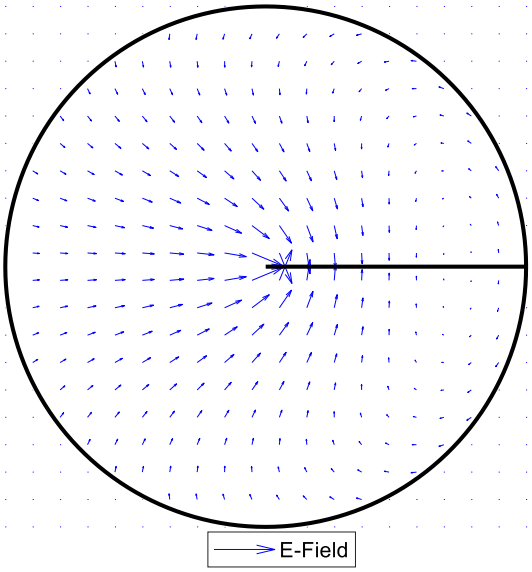

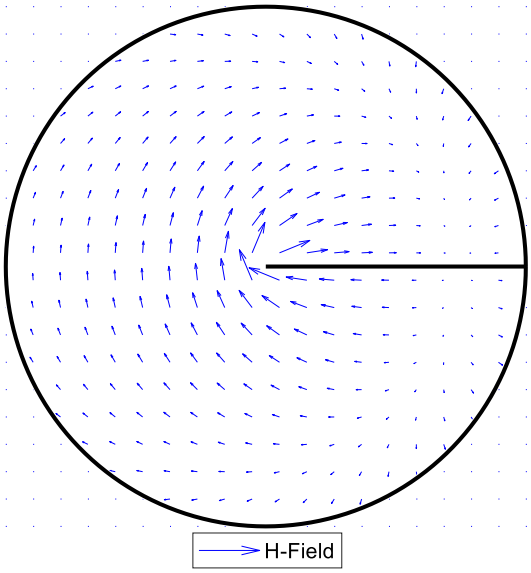

Figure 4.38. :Vector plot of Baffle waveguide for TE_{11} mode.

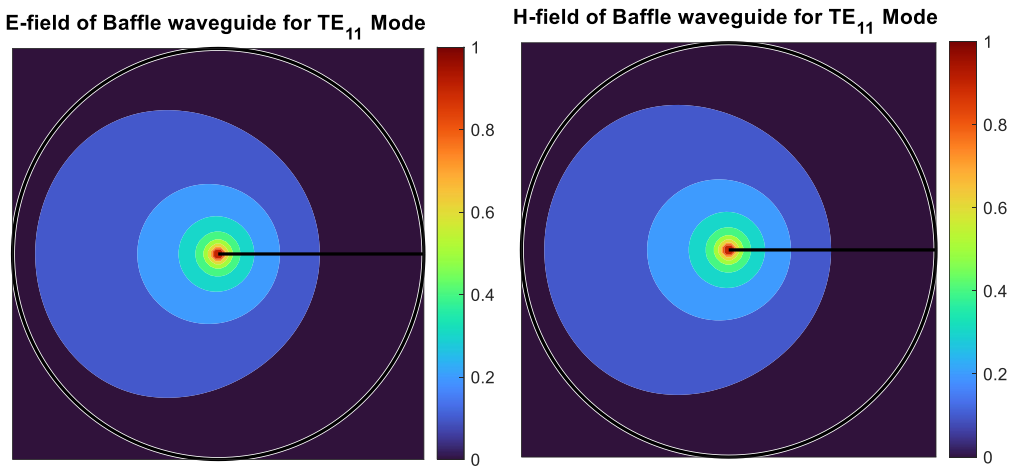

Figure 4.39. : E-field and H-field of baffle waveguide for TM_{11}

To validate our work, vector field pattern of some modes of operation were analyzed and compared with the figures documented in [24]. Those figures are given below.

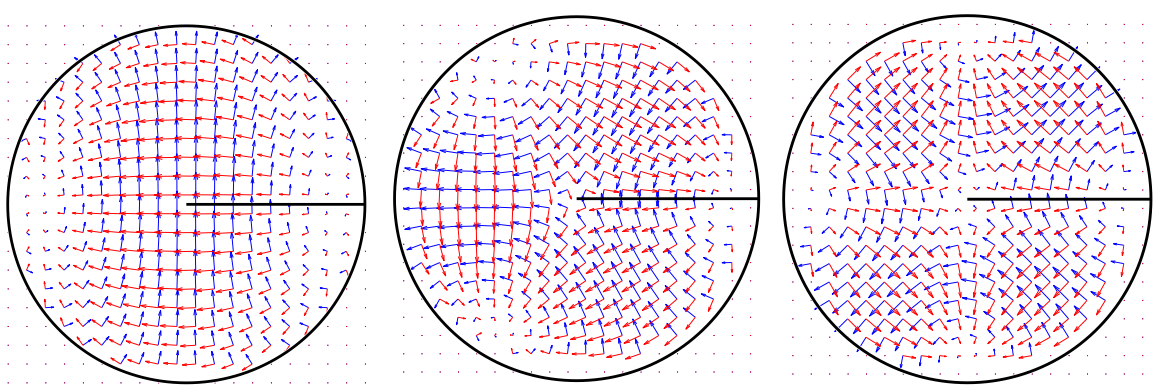

(a) TE_{21} (b) TE_{31} (c) TE_{41}

Figure 4.40: Field vectors for (a) TE_{21} (b) TE_{31} (c) TE_{41} mode in baffle waveguide.

4.1.6 Sectoral-Coaxial Waveguide

Sectoral-Coaxial waveguide is combination of sectoral and coaxial cross-sections. Like sectoral cross-section this is also for an arbitrary angle from 0° to 360°. As the conducting core is

placed inside the waveguide, from the center to radius of the conducting core no field vectors are present. The parameters screen of this cross-section is shown in Figure 4.41. Illustrated examples have been given for 90° and 180° sectoral-coaxial waveguide in Figure 4.42 and 4.43.

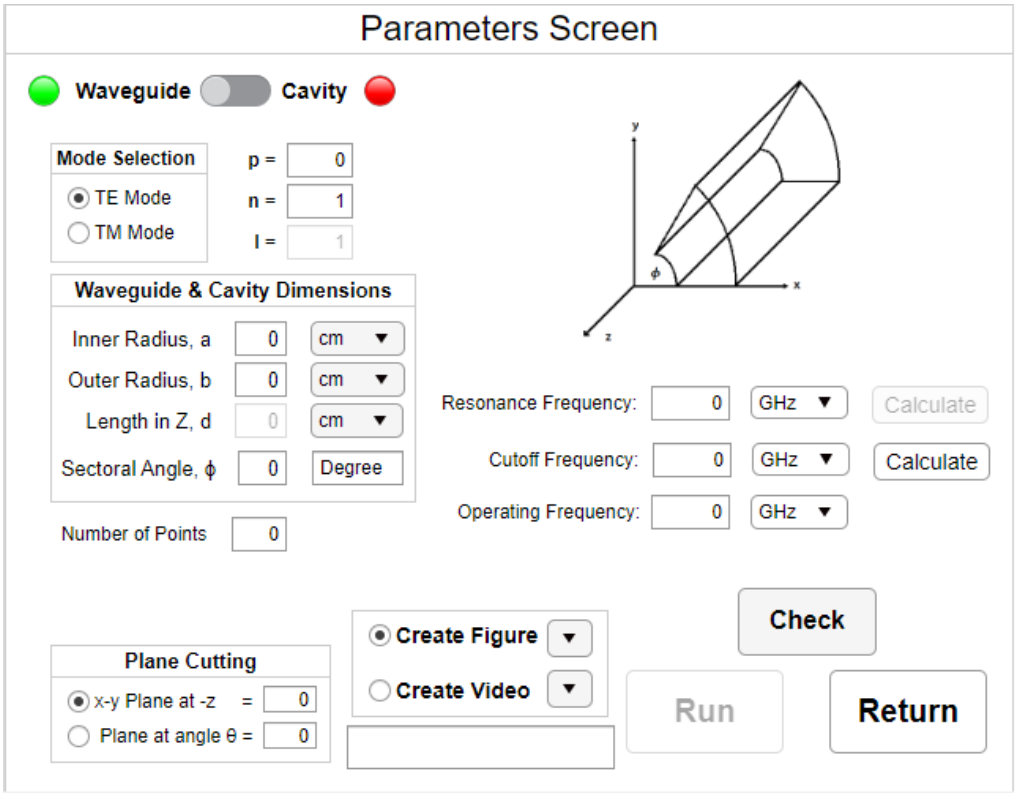

Figure 4.41: Parameters screen for sectoral-coaxial waveguide.

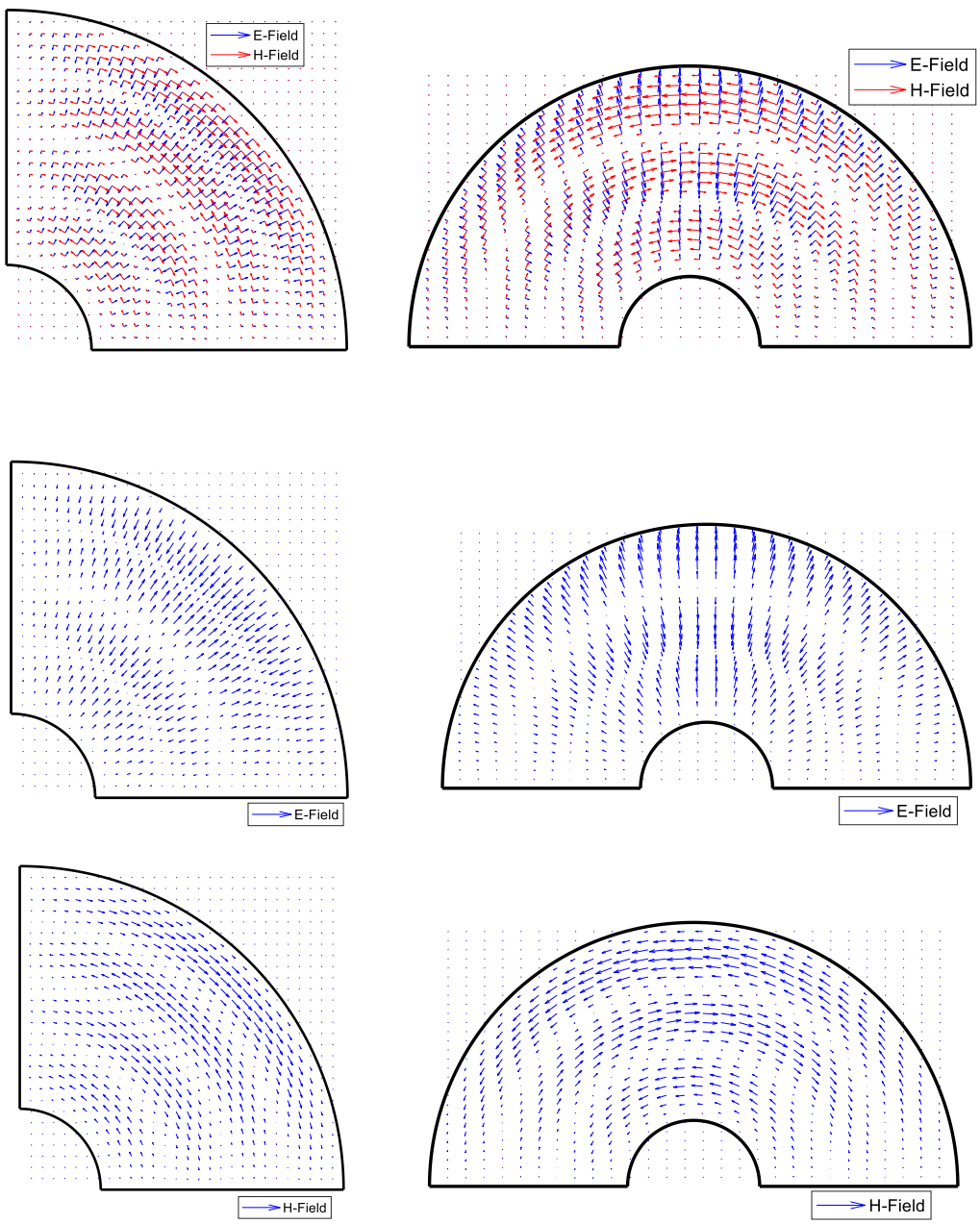

TM_{11} mode 90° sectoral-coaxial	TM_{11} mode 180° sectoral-coaxial
Inner radius, a = 1 cm	Inner radius, a = 1 cm
Outer radius, b = 4 cm	Outer radius, b = 4 cm
Cutoff frequency, fc = 24.5 GHz	Cutoff frequency, fc = 18.3 GHz
Operating frequency, f = 26 GHz	Operating frequency, f = 20 GHz

Figure 4.42: Field vectors of 90° and 180° sectoral coaxial waveguide for TM_{11} mode.

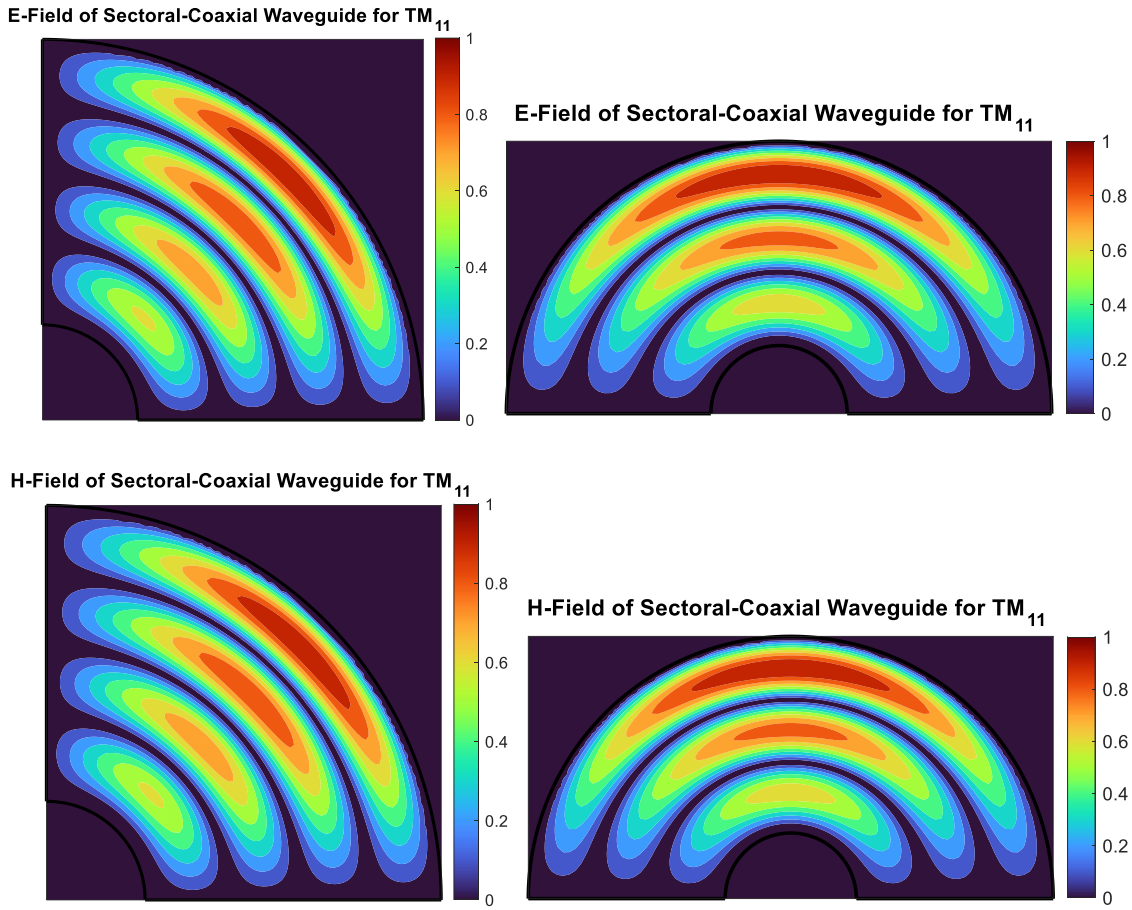

Figure 4.43: E-Field and H-Field of 90°and 180° sectoral-coaxial waveguide.

4.1.7 Baffle-Coaxial Waveguide

In the baffle-coaxial waveguide a conducting core and a metal plate is placed into the cylindrical waveguide as shown in Figure 2.5. Parameters screen of baffle-coaxial waveguide is shown in Figure 4.44. Like coaxial waveguide, it has inner and outer radius and since the baffle is inserted, the mode number m is replaced with p as the value of m is non integer.

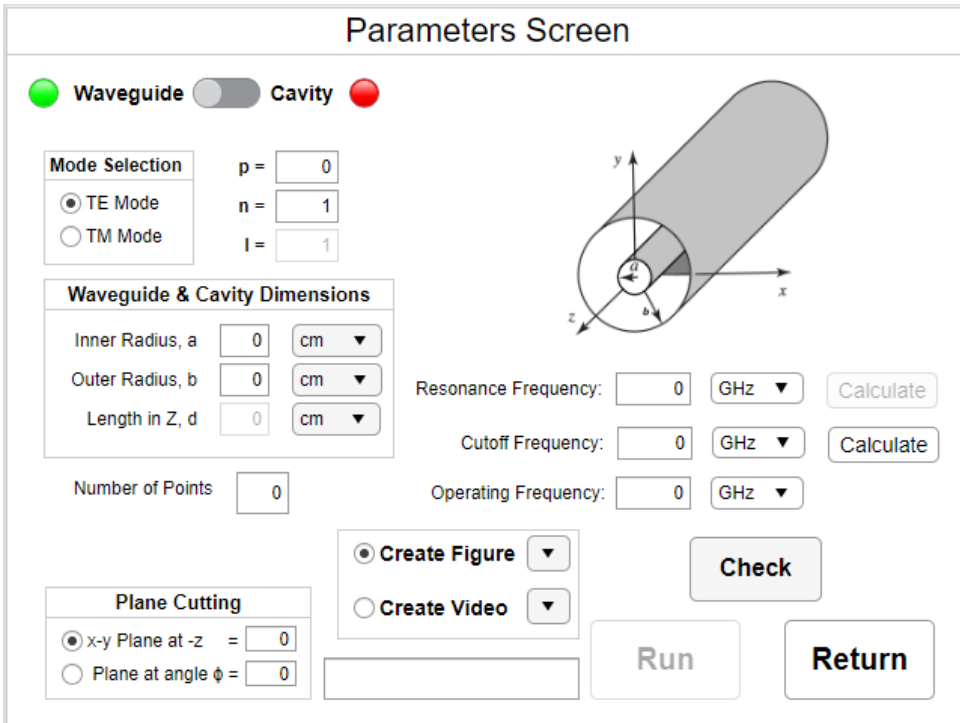

Figure 4.44: Parameters screen of baffle-coaxial waveguide.

Field vectors are shown in Figure 4.45.

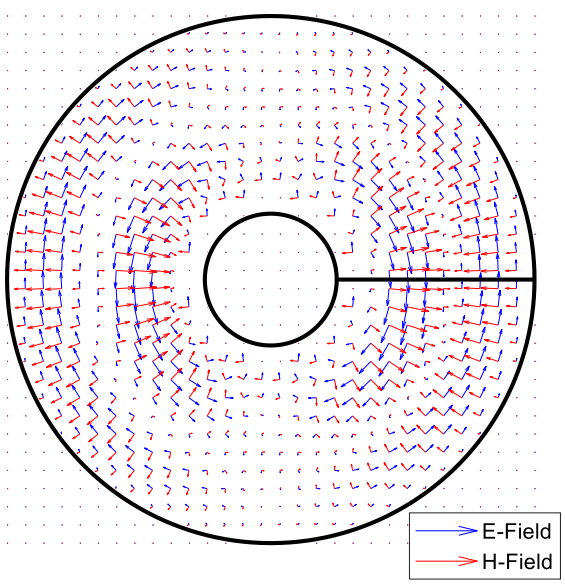

TE_{21} *mode*

Inner radius, a = 1 cm

Outer radius, b = 4 cm

fc = 8.78 GHz

f = 9 GHz

Figure 4.45: Field vectors of baffle-coaxial waveguide for TE_{21} mode.

Figure 4.45 continued.

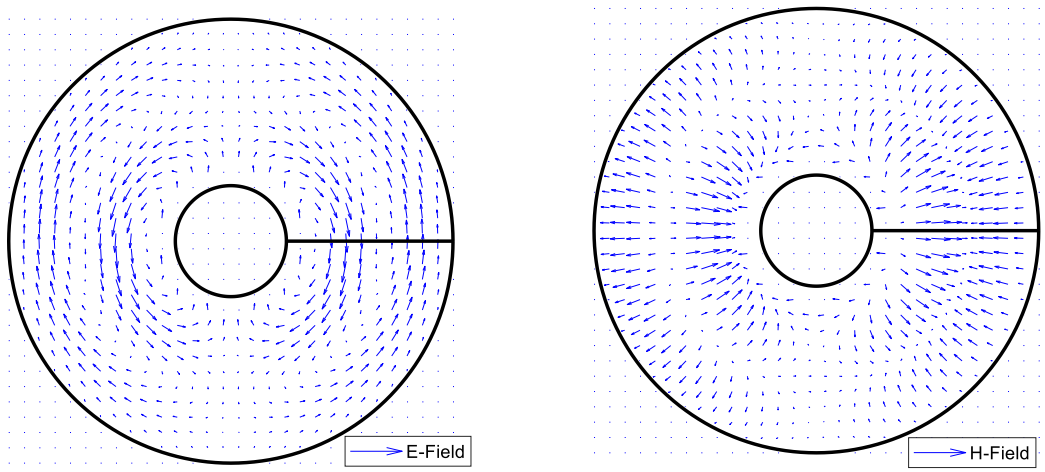

Electric and magnetic field intensity is shown in Figure 4.46.

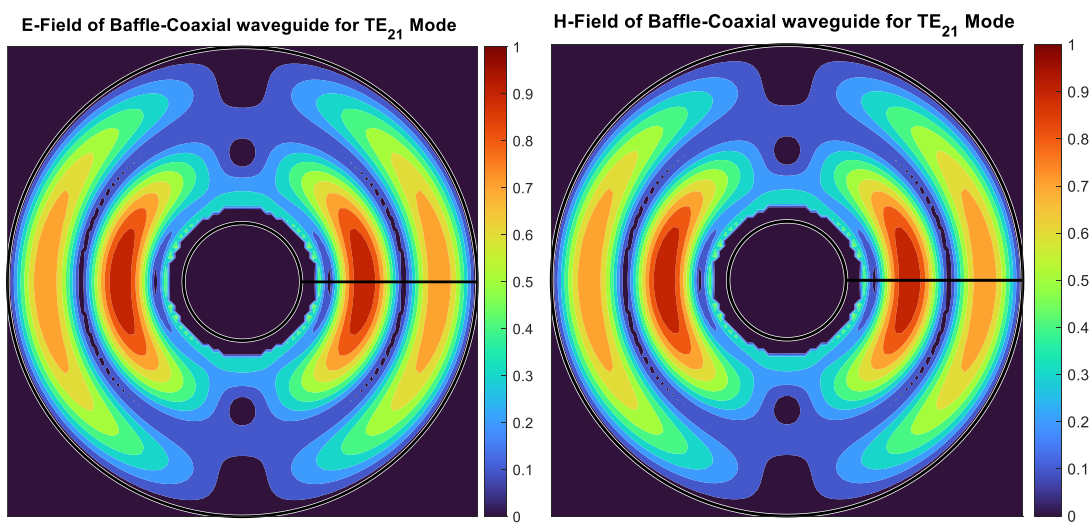

Figure 4.46: E-Field and H-Field of baffle-coaxial waveguide for TE_{21} mode.

4.2 Cavity

Switching to cavity mode, activates some input parameters in the parameters screen. Those input parameters have no function in the waveguide mode and that is why those are inactive in the waveguide mode. Illustrated examples have been given for rectangular and circular cavity.

4.2.1 Rectangular Cavity

Figure 4.47 shows the parameters screen for the rectangular cavity option. Green circles are activated after switching to the cavity and the red circle is deactivated. Proper valid input will draw electric and magnetic field distribution inside this shape. As in waveguide mode, warning messages are generated for invalid inputs.

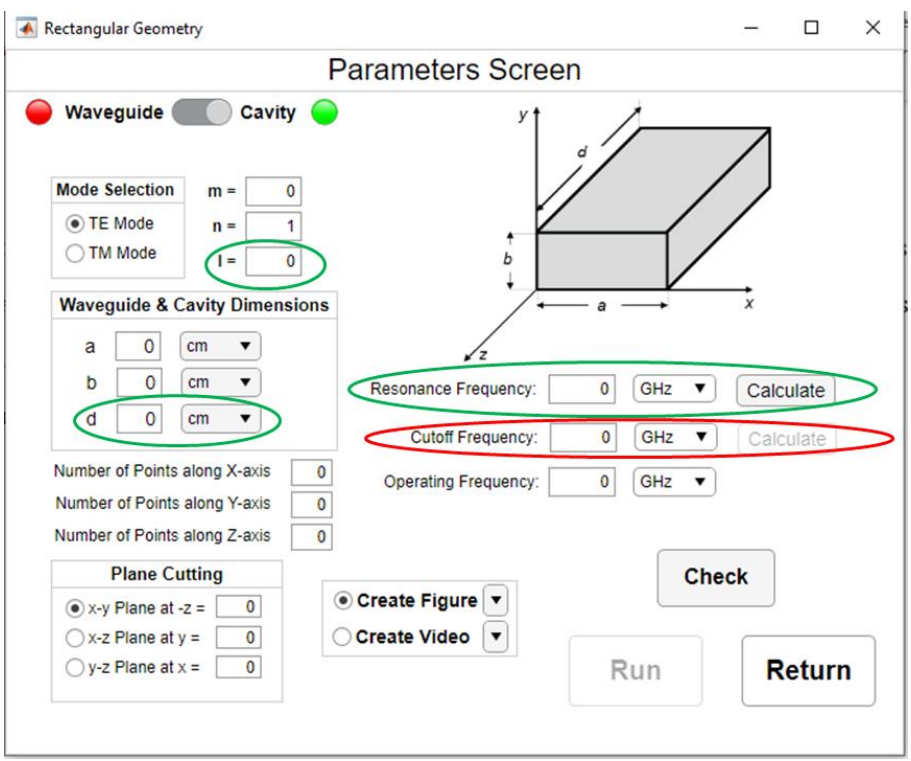

Figure 4.47: Parameters screen for rectangular cavity.

For some valid inputs, field distribution inside the rectangular cavity at different plane cuts is shown in Figures 4.48, 4.50, and 4.52. Electric and magnetic field strength at different plane cuts is shown in Figures 4.49, 4.51, and 4.53.

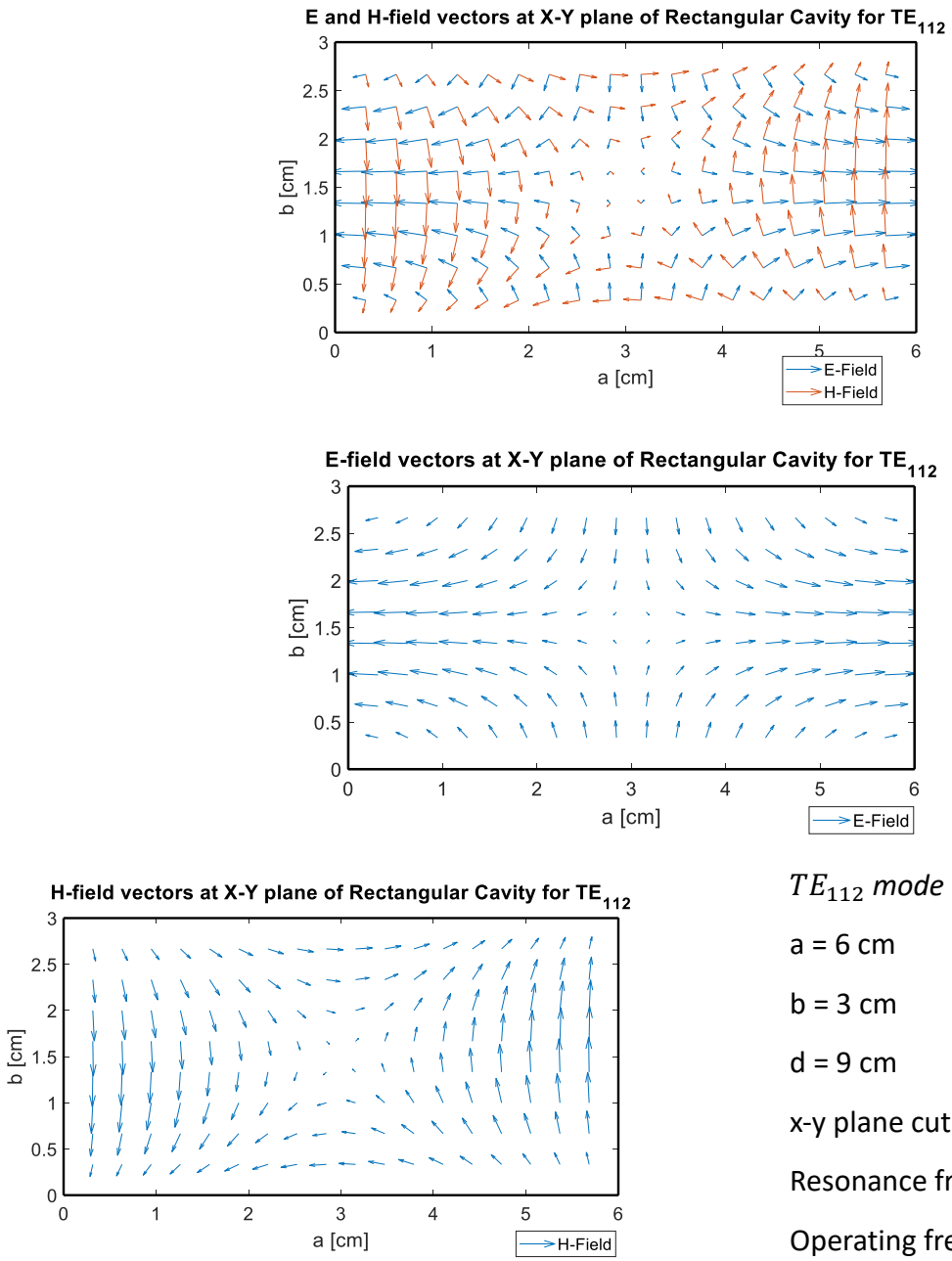

TE_{112} *mode*

a = 6 cm

b = 3 cm

d = 9 cm

x-y plane cut in -z = 8 cm

Resonance frequency, fr = 2.06 GHz

Operating frequency, f =2.0 GHz

Figure 4.48: Vector plot of rectangular cavity at x-y plane for TE_{112}.

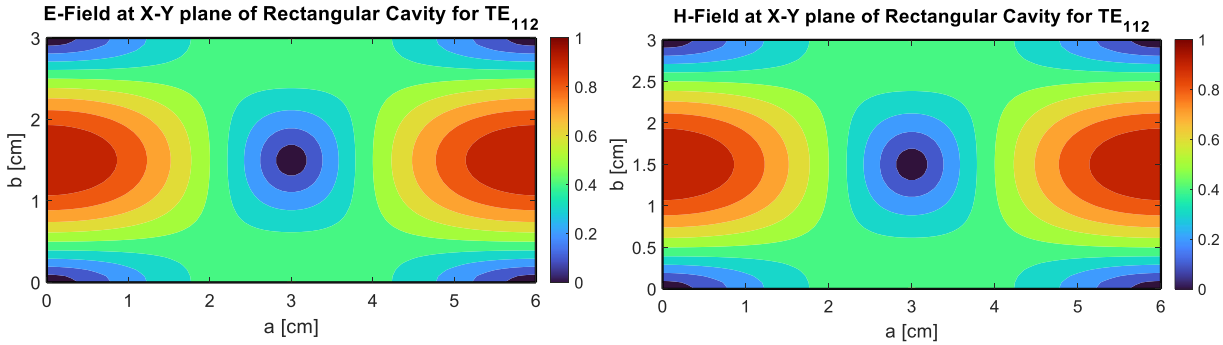

Figure 4.49: E-field and H-field of rectangular cavity at x-y plane for TE_{112}.

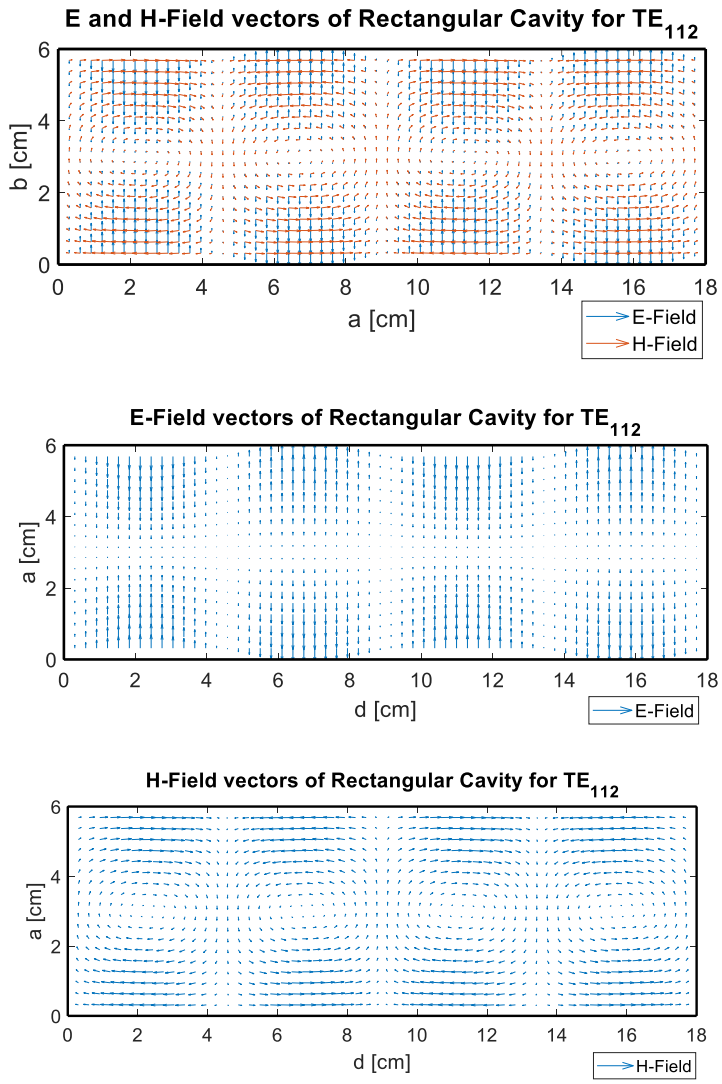

Figure 4.50: Vector plot of rectangular cavity at x-z plane for TE_{112}.

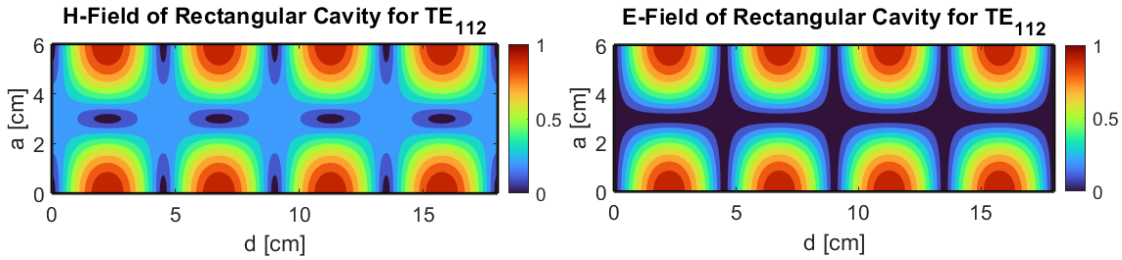

Figure 4.51: E-field and H-field of rectangular cavity at x-z plane for TE_{112}.

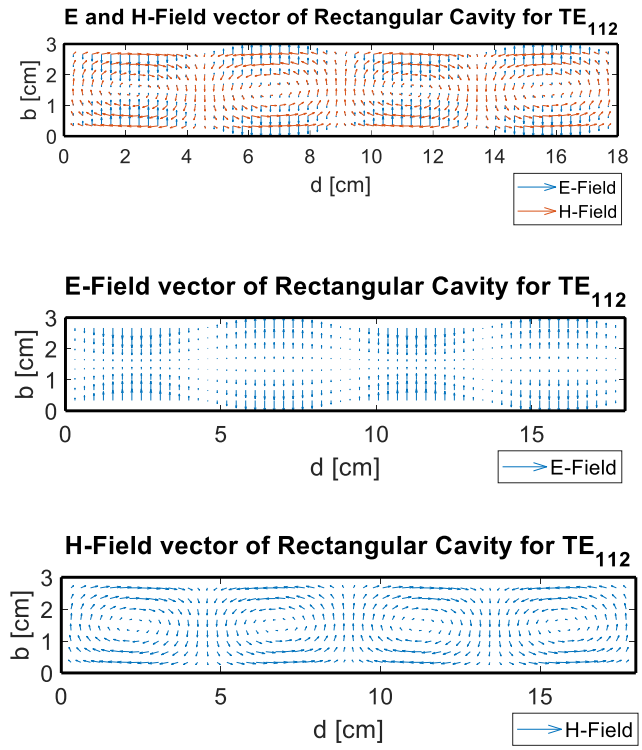

Figure 4.52: Vector plot of rectangular cavity at y-z plane for TE_{112}.

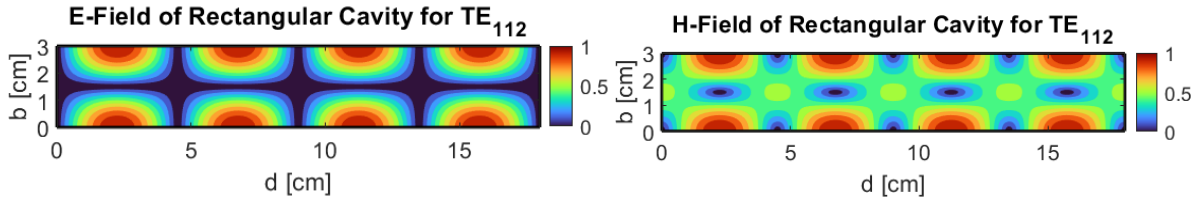

Figure 4.53: E-field and H-field with vector plot of rectangular cavity at y-z plane for TE_{112}.

4.2.2 Circular Cavity

As in the rectangular cavity parameters screen, circular cavity mode also enables the input of l in mode number and d in cavity dimension. It also activates the calculate button for resonant frequency (green circles) and deactivates the cut-off frequency calculate button (red circle). The parameters screen of the circular cavity is shown in Figure 4.54.

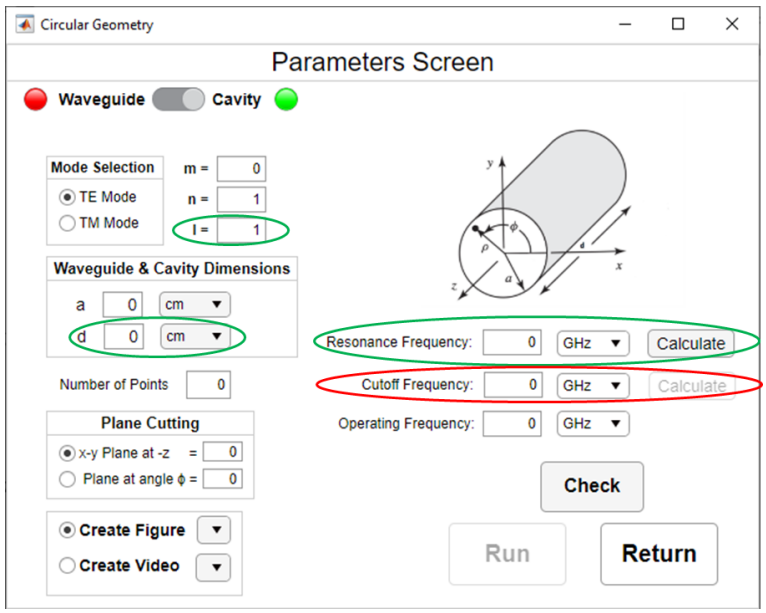

Figure 4.54: Parameters screen for circular cavity.

Figure 4.55 shows the E-field and H-field vectors inside the circular cavity by blue and red arrows, respectively. Electric and magnetic field strength inside that circular cavity is also shown in Figure 4.56 for TE_{221} mode.

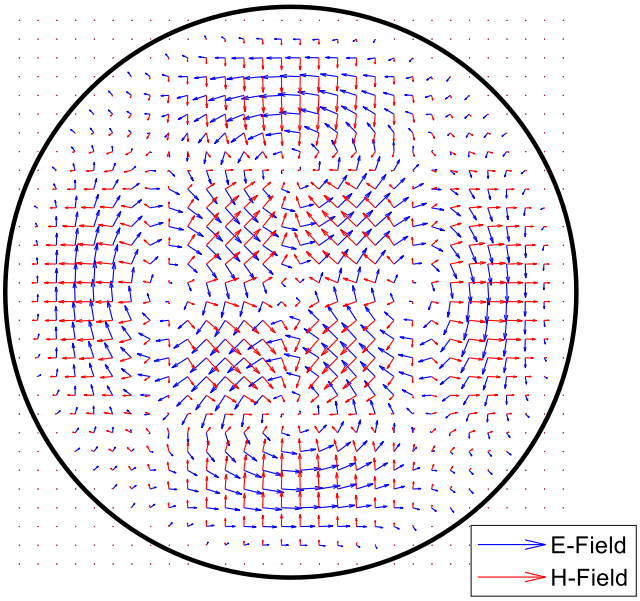

TE_{221} *mode*

Radius, a = 4 cm

Length, d = 9 cm

Resonance frequency, fr = 6.61 GHz

Operating frequency, f = 7 GHz

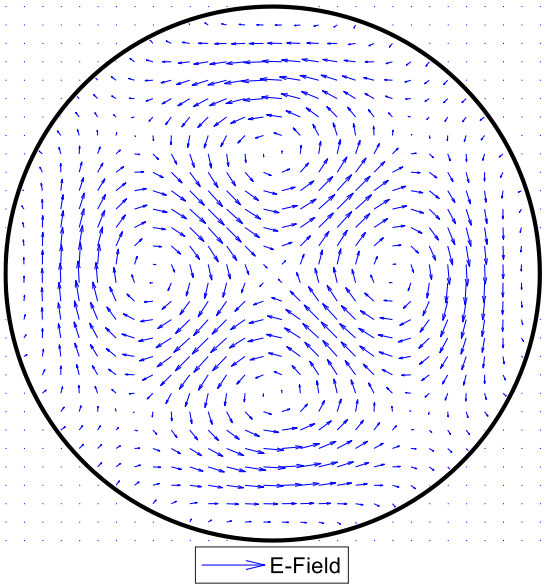

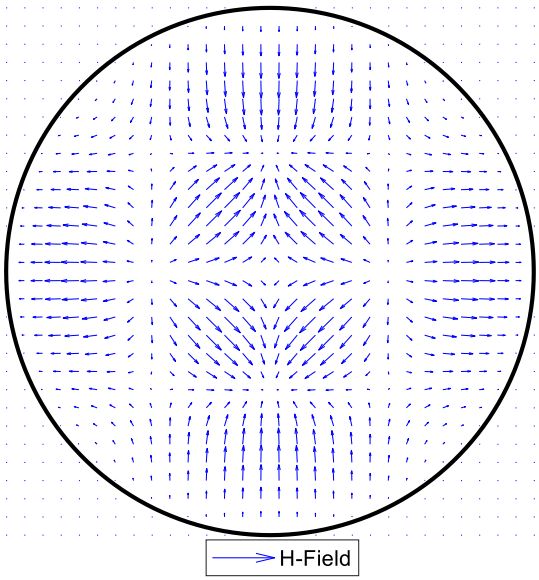

Figure 4.55: Vector plot of circular cavity at x-y plane for TE_{221}.

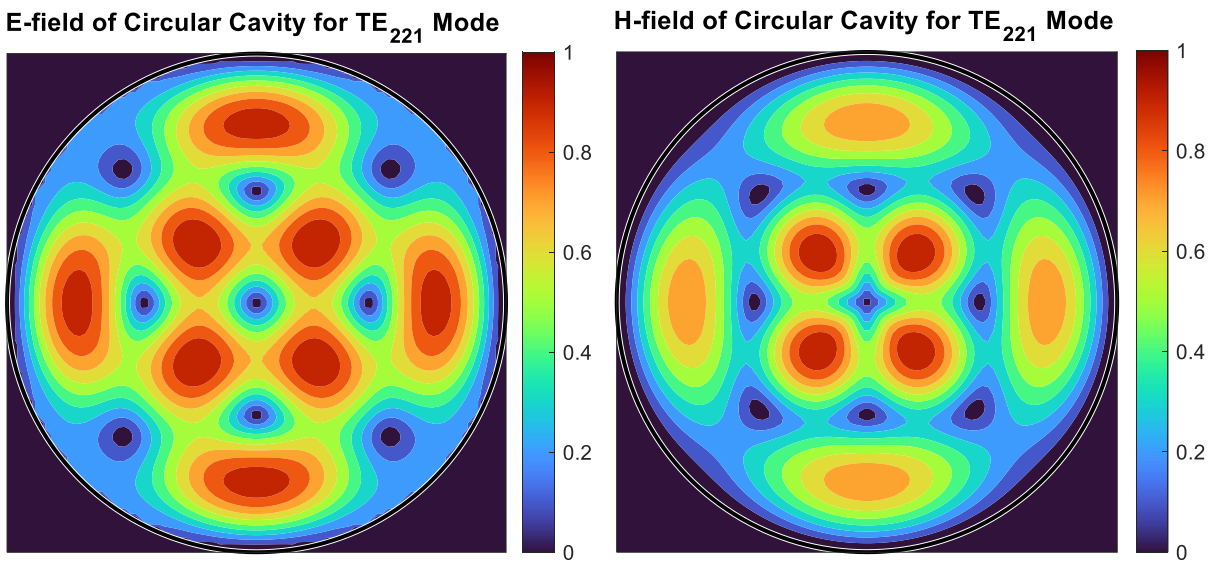

Figure 4.56: E-field and H-field of circular cavity at x-y plane for TE_{221}.

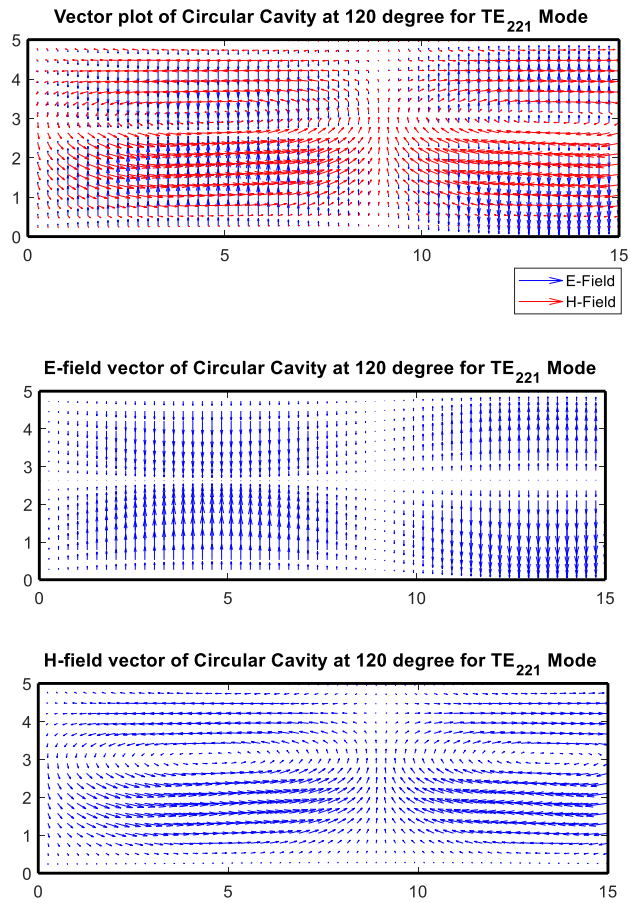

Figure 4.57: Vector plot of circular cavity at 120° plane cut for TE_{111}.

Similarly, at 120° plane cut of the circular cavity, vector plot and E-field and H-field distribution with strength are shown in Figure 4.57 and 4.58 for the same mode number TE_{221}.

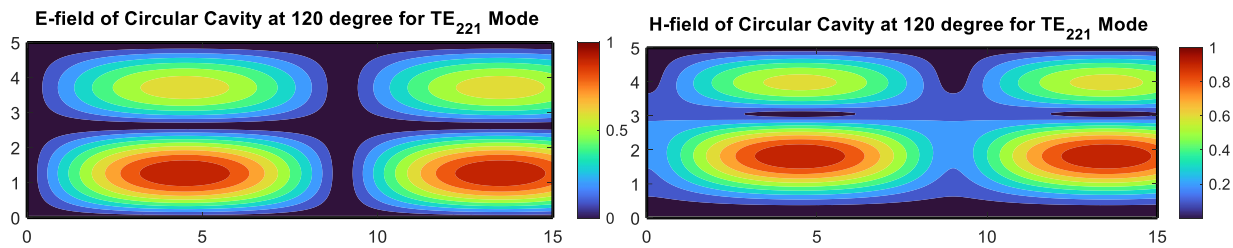

Figure 4.58: E-field and H-field of circular cavity at 120°plane cut for TE_{111}.

The rest of the parameters screen for different cross-sections are similar to the parameters screen presented in the previous section. Only the cavity switch activates some input parameters and calculates resonance frequency for the cavity. Meanwhile, switching to cavity, nulls the cut-off frequency value which was calculated in the waveguide mode. For this reason, no parameters screen is shown for the rest of the cross-sections.

4.2.3 Coaxial Cavity

Vector plot of coaxial cavity is shown in Figure 4.59. For example, TM mode is selected, and the mode value is taken $m = 2, n = 1, l = 1$.

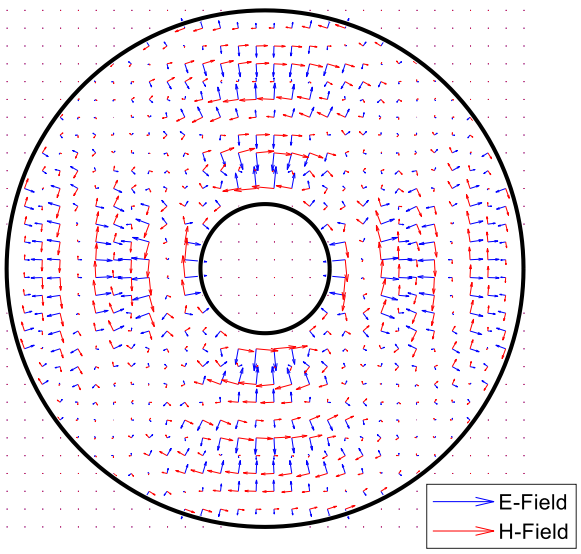

TM_{211} *mode*

Inner radius, a = 1 cm

Outer radius, b = 4 cm

Length, d = 9 cm

Resonance frequency, fr = 24.56 GHz

Operating frequency, f = 25 GHz

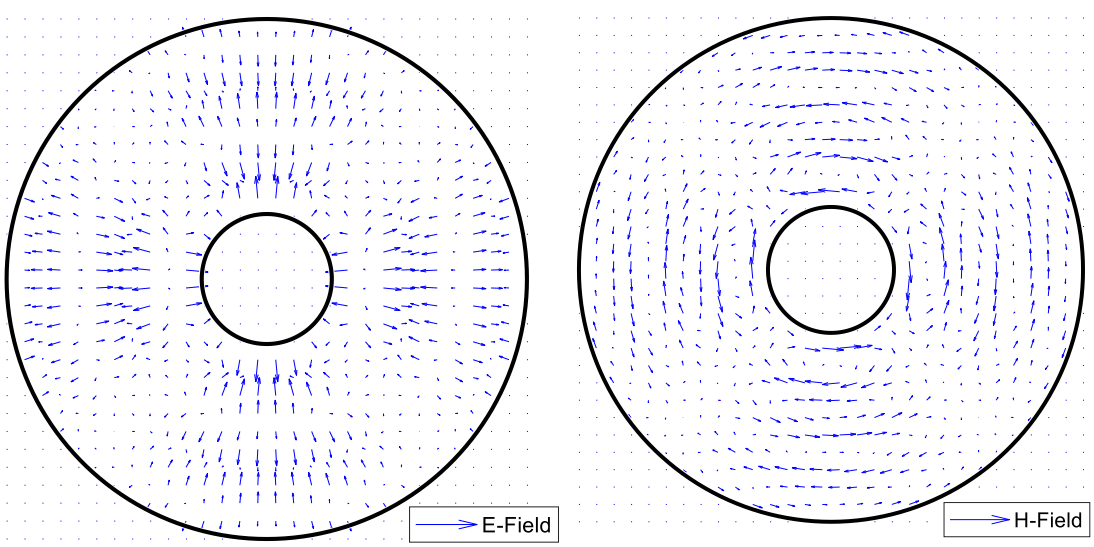

Figure 4.59: Field vectors of coaxial cavity for TM_{211} mode.

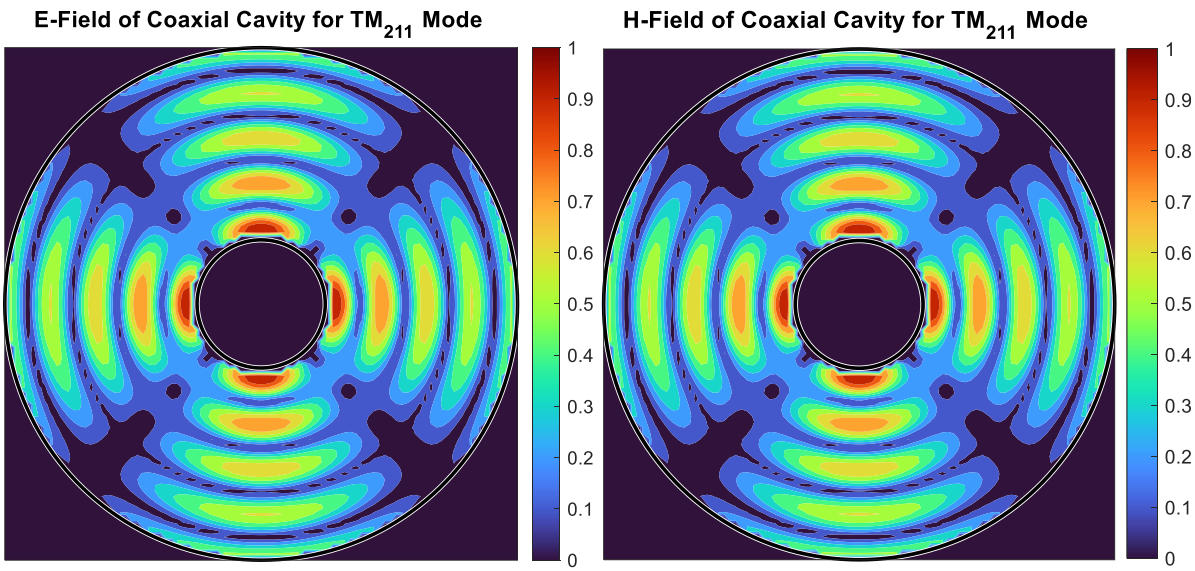

Figure 4.60: E-field and H-field of coaxial cavity for TM_{211} mode.

4.2.4 Sectoral Cavity

Similarly sectoral waveguide, sectoral cavity has the flexibility to have any angle from 0 to 360-degree. Field vectors for 180° and 120° sectoral cavity are illustrated in Figure 4.61 and 4.63, respectively. TM_{212} mode is selected for 180° sectoral and TM_{121} mode is selected for 120-degree sectoral cavity. E-Field and H-Field of both sectoral cavity resonators are shown in Figure 4.62 and Figure 4.64.

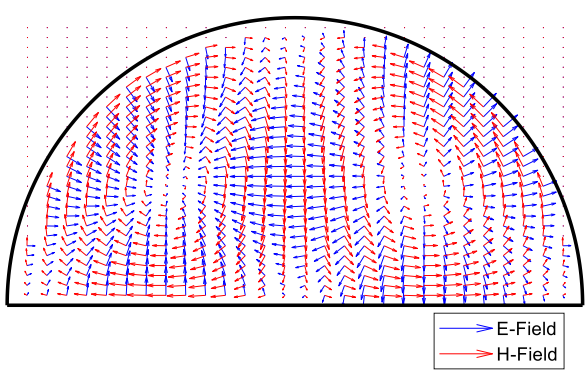

TM_{212} mode

Radius, a = 5 cm

Length, d = 9 cm

Resonance frequency, fr = 5.93 GHz

Operating frequency, f = 6 GHz

Figure 4.61: Field vectors of 180° sectoral cavity for TM_{212} mode.

Figure 4.61 continued.

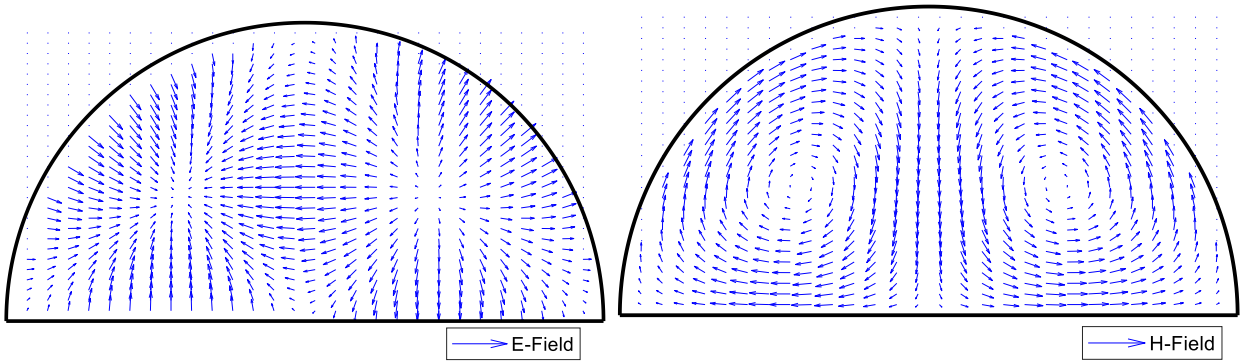

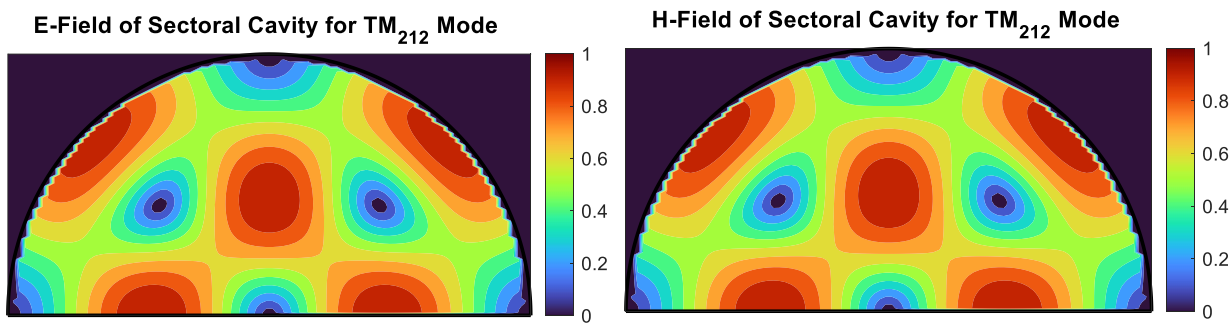

Figure 4.62: E-Field and H-Field of 180° sectoral cavity for TM_{212} mode.

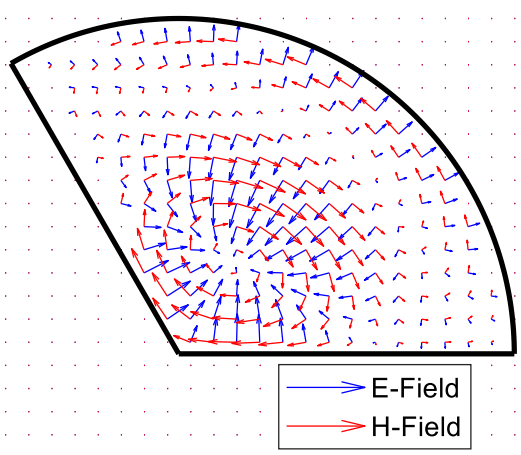

TM_{121} mode

Radius, a = 5 cm

Length, d = 9 cm

Resonance frequency, fr = 7.56 GHz

Operating frequency, f = 7 GHz

Figure 4.63: Field vectors of 120° sectoral cavity for TM_{121} mode.

Figure 4.63 continued.

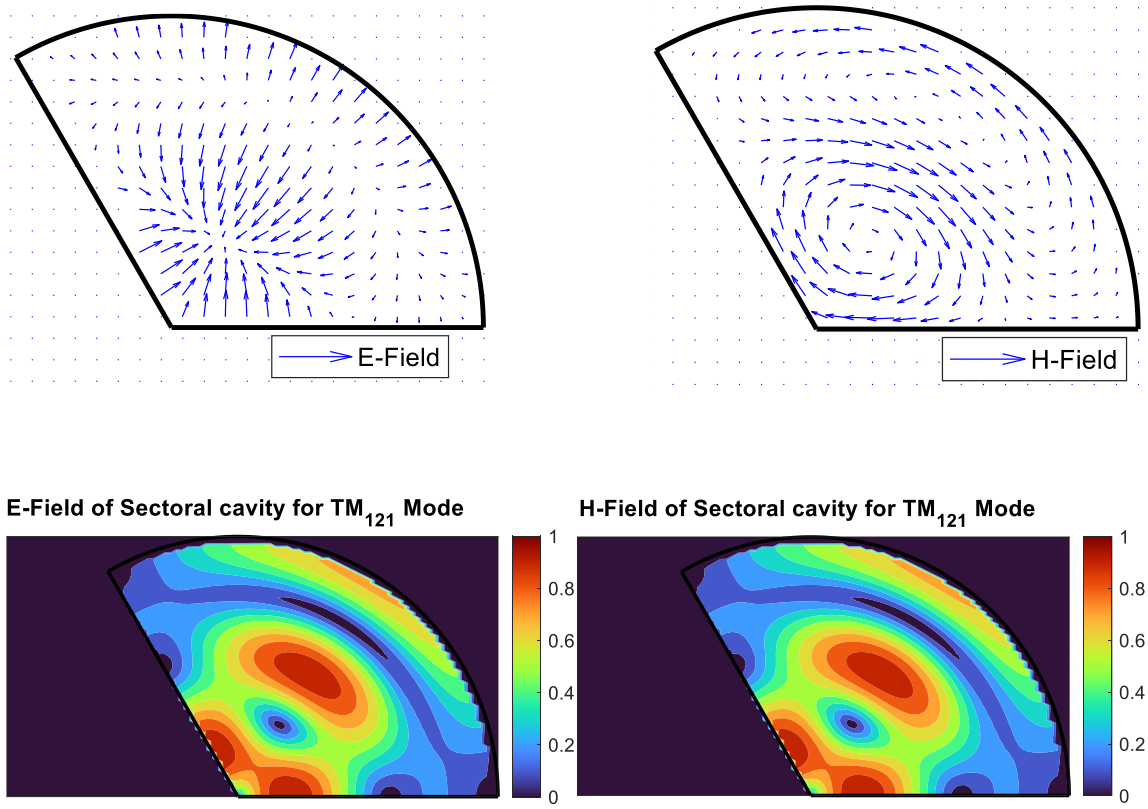

Figure 4.64: E-Field and H-Field of 120° sectoral cavity for TM_{121} mode.

4.2.5 Baffle Cavity

Electric and magnetic field vectors of the baffle cavity are shown in Figure 4.65. These figures show the electric and magnetic field orientations inside this cross-section. Figure 4.66 shows where the intensity of the field is higher. It can be shown that at the center of the cavity field strength is much higher than around the boundary wall.

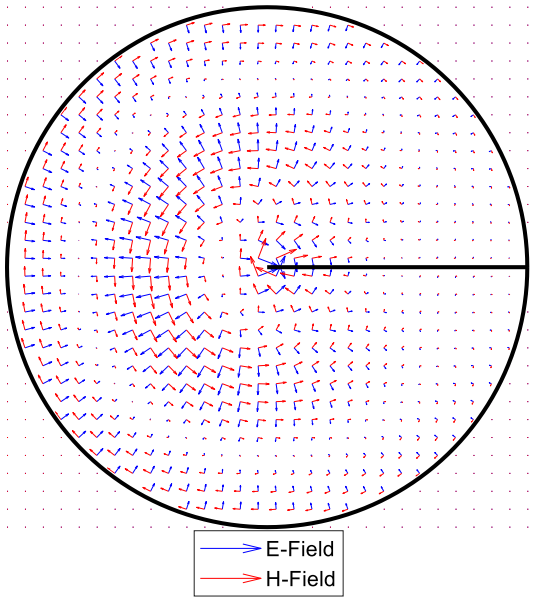

TM_{122} *mode*

Radius, a = 5 cm

Length, d = 9 cm

fr = 6.86 GHz

f = 7 GHz

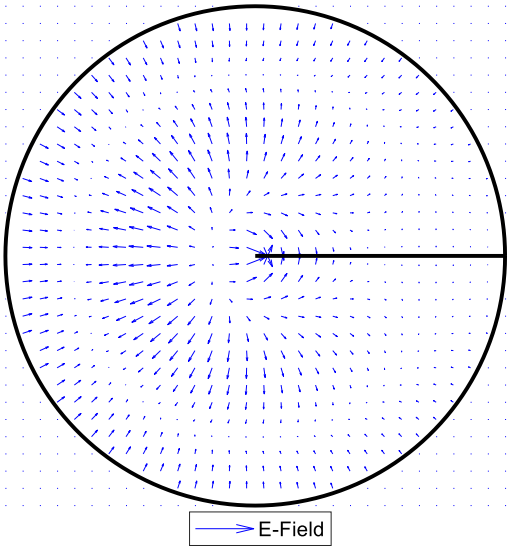

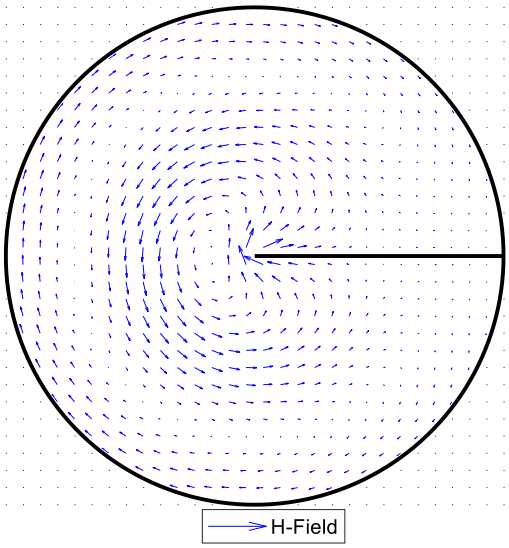

Figure 4.65: Field vectors of baffle cavity for TM_{122} mode.

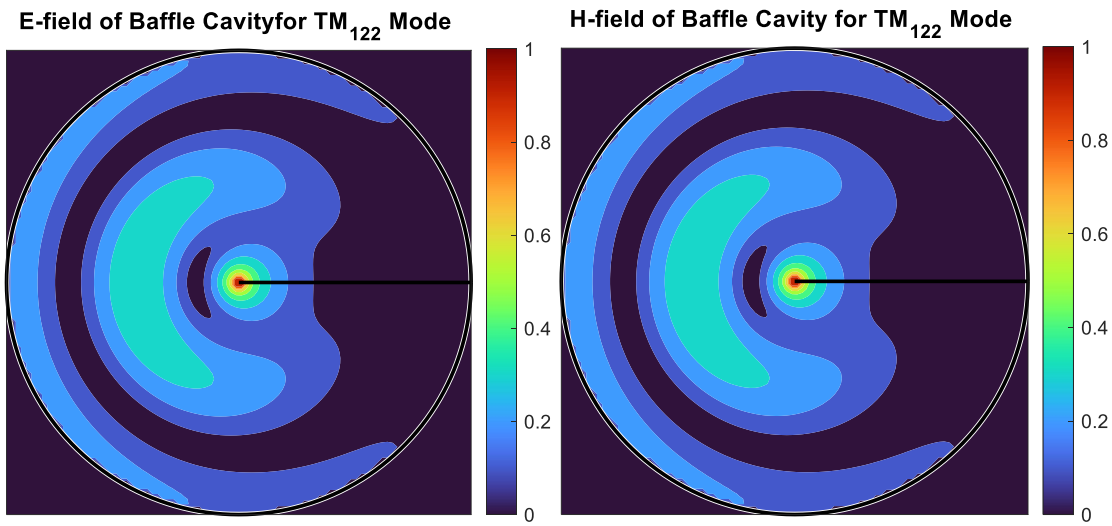

Figure 4.66: E-Field and H-Field of baffle-coaxial cavity for TM_{122} mode.

4.2.6 Sectoral-Coaxial Cavity

Like the sectoral-coaxial waveguide, this cavity structure has a conducting core inside and may be formed by arbitrary angles. Field vectors of 45° sectoral-coaxial cavity for TM_{211} mode is shown is Figure 4.67. Field strength is also presented in Figure 4.68.

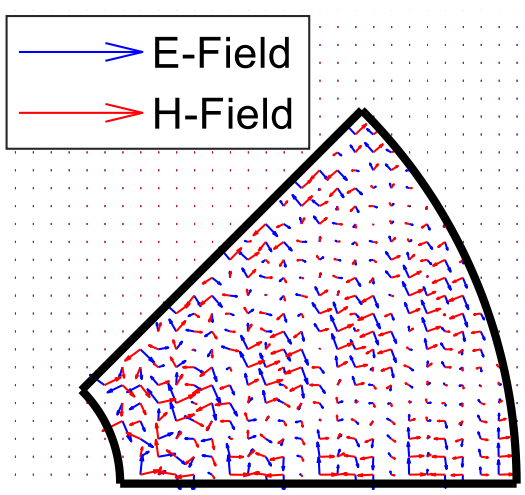

TE_{211} *mode*

Inner radius, a = 1 cm

Outer radius, b = 4 cm

Length, d = 9 cm

Resonance frequency, fr = 46.06 GHz

Operating frequency, f = 46 GHz

Figure 4.67: Field vectors of 45° sectoral-coaxial cavity for TM_{211} mode.

Figure 4.67 continued.

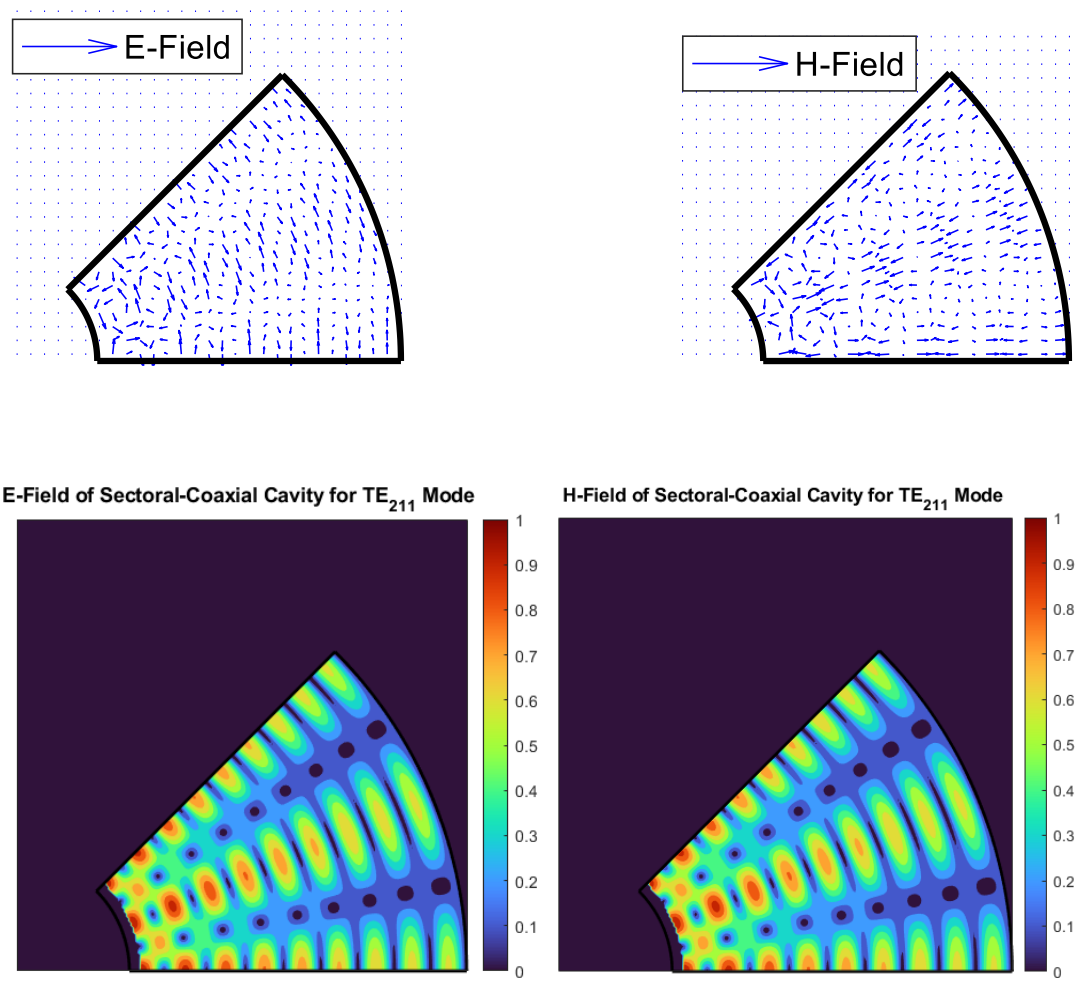

Figure 4.68: E-Field and H-Field of sectoral-coaxial cavity for TM_{211} mode.

4.2.7 Baffle-Coaxial Cavity

As previously mentioned, a conducting core and a metal plate is placed inside the baffle-coaxial cross-section. Unlike waveguide, cavity has a finite dimension along -z axis direction. Here, TE_{212} mode is selected to show the field vectors and field intensity of this cavity structure (see Figure 4.69 and Figure 4.70). From both figures, it is clearly noticeable that fields is only present in the hollow region and not in the conduction core.

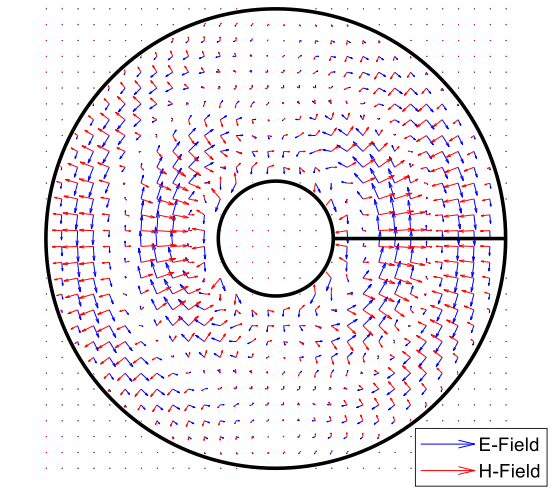

TE_{212} mode

Inner radius, a = 1 cm

Outer radius, b = 4 cm

Length, d = 9 cm

Resonance frequency, fr = 9.39 GHz

Operating frequency, f = 9 GHz

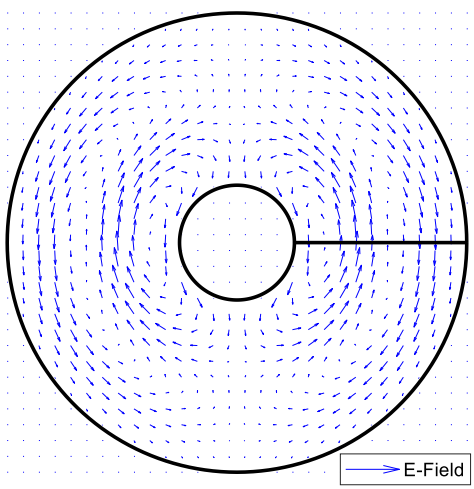

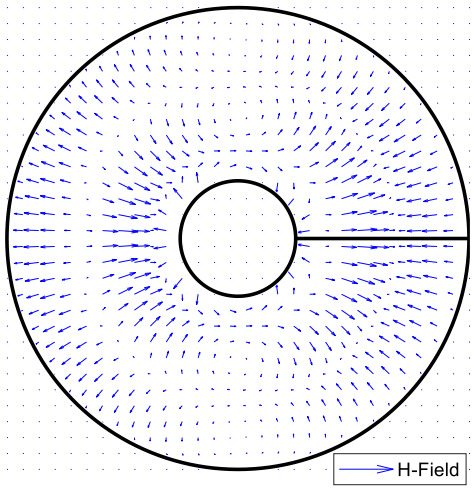

Figure 4.69: Field vectors of baffle-coaxial cavity for TE_{212} mode.

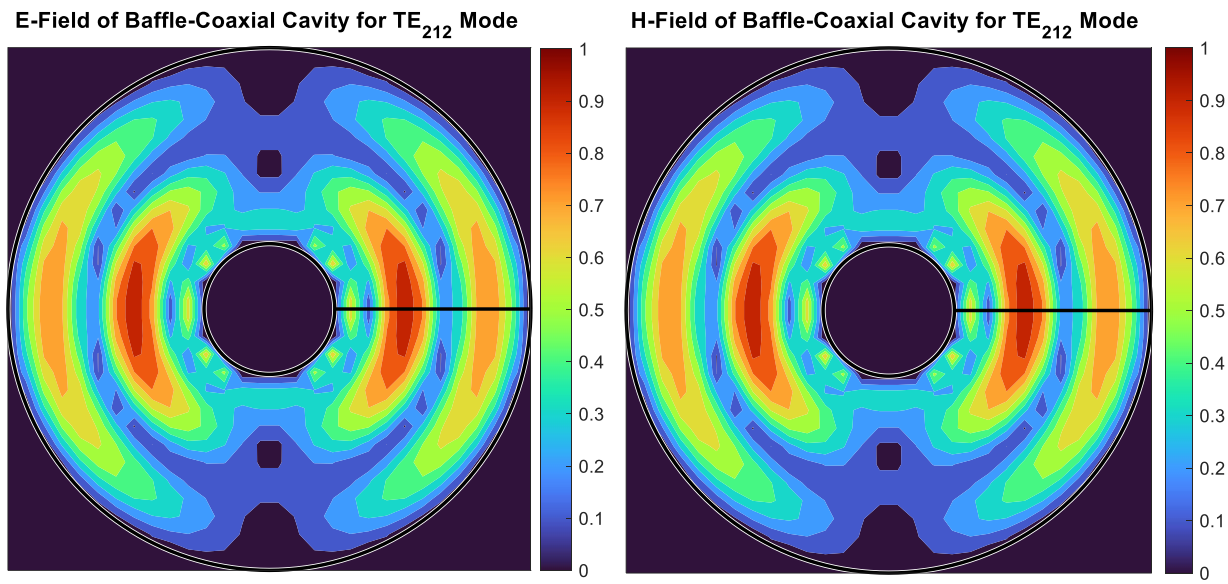

Figure 4.70: E-Field and H-Field of baffle-coaxial cavity for TE_{212} mode.

This chapter provided illustrated examples for various cross-sections of waveguide and cavity resonator configurations. For rectangular cross-section, users can view the field pattern in x-y, x-z and y-z axis. For cylindrical cross-sections, users can view field distribution in x-y axis and in any arbitrary angle between 0° and 360°. However, since the sectoral cross-sections limits the geometry structure with the angle ϕ_0, users can observe field pattern between 0° and ϕ_0 degrees. If users input in the view angle is greater than the sectoral angle ϕ_0, for sectoral and sectoral-coaxial cross-sections, WGC will show warning messages.

CHAPTER 5

CONCLUSIONS

This thesis is the rework of the waveguide and cavity software (WGC version 2.1) built by Dr. Atef Z. Elsherbeni and Dr. Clayborne Taylor for the IBM-PC computer family. Coding languages used to build WGC (version 2.1) are no longer available which rendered the software unusable. The revival of the software was essential to compute and visualize the electric and magnetic fields inside waveguides and cavity resonators on current computing platforms. Several enhancements were made to make the software more powerful and user-friendly.

5.1 Summary of Results

The software package presented in this thesis WGC (version 3) has been developed in the MATLAB App designer platform. WGC's graphical user interface (GUI) is easy to use and self-explanatory. The main window provides information about the software and the contact info of the authors. Users are able to select one of the seven cross-sections listed by names along with graphical representation. Based on selected cross-section, the appropriate parameters screen is displayed to allow the user to enter physical dimensions, operating frequency and select how to visualize the results. Warning messages are generated for invalid input parameters. WGC allows users to save the computed field values for comparison and validation against theoretical calculations and measurements.

5.2 Implications

With the growing needs of modern technology, microwave engineering has been developed in an unprecedented way. New technology and new research ideas are coming from the people's

demand. To enhance the technology further, researchers need to understand the core of this field and that is how electromagnetic wave propagation through the transmission lines and how it reacts in an enclosed boundary wall. This thesis work provides the electromagnetic field characteristics inside transmission lines (waveguide) and cavity resonators by designing user friendly software. It presents the field distribution inside seven different geometrical shapes not only by showing pictures but also by creating videos of those. Researchers and students can fully visualize the electric and magnetic field distribution inside those cross-sections for a different mode of operations.

5.3 Future Work

Performance evaluation of WGC through comparisons with HFSS and CST's computational time and memory requirements for similar waveguides and cavity resonators problem, may be conducted for benchmarking purposes. Future work also includes research on the development of mathematical expressions for dielectric, partially filled, and rigid waveguides and cavity resonators for inclusion as modelling options in the software.

REFERENCES

[1] K. S. Packard, “The origin of waveguides: A case of multiple rediscovery,” IEEE Transactions on Microwave Theory and Techniques, vol. 32, no. 9, pp. 961–969, 1984.

[2] S. Farjana, M. Ghaderi, A. U. Zaman, S. Rahiminejad, P. Lundgren, and P. Enoksson, “Low-loss gap waveguide transmission line and transitions at 220–320 GHz Using Dry Film Micromachining,” IEEE Transactions on Components, Packaging and Manufacturing Technology, vol. 11, no. 11, pp. 2012–2021, 2021.

[3] Y. Zhao et al., “RF evanescent-mode cavity resonator for passive wireless sensor applications,” Sensors and Actuators A: Physical, vol. 161, no. 1–2, pp. 322–328, 2010.

[4] A. Sahu, V. K. Devabhaktuni, R. K. Mishra, and P. H. Aaen, “Recent advances in theory and applications of substrate-integrated waveguides: a review,” International Journal of RF and Microwave Computer-Aided Engineering, vol. 26, no. 2, pp. 129–145, 2016.

[5] A. Z. Elsherbeni and C. D. Taylor, “Interactive visualizations of electromagnetic fields inside waveguides and cavity resonators using the WGC program,” Computer Applications in Engineering Education, vol. 2, no. 2, pp. 97–107, 1994.

[6] F. D. Mbairi and H. Hesselbom, “High frequency design and characterization of SU-8 based conductor backed coplanar waveguide transmission lines,” in Proceedings. International Symposium on Advanced Packaging Materials: Processes, Properties and Interfaces, 2005., 2005, pp. 243–248.

[7] I. Jeong et al., “High-performance air-gap transmission lines and inductors for millimeter-wave applications,” IEEE Transactions on Microwave Theory and Techniques, vol. 50, no. 12, pp. 2850–2855, 2002.

[8] F. Taringou, D. Dousset, J. Bornemann, and K. Wu, “Substrate-integrated waveguide transitions to planar transmission-line technologies,” in 2012 IEEE/MTT-S International Microwave Symposium Digest, 2012, pp. 1–3.

[9] J. Shi, H. Chen, S. Zheng, D. Li, R. Rimmer, and H. Wang, “Comparison of measured and calculated coupling between a waveguide and an RF cavity using CST microwave studio,” Thomas Jefferson National Accelerator Facility, Newport News, VA, techreport, 2006.

[10] E. Pucci, A. U. Zaman, E. Rajo-Iglesias, P.-S. Kildal, and A. Kishk, “Losses in ridge gap waveguide compared with rectangular waveguides and microstrip transmission lines,” in Proceedings of the Fourth European Conference on Antennas and Propagation, 2010, pp. 1–4.

[11] N. A. Amoli et al., “Screen-Printed Flexible Coplanar Waveguide Transmission Lines: Multi-Physics Modeling and Measurement,” in 2019 IEEE 69th Electronic Components and Technology Conference (ECTC), 2019, pp. 249–257.

[12] S. H. Kamath, R. Arora, and V. Agarwal, “Studying the characteristics of a rectangular Waveguide using HFSS,” International Journal of Computer Applications, vol. 118, no. 21, pp. 5–8, 2015.

[13] Y. Zhou, H. Liu, E. Li, G. Guo, and T. Yang, “Design of a wideband transition from double-ridge waveguide to microstrip line,” in 2010 International Conference on Microwave and Millimeter Wave Technology, 2010, pp. 737–740.

[14] Microwave Journal, “Software for optimizing the design and low-cost production of waveguide filters,” *Zeland Software Inc., Fremont, CA*, [Online]. Available: https://www.microwavejournal.com [Accessed: March 24, 2022].

[15] REMCOM, “How to build a rectangular waveguide in XFdtd,” *Remcom Inc State College, PA*, [Online]. Available: https://www.remcom.com [Accessed: March 22, 2022]

[16] M. Al Ameen, J. Liu, and K. Kwak, “Security and privacy issues in wireless sensor networks for healthcare applications,” Journal of medical systems, vol. 36, no. 1, pp. 93–101, 2012.

[17] N. N. Rao, “PC-assisted instruction of introductory electromagnetics,” IEEE Transactions on Education, vol. 33, no. 1, pp. 51–59, 1990.

[18] E. Sheina, A. Smirnov, and Y. Shestopalov, “Optimal parameters of a multi-frequency experiment in an inverse problem of determining the dielectric constant of an inclusion in free space and in a waveguide,” Measurement, vol. 187, p. 110357, 2022.

[19] M. Benson, Fields, waves and transmission lines. Springer Science & Business Media, 2012.

[20] A.Z. Elsherbeni and C.D. Taylor, Jr., Electromagnetic Fields Inside Waveguides and cavity resonators; WGC (version 2.1). Software Book II, Center on Computer Applications for Electromagnetic Education (CAEME), 1994.

[21] A. E. Forooshani, S. Bashir, D. G. Michelson, and S. Noghanian, “A survey of wireless communications and propagation modeling in underground mines,” IEEE Communications surveys & tutorials, vol. 15, no. 4, pp. 1524–1545, 2013.

[22] A. Webb, “Cavity-and waveguide-resonators in electron paramagnetic resonance, nuclear magnetic resonance, and magnetic resonance imaging,” Progress in nuclear magnetic resonance spectroscopy, vol. 83, pp. 1–20, 2014.

[23] MathWorks, “App Designer-Create desktop and web apps in MATLAB,” *Mathworks Natick, MA*, [Online]. Available: https://www.mathworks.com [Accessed: August 01, 2021].

[24] C. A. Balanis, Advanced engineering electromagnetics. John Wiley & Sons, 2012.

[25] A. Elsherbeni, D. Kajfez, and S. Zeng, “Circular sectoral waveguides,” IEEE Antennas and Propagation Magazine, vol. 33, no. 6, pp. 20–27, 1991.

[26] Mitheran, S., Narayanan, R. T., & Singaravelu, R. (2022). User-Friendly Waveguide Mode Visualizer [Educator’s Corner]. IEEE Microwave Magazine, 23(5), 96–100.

[27] Jason Nicholson (2022). Bessel Zero Solver (https://www.mathworks.com/matlabcentral/fileexchange/48403-bessel-zero-solver), MATLAB Central File Exchange. Retrieved April 22, 2022.

[28] Arfken, G. B., & Weber, H. J. (1999). Mathematical methods for physicists. American Association of Physics Teachers.

APPENDIX A

ZEROS FOR BESSEL FUNCTION

In the above equations, the term X_{mn} and X'_{mn} are the zeros of the 1st and the derivative of the 1st kind of the Bessel function. There are numerous ways to find the roots of the Bessel function. The programming code that is used in the software package uses Halley's method to generate zeros. There are two MATLAB files developed, one to generate zeros for the Bessel function for 1st kind and its derivative, another one is to generate zeros for the combination of 1st and 2nd kind of Bessel function and their derivatives. The latter one is described in section 2, equation number 2.31 which is used for TE and TM modes for coaxial cross-section. Two files are documented as “besselzeros.m” and “gmzeros.m.” The programming of these two files is based on the program provided in [27].

For the “besselzeros.m” there are three inputs. “m” is the order of the Bessel function which can be a scalar, vector, or matrix. “m” can be positive, negative, fractional, or any combination. “n” is the number of zeros to calculate. “kind” is either 1 or 2. The selection of kind = 1 generates zeros for the Bessel function 1st kind and the selection of 2 will generate zeros for the derivative of the 1st kind Bessel function. When kind is not supplied, the default is kind = 1.

“gmzeros.m” coding script has been developed to calculate the zeros of the combination of Bessel and Neuman functions. This coding script has four inputs (m, k, B, kind). The functionality of the inputs m, k, and kind is the same as “besselzeros.m.” “m” is the order of the Bessel and Neuman function, “k” is the number of zeros and “kind” is either 1 or 2. The input

“B” is the constant which is used to calculate values of Bessel and Neuman function. This “gmzeros.m” code calculates the zeros for the combination of Bessel and Neuman functions and the derivative of the combination of Bessel and Neuman functions.

The algorithm for finding the zeroes is based on the approximation of the first three roots of any order Bessel by a simple equation. These equations were generated using a least-squares fit of the roots. The approximation is used to start the iteration of Halley's method. The 4th and higher roots can be approximated by understanding the roots are regularly spaced for a given order. Once the 2nd and 3rd roots are found, the spacing can be approximated by the distance between the 2nd and 3rd root. Then again Halley's method can be applied to precisely locate the root. Some modifications of the program from [27] were necessary to generate zeros for the purpose of the thesis. The function used in this thesis is given below.

A1: Matlab Programming

```
%-----------------------------------------------
%% besselzeros.m
% Program to find roots of the Bessel function
% Last Modified on April 16, 2022
%%%%% Modified By Zahid Hasan %%%%%%
%-----------------------------------------------

 function x = besselzeros(m, n, kind)
%% Input checking
assert(nargin >=1 | nargin <=3,'Wrong number of input arguments.');
% Take care of default cases of k and kind
if nargin < 2
    n = 5;
end
if nargin < 3
    kind = 1;
end
assert(isscalar(kind) & any(kind == [1 2]), '''kind''must be a scalar with
value 1 or 2 only.');
assert(isscalar(n) & fix(n)==n & n>0, 'k must a positive scalar integer.');
assert(all(isreal(m(:))), 'n must be a real number.');
% negative orders have the same roots as the positive orders
m = abs(m);
% Check for that n is less than the ORDER_MAX
if kind==1
    ORDER_MAX = 146222.16674537213;
    assert(all(m <= ORDER_MAX), 'all n values must be less than or equal
%6.10f for kind=1.', ORDER_MAX);
elseif kind==2
    ORDER_MAX = 370030.762407380;
    assert(all(m(:) <= ORDER_MAX), 'all n values must be less than or equal
%6.10f for kind=2.', ORDER_MAX);
end
%% Setup Arrays
% output size
mSize = size(m);
if mSize(end) ==1
    outputSize = [mSize(1) n];
else
    outputSize = [mSize(1) n];
end
% number of orders for each kth root
nOrdersPerRoot = prod(outputSize(1:end-1));
x = nan(outputSize);
%% Solve for Roots
switch kind
    case 1
        % coefficients and exponent are from least squares fitting the k=1,
        % n=0:10000.
        coefficients1j =
[0.411557013144507;0.999986723293410;0.698028985524484;1.06977507291468];
        exponent1j = [0.335300369843979,0.339671493811664];
        % guess for k = 1
```

```
        x((1:nOrdersPerRoot)') = coefficients1j(1) + coefficients1j(2)*m(:) +
coefficients1j(3)*(m(:)+1).^(exponent1j(1)) +
coefficients1j(4)*(m(:)+1).^(exponent1j(2));
        % find first zero
        x((1:nOrdersPerRoot)') = arrayfun(@(n, x0) findzero(n, 1, x0, kind),
m(:), x((1:nOrdersPerRoot)'));

        if n >= 2
            % coefficients and exponent are from least squares fitting the
k=2,
            % n=0:10000.
            coefficients2j = [1.93395115137444;1.00007656297072;-
0.805720018377132;3.38764629174694];
            exponent2j = [0.456215294517928,0.388380341189200];
            % guess for k = 2
            x((nOrdersPerRoot+1:2*nOrdersPerRoot)') = coefficients2j(1) +
coefficients2j(2)*m(:) + coefficients2j(3)*(m(:)+1).^(exponent2j(1)) +
coefficients2j(4)*(m(:)+1).^(exponent2j(2));
            % find second zero
            x((nOrdersPerRoot+1:2*nOrdersPerRoot)') = arrayfun(@(n, x0)
findzero(n, 2, x0, kind), m(:), x((nOrdersPerRoot+1:2*nOrdersPerRoot)'));
        end

        if n >= 3
            % coefficients and exponent are from least squares fitting the
k=3,
            % n=0:10000.
            coefficients3j =
[5.40770803992613;1.00093850589418;2.66926179799040;-0.174925559314932];
            exponent3j = [0.429702214054531,0.633480051735955];
            % guess for k = 3
            x((2*nOrdersPerRoot+1:3*nOrdersPerRoot)') = coefficients3j(1) +
coefficients3j(2)*m(:) + coefficients3j(3)*(m(:)+1).^(exponent3j(1)) +
coefficients3j(4)*(m(:)+1).^(exponent3j(2));
            % find second zero
            x((2*nOrdersPerRoot+1:3*nOrdersPerRoot)') = arrayfun(@(n, x0)
findzero(n, 3, x0, kind), m(:), x((2*nOrdersPerRoot+1:3*nOrdersPerRoot)'));
        end
    case 2
        % coefficients and exponent are from least squares fitting the k=1,
        % n=0:10000.
        coefficients1y =
[0.0795046982450635;0.999998378297752;0.890380645613825;0.0270604048106402];
        exponent1y = [0.335377217953294,0.308720059086699];
        % guess for k = 1
        x((1:nOrdersPerRoot)') = coefficients1y(1) + coefficients1y(2)*m(:) +
coefficients1y(3)*(m(:)+1).^(exponent1y(1)) +
coefficients1y(4)*(m(:)+1).^(exponent1y(2));
        % find first zero
        x((1:nOrdersPerRoot)') = arrayfun(@(n, x0) findzero(n, 1, x0, kind),
m(:), x((1:nOrdersPerRoot)'));

        if n >= 2
            % coefficients and exponent are from least squares fitting the
k=2,
            % n=0:10000.
```

```
            coefficients2y = [1.04502538172394;1.00002054874161;-
0.437921325402985;2.70113114990400];
            exponent2y = [0.434823025111322,0.366245194174671];
            % guess for k = 2
            x((nOrdersPerRoot+1:2*nOrdersPerRoot)') = coefficients2y(1) +
coefficients2y(2)*m(:) + coefficients2y(3)*(m(:)+1).^(exponent2y(1)) +
coefficients2y(4)*(m(:)+1).^(exponent2y(2));
            % find second zero
            x((nOrdersPerRoot+1:2*nOrdersPerRoot)') = arrayfun(@(n, x0)
findzero(n, 2, x0, kind), m(:), x((nOrdersPerRoot+1:2*nOrdersPerRoot)'));
        end

        if n >= 3
            % coefficients and exponent are from least squares fitting the
k=3,
            % n=0:10000.
            coefficients3y =
[3.72777931751914;1.00035294977757;2.68566718444899;-0.112980454967090];
            exponent3y = [0.398247585896959,0.604770035236606];
            % guess for k = 3
            x((2*nOrdersPerRoot+1:3*nOrdersPerRoot)') = coefficients3y(1) +
coefficients3y(2)*m(:) + coefficients3y(3)*(m(:)+1).^(exponent3y(1)) +
coefficients3y(4)*(m(:)+1).^(exponent3y(2));
            % find second zero
            x((2*nOrdersPerRoot+1:3*nOrdersPerRoot)') = arrayfun(@(n, x0)
findzero(n, 3, x0, kind), m(:), x((2*nOrdersPerRoot+1:3*nOrdersPerRoot)'));
        end
    otherwise
        error('Code should never get here.');
end
if n >= 4
    for iRoot = 4:n
        % guesses for remaining roots x[k] = rootSpacing + x[k-1]
        x(((iRoot-1)*nOrdersPerRoot+1:iRoot*nOrdersPerRoot)') = 2*x(((iRoot-
2)*nOrdersPerRoot+1:(iRoot-1)*nOrdersPerRoot)')- x(((iRoot-
3)*nOrdersPerRoot+1:(iRoot-2)*nOrdersPerRoot)');
        % find the remaining zeros
        x(((iRoot-1)*nOrdersPerRoot+1:iRoot*nOrdersPerRoot)') = arrayfun(@(n,
x0) findzero(n, n, x0, kind), m, x(((iRoot-
1)*nOrdersPerRoot+1:iRoot*nOrdersPerRoot)'));
    end
end
end
function x=findzero(n,k,x0,kind)
% Uses Halley's method to find a zero given the starting point x0
% http://en.wikipedia.org/wiki/Halley's_method
ITERATIONS_MAX = 100;       % Maximum number of iteration
TOLERANCE_RELATIVE = 1e4;
% Setup loop
error = 1;
loopCount = 0;
x = 1; % Initialization value only.
% Begin loop
while abs(error)>eps(x)*TOLERANCE_RELATIVE && loopCount<ITERATIONS_MAX

    switch kind
```

```
        case 1
            a = besselj(n,x0);
            b = besselj((n+1),x0);
        case 2
            a = (n/x0)*besselj(n,x0)-besselj(n+1,x0);
            b = ((n+1)/x0)*besselj(n+1,x0)-besselj(n+2,x0);
    end

    xSquared = x0*x0;

    error = 2*a*x0*(n*a-b*x0)/(2*b*b*xSquared-
a*b*x0*(4*n+1)+(n*(n+1)+xSquared)*a*a);

    % Prepare for next loop
    x=x0-error;
    x0=x;
    loopCount=loopCount+1;

end
% Handle maximum iterations
if loopCount>ITERATIONS_MAX-1
    warning('Failed to converge to within relative tolerance of %e for n=%f
and k=%d in %d iterations', eps(x)*TOLERANCE_RELATIVE, n, k, ITERATIONS_MAX);
end
end
```

```
%-----------------------------------------------
%% gmzeros.m
% Program to find roots of the Bessel and Neuman function
% Last Modified on April 16, 2022
%%%%% Modified By Zahid Hasan %%%%%%
%-----------------------------------------------

function x = gmzeros(m, k, B, kind)
%% Input checking
assert(nargin >=1 | nargin <=3,'Wrong number of input arguments.');
% Take care of default cases of k and kind
if nargin < 2
    k = 5;
end
if nargin < 3
    kind = 1;
end
assert(isscalar(kind) & any(kind == [1 2]), '''kind''must be a scalar with
value 1 or 2 only.');
assert(isscalar(k) & fix(k)==k & k>0, 'k must a positive scalar integer.');
assert(all(isreal(m(:))), 'n must be a real number.');

% negative orders have the same roots as the positive orders
m = abs(m);
% Check for that n is less than the ORDER_MAX
if kind==1
    ORDER_MAX = 146222.16674537213;
    assert(all(m <= ORDER_MAX), 'all n values must be less than or equal
%6.10f for kind=1.', ORDER_MAX);
elseif kind==2
    ORDER_MAX = 370030.762407380;
    assert(all(m(:) <= ORDER_MAX), 'all n values must be less than or equal
%6.10f for kind=2.', ORDER_MAX);
end
%% Setup Arrays
% output size
nSize = size(m);
if nSize(end) ==1
    outputSize = [nSize(1) k];
else
    outputSize = [nSize(1) k];
end
% number of orders for each kth root
nOrdersPerRoot = prod(outputSize(1:end-1));
x = nan(outputSize);
%% Solve for Roots
switch kind
    case 1
        % coefficients and exponent are from least squares fitting the k=1,
        % n=0:10000.
        coefficients1j =
[0.411557013144507;0.999986723293410;0.698028985524484;1.06977507291468];
        exponent1j = [0.335300369843979,0.339671493811664];
        % guess for k = 1
        x((1:nOrdersPerRoot)') = coefficients1j(1) + coefficients1j(2)*m(:) +
coefficients1j(3)*(m(:)+1).^(exponent1j(1)) +
coefficients1j(4)*(m(:)+1).^(exponent1j(2));
```

```
        % find first zero
        x((1:nOrdersPerRoot)') = arrayfun(@(n, x0) findzero(n, 1, x0, B,
kind), m(:), x((1:nOrdersPerRoot)'));

        if k >= 2
            % coefficients and exponent are from least squares fitting the
k=2,
            % n=0:10000.
            coefficients2j = [1.93395115137444;1.00007656297072;-
0.805720018377132;3.38764629174694];
            exponent2j = [0.456215294517928,0.388380341189200];
            % guess for k = 2
            x((nOrdersPerRoot+1:2*nOrdersPerRoot)') = coefficients2j(1) +
coefficients2j(2)*m(:) + coefficients2j(3)*(m(:)+1).^(exponent2j(1)) +
coefficients2j(4)*(m(:)+1).^(exponent2j(2));
            % find second zero
            x((nOrdersPerRoot+1:2*nOrdersPerRoot)') = arrayfun(@(n, x0)
findzero(n, 2, x0, B, kind), m(:), x((nOrdersPerRoot+1:2*nOrdersPerRoot)'));
        end

        if k >= 3
            % coefficients and exponent are from least squares fitting the
k=3,
            % n=0:10000.
            coefficients3j =
[5.40770803992613;1.00093850589418;2.66926179799040;-0.174925559314932];
            exponent3j = [0.429702214054531,0.633480051735955];
            % guess for k = 3
            x((2*nOrdersPerRoot+1:3*nOrdersPerRoot)') = coefficients3j(1) +
coefficients3j(2)*m(:) + coefficients3j(3)*(m(:)+1).^(exponent3j(1)) +
coefficients3j(4)*(m(:)+1).^(exponent3j(2));
            % find second zero
            x((2*nOrdersPerRoot+1:3*nOrdersPerRoot)') = arrayfun(@(n, x0)
findzero(n, 3, x0, B, kind), m(:),
x((2*nOrdersPerRoot+1:3*nOrdersPerRoot)'));
        end
    case 2
        % coefficients and exponent are from least squares fitting the k=1,
        % n=0:10000.
        coefficients1y =
[0.0795046982450635;0.999998378297752;0.890380645613825;0.0270604048106402];
        exponent1y = [0.335377217953294,0.308720059086699];
        % guess for k = 1
        x((1:nOrdersPerRoot)') = coefficients1y(1) + coefficients1y(2)*m(:) +
coefficients1y(3)*(m(:)+1).^(exponent1y(1)) +
coefficients1y(4)*(m(:)+1).^(exponent1y(2));
        % find first zero
        x((1:nOrdersPerRoot)') = arrayfun(@(n, x0) findzero(n, 1, x0, B,
kind), m(:), x((1:nOrdersPerRoot)'));

        if k >= 2
            % coefficients and exponent are from least squares fitting the
k=2,
            % n=0:10000.
            coefficients2y = [1.04502538172394;1.00002054874161;-
0.437921325402985;2.70113114990400];
```

```
            exponent2y = [0.434823025111322,0.366245194174671];
            % guess for k = 2
            x((nOrdersPerRoot+1:2*nOrdersPerRoot)') = coefficients2y(1) +
coefficients2y(2)*m(:) + coefficients2y(3)*(m(:)+1).^(exponent2y(1)) +
coefficients2y(4)*(m(:)+1).^(exponent2y(2));
            % find second zero
            x((nOrdersPerRoot+1:2*nOrdersPerRoot)') = arrayfun(@(n, x0)
findzero(n, 2, x0, B, kind), m(:), x((nOrdersPerRoot+1:2*nOrdersPerRoot)'));
        end

        if k >= 3
            % coefficients and exponent are from least squares fitting the
k=3,
            % n=0:10000.
            coefficients3y =
[3.72777931751914;1.00035294977757;2.68566718444899;-0.112980454967090];
            exponent3y = [0.398247585896959,0.604770035236606];
            % guess for k = 3
            x((2*nOrdersPerRoot+1:3*nOrdersPerRoot)') = coefficients3y(1) +
coefficients3y(2)*m(:) + coefficients3y(3)*(m(:)+1).^(exponent3y(1)) +
coefficients3y(4)*(m(:)+1).^(exponent3y(2));
            % find second zero
            x((2*nOrdersPerRoot+1:3*nOrdersPerRoot)') = arrayfun(@(n, x0)
findzero(n, 3, x0, B, kind), m(:),
x((2*nOrdersPerRoot+1:3*nOrdersPerRoot)'));
        end
    otherwise
        error('Code should never get here.');
end
if k >= 4
    for iRoot = 4:k
        % guesses for remaining roots x[k] = rootSpacing + x[k-1]
        x(((iRoot-1)*nOrdersPerRoot+1:iRoot*nOrdersPerRoot)') = 2*x(((iRoot-
2)*nOrdersPerRoot+1:(iRoot-1)*nOrdersPerRoot)')- x(((iRoot-
3)*nOrdersPerRoot+1:(iRoot-2)*nOrdersPerRoot)');
        % find the remaining zeros
        x(((iRoot-1)*nOrdersPerRoot+1:iRoot*nOrdersPerRoot)') = arrayfun(@(n,
x0) findzero(n, k, x0, B, kind), m, x(((iRoot-
1)*nOrdersPerRoot+1:iRoot*nOrdersPerRoot)'));
    end
end
end
function x=findzero(n,k,x0,B,kind)
% Uses Halley's method to find a zero given the starting point x0
% http://en.wikipedia.org/wiki/Halley's_method
ITERATIONS_MAX = 100;       % Maximum number of iteration
TOLERANCE_RELATIVE = 1e4;
% Setup loop
error = 1;
loopCount = 0;
x = 1; % Initialization value only.
% Begin loop

while abs(error)>eps(x)*TOLERANCE_RELATIVE && loopCount<ITERATIONS_MAX

    switch kind
```

```
        case 1
            p = bessely(n,B)/besselj(n,B);
            a = bessely(n,x0)-besselj(n,x0)*p;
            b = bessely(n+1,x0)-besselj(n+1,x0)*p;
        case 2
            q = ((n/B)*bessely(n,B)-bessely(n+1,B))/((n/B)*besselj(n,B)-
besselj(n+1,B));
            a = ((n/x0)*bessely(n,x0)-bessely(n+1,x0))-((n/x0)*besselj(n,x0)-
besselj(n+1,x0))*q;
            b = (((n+1)/x0)*bessely(n+1,x0)-bessely(n+2,x0))-
(((n+1)/x0)*besselj(n+1,x0)-besselj(n+2,x0))*(q);
    end

    xSquared = x0*x0;

    error = 2*a*x0*(n*a-b*x0)/(2*b*b*xSquared-
a*b*x0*(4*n+1)+(n*(n+1)+xSquared)*a*a);

    % Prepare for next loop
    x=x0-error;
    x0=x;
    loopCount=loopCount+1;

end
% Handle maximum iterations
if loopCount>ITERATIONS_MAX-1
    warning('Failed to converge to within relative tolerance of %e for n=%f
and k=%d in %d iterations', eps(x)*TOLERANCE_RELATIVE, n, k, ITERATIONS_MAX);
end
end
```